

ESL-TR-92-61

**EFFECTIVENESS OF YAW-INDUCING
DEFLECTION GRIDS FOR DEFEATING
ADVANCED PENETRATING WEAPONS**

J.M. UNDERWOOD

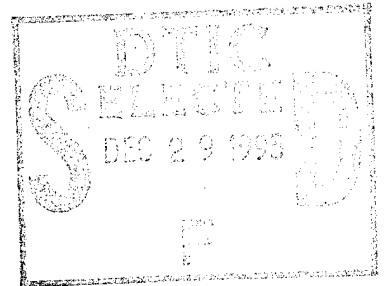
**APPLIED RESEARCH ASSOCIATES, INC.
P.O. BOX 40128
TYNDALL AFB FL 32403**

APRIL 1995

FINAL REPORT

OCTOBER 1991 - NOVEMBER 1992

**APPROVED FOR PUBLIC RELEASE:
DISTRIBUTION UNLIMITED**



19951228 022



ENGINEERING RESEARCH DIVISION
Air Force Civil Engineering Support Agency
Civil Engineering Laboratory
Tyndall Air Force Base, Florida 32403



NOTICE

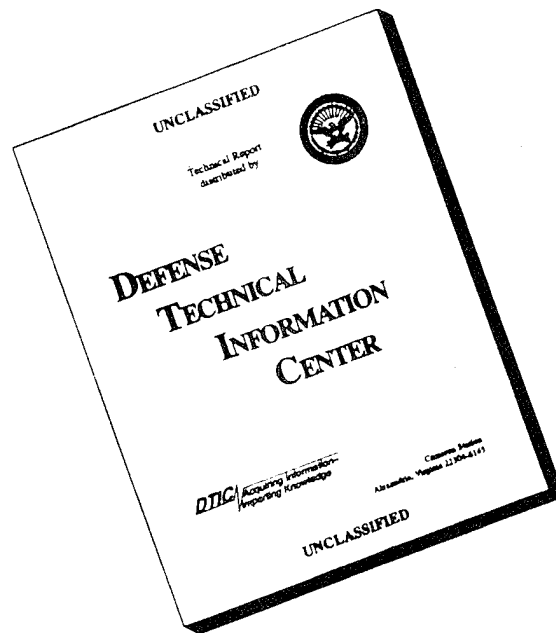
PLEASE DO NOT REQUEST COPIES OF THIS REPORT FROM HQ AFCEA/RA (AIR FORCE CIVIL ENGINEERING SUPPORT AGENCY). ADDITIONAL COPIES MAY BE PURCHASED FROM:

**NATIONAL TECHNICAL INFORMATION SERVICE
5285 PORT ROYAL ROAD
SPRINGFIELD, VIRGINIA 22161**

FEDERAL GOVERNMENT AGENCIES AND THEIR CONTRACTORS REGISTERED WITH DEFENSE TECHNICAL INFORMATION CENTER SHOULD DIRECT REQUESTS FOR COPIES OF THIS REPORT TO:

**DEFENSE TECHNICAL INFORMATION CENTER
CAMERON STATION
ALEXANDRIA, VIRGINIA 22314**

DISCLAIMER NOTICE



THIS DOCUMENT IS BEST QUALITY AVAILABLE. THE COPY FURNISHED TO DTIC CONTAINED A SIGNIFICANT NUMBER OF PAGES WHICH DO NOT REPRODUCE LEGIBLY.

REPORT DOCUMENTATION PAGE

Form Approved
OMB No. 0704-0188

Public reporting burden for this collection of information is estimated to average 1 hour per response, including the time for reviewing instructions, searching existing data sources, gathering and maintaining the data needed, and completing and reviewing the collection of information. Send comments regarding this burden estimate or any other aspect of this collection of information, including suggestions for reducing this burden, to Washington Headquarters Services, Directorate for Information Operations and Reports, 1215 Jefferson Davis Highway, Suite 1204, Arlington, VA 22202-4302, and to the Office of Management and Budget, Paperwork Reduction Project (0704-0188), Washington, DC 20503.

1. AGENCY USE ONLY (Leave blank)		2. REPORT DATE April 1995		3. REPORT TYPE AND DATES COVERED Final 28 Oct 91 - 30 Nov 92	
4. TITLE AND SUBTITLE Effectiveness of Yaw-Inducing Deflection Grids for Defeating Advanced Penetrating Weapons				5. FUNDING NUMBERS C: F08635-88-c-0067	
6. AUTHOR(S) Underwood, J. M.					
7. PERFORMING ORGANIZATION NAME(S) AND ADDRESS(ES) Applied Research Associates, Inc. P.O. Box 40128 Tyndall AFB, FL 32403				8. PERFORMING ORGANIZATION REPORT NUMBER ESL-TR-92-61	
9. SPONSORING/MONITORING AGENCY NAME(S) AND ADDRESS(ES) Headquarters Air Force Civil Engineering Support Agency Civil Engineering Laboratory Tyndall AFB, FL 32403-6001				10. SPONSORING/MONITORING AGENCY REPORT NUMBER ESL-TR-92-61	
11. SUPPLEMENTARY NOTES					
12a. DISTRIBUTION/AVAILABILITY STATEMENT Approved for public release. Distribution unlimited.				12b. DISTRIBUTION CODE	
13. ABSTRACT (Maximum 200 words) The objective of this effort was to develop a new layered protective system effective in defeating advanced penetrating weapons. The system consists of a reinforced concrete deflection grid and a burster slab to deflect and stop the penetrator. The design was to be cost effective, improve survivability and be used in both new and retrofit construction.					
14. SUBJECT TERMS Antipenetration Systems Protective Construction Layered Media				15. NUMBER OF PAGES	
				16. PRICE CODE	
17. SECURITY CLASSIFICATION OF REPORT U	18. SECURITY CLASSIFICATION OF THIS PAGE U	19. SECURITY CLASSIFICATION OF ABSTRACT U	20. LIMITATION OF ABSTRACT UL		

EXECUTIVE SUMMARY

A. OBJECTIVE

In response to a letter dated 23 May 1991 from Headquarters United States Air Forces in Europe, the Air Force Civil Engineering Support Agency, Engineering Research Division stepped up an effort for a new layered protective system effective in defeating advanced penetrating weapons. The system consists of a reinforced concrete deflection grid and a burster slab to deflect and stop the penetrator. The objective of this subtask was to develop a design which would be cost effective and could be implemented in both new and retrofit construction.

B. BACKGROUND

Current protective construction practice in the USAFE and PACAF areas consists of heavily reinforced concrete, which requires massive amounts of materials and labor. This type of construction is designed to prevent breaching, and to reduce spall on the inside of exterior walls. Various combinations of soil layers, burster slabs, and rock rubble overlays have been used to trap penetrating weapons. Semihardened and hardened facilities are protected from aerial bombardment by a burster slab, designed for a particular threat. Weapon shape, weight, case material properties, charge-to-weight ratio, velocity, and fusing are the principal variables considered in the design of a burster slab. Its purpose is to break up or detonate the weapon at a sufficient distance to prevent serious damage to the target. With the increased accuracy of today's weapons, existing construction techniques do not provide guaranteed protection against weapon penetration, and the cost to do so could be prohibitive due to the shear mass required to defeat a deep penetrating weapon. In tests conducted by the Waterways Experiment Station (WES), it was found that yaw, the angle between the penetrator's center of gravity translational velocity vector and its geometric centerline, induced into the projectile prior to striking the burster slab, greatly affects its penetration capability. Stress levels generated in the weapon case during impact can trigger a variety of failure mechanisms.

Various antipenetration systems have been tested using rock rubble as an overlay against various types of weapons, but rock rubble is not practical if the rock is not readily available. Oblique impacts showed a tendency of the weapon to rotate in the boulder layer, revealing the importance of local impact conditions.

A yaw-inducing concept tested by WES using steel bars showed how effective a simple design could be in defeating low length to diameter, armor-piercing projectiles.

<input checked="checked" type="checkbox"/>
<input type="checkbox"/>
<input type="checkbox"/>
Codes

Dist	and/or Special
A-1	

The bars provided an unsymmetrical load on the projectile nose, which in turn caused a rotation of the projectile around its center of gravity.

Previous AFCESA tests at the Tyndall AFB Sky X Test Area had been conducted with deflection type devices constructed of cementitious materials. A basic deflection grid geometry was tested to observe the reaction between the deflection grid and the projectile. Data reduced from these exploratory tests showed a variance in induced projectile rotational rate as the physical properties of the concrete changed. The magnitude of the effect of each material variable, such as compressive strength, density, and toughness, was not determined, nor was the effect of impact point. Due to the irregular design of the deflection grid, projectile rotation was induced, at least in part, by unsymmetrical loading. The findings of this earlier work indicated the material properties of the concrete provide a significant contribution to projectile tumble rate. For a system to be effective, it must have an overall weight advantage over existing construction techniques, and provide the structural integrity to resist multiple strikes and maintain consistent performance.

C. SCOPE

A theoretical analysis of the ballistic penetration of a deflection grid is presented in Section II. Test procedures and laboratory setup are discussed in Section III. The test programs for FY 91 and FY 92 are presented in Section IV. Section V discusses the analysis of the test results for both test programs, based on geometry type, with conclusions and recommendations in Section VI and VII.

D. METHODOLOGY

Many variables affect the behavior of dynamically loaded concrete. In the case of a deflection grid, the interaction of the projectile and the grid is very complex due to the grid's nonhomogeneous nature. Various computer modeling programs investigated failed to provide a good constitutive model for the unique design of the deflection grid. Experiments were conducted to determine the key variables relating to the destabilization of advanced penetrating weapons. The FY 91 test program was an exploratory experimental effort to determine the effect of perforated concrete slab sections on the stability of a weapon. In its early stages, this effort focused on the geometry of the deflection grid, and the influence of compressive strength. Due to a wide variance in projectile rotational rates, and the catastrophic damage to the deflection grids at high compressive strengths, steel and nylon fibers were added to the mix designs. Bursting slabs were not incorporated into the tests until FY 92, since observation of the projectile's induced rotation was the objective of the FY 91 tests. The projectile was allowed to

travel freely for 20 feet after striking the deflection grid, to obtain sufficient high speed photography of the event. Based on the FY 91 test results, the FY 92 test program systematically varied deflection grid and burster slab configuration parameters to obtain response data from which to develop an antipenetration system design procedure. For each fiscal year program, the test schedule, test item configuration, material properties, and field test results are presented.

E. RESULTS

All penetrators stopped by the burster slab had angles of attack of at least 12.5 degrees. The lightweight concretes showed increased fracturing as the compressive strength was increased, and did not perform as well as did the heavier concretes. This could be related to the contact time of the penetrator and the deflection grid and the associated angular impulse. Lightweight, high-strength concretes have a shorter time to failure, and do not provide the contact time required to overcome inertia forces in the shorter distances. Since the heavier concrete mixes performed 100 percent of the time in preventing perforation, a hypothetical case was developed for a deflection grid system, resulting in a unit weight of 207 pcf. Using the design parameters in the FY 92 test program, the deflection grid required a thickness of 4 inches, followed by a 72-inch air gap, terminating at an 18-inch burster slab. The overall depth of the combined system was 94 inches. The weight of the deflection grid, for a 10-foot by 10-foot section, was 5,520 pounds for 26.6 cf of concrete at 207 pcf. The weight of an 18-inch burster slab was 22,500 pounds, for a combined weight of 28,020 pounds. If a standard burster slab were to be implemented in lieu of the deflection grid, a thickness of 28 inches would be required to prevent perforation. Total weight of the burster slab would be 34,000 pounds, based on a unit weight of 150 pcf. This resulted in a 17 percent weight reduction and a 22 percent volume reduction through the use of a deflection grid system.

F. CONCLUSIONS

In reviewing the laboratory data on the flexural beam tests, a significant relationship was observed between unit weight and material toughness. An almost linear relationship exists when toughness is calculated using the JCI Method. Total yaw was related to unit weight, compressive strength, and toughness, where again toughness exhibited excellent linearity based on the FY 92 data. For this particular penetrator, angles of attack greater than 12 degrees upon impact with the burster slab defeated the weapon.

In designing a deflection system, the threat must be known, as well as the depth of the protected facility. This information will be used to compute the physical dimensions of

the deflection grid, length of the air gap, and thickness of the burster slab. The following computational procedures are valid only within the range of conditions described in the body of this report, and require modification to account for scale effects. Change in weapon characteristics will have a definite impact on the procedure. Efforts are being investigated to augment these calculations for a variety of weapon types, and will be presented in a subsequent report.

G. RECOMMENDATIONS

Investigations should be conducted to evaluate additional mix design performance with variations of velocity and projectile size, to increase the existing data base. Full scale tests should be conducted against inert and live 2000-pound class weapons, once scaling issues have been investigated. The deflection grids should be constructed as modular panels in a factory environment, to ensure strict quality control.

PREFACE

This report was prepared by Applied Research Associates, Inc. (ARA), under contract F08635-88-C-0067 for the Air Force Civil Engineering Support Agency (AFCESA), Tyndall Air Force Base, Florida.

This report summarizes work done between 28 October 1991 and 30 November 1992. LT Michael K. Westmoreland (USN) was the AFCESA/RACS Project Officer for the subtask under which this work was accomplished.

This report has been reviewed by the Public Affairs Office and is releasable to the National Technical Information Service (NTIS). At NTIS, it will be available to the public.

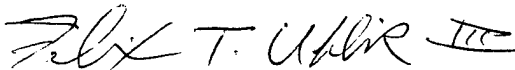
This technical report has been reviewed and is approved for publication.



MICHAEL K. WESTMORELAND, LT, USN
Project Officer



WILLIAM S. STRICKLAND
Chief, Air Base Survivability Section



FELIX T. UHLIR, III, Lt Col, USAF
Chief, Air Base Systems Branch

TABLE OF CONTENTS

Section	Title	Page
I	INTRODUCTION.....	1
	A. OBJECTIVE.....	1
	B. BACKGROUND.....	1
	C. SCOPE.....	2
II	BALLISTIC PENETRATION ANALYSIS.....	3
	A. APPROACH.....	3
	B. COMPUTER SIMULATION.....	7
III	TEST SETUP.....	14
	A. ANTIPENETRATION GUN FACILITY.....	14
	B. MATERIAL TEST LABORATORY.....	17
IV	TEST PROGRAMS.....	20
	A. INTRODUCTION.....	20
	B. FY 91 TEST PROGRAM.....	20
	1. Test Schedule.....	20
	2. Test Item Configuration.....	20
	3. Material Properties.....	25
	4. Field Test Results.....	26
	C. FY 92 TEST PROGRAM.....	28
	1. Test Schedule.....	28
	2. Test Item Configuration.....	28
	3. Material Properties.....	28
	4. Field Test Results.....	48
V	ANALYSIS OF TEST RESULTS.....	56
	A. FY 91 ANALYSIS.....	56
	1. Grid Type 01.....	56
	2. Grid Type 02.....	62
	3. Grid Type 03.....	62
	B. FY 92 ANALYSIS.....	62
	1. Grid Type 16.....	62
	2. Grid Type 20.....	71
	3. Grid Type 25.....	90
	C. COST ANALYSIS.....	97
	1. Burster Slab Upgrade.....	101
	2. Deflection Grid with Burster Slab Upgrade.....	101

TABLE OF CONTENTS (CONTINUED)

Section	Title	Page
VI	CONCLUSIONS.....	103
VII	RECOMMENDATIONS.....	106
	REFERENCES.....	107

LIST OF FIGURES

Figure	Title	Page
1	Projectile Rotation versus Body Lengths of Travel.....	4
2	Projectile Rotation versus Body Lengths of Travel.....	5
3	Plot of Projectile Shape.....	8
4	Plot of Projectile Penetration Depth at 0-degree Angle of Attack.....	9
5	Plot of Projectile Penetration Depth at 4-degree Angle of Attack.....	10
6	Plot of Projectile Penetration Depth at 8-degree Angle of Attack.....	11
7	Plot of Projectile Penetration Depth at 10-degree Angle of Attack.....	12
8	Plot of Projectile Penetration Depth at 12-degree Angle of Attack.....	13
9	Schematic of Penetrator used in AFCESA Test.....	15
10	Layout of Antipenetration Laboratory and Equipment.....	16
11	Pretest and Posttest Photographs of Static Compression Tests.....	18
12	Deflection Grid Type 01.....	22
13	Deflection Grid Type 02.....	23
14	Deflection Grid Type 03.....	24
15	Deflection Grid Type 16.....	30
16	Deflection Grid Type 20.....	31
17	Deflection Grid Type 25.....	32
18	Pretest Photographs of 155 mm Howitzer and Grid Type 20.....	33
19	Pretest Photographs of Grid Type 16.....	34
20	Pretest Photographs of Grid Type 25.....	34
21	Load versus Deflection Curve for LW4000 6" by 12" Cylinder Static Compressive Strength Test.....	36
22	Deflection versus Time Curve for LW4000 Flexural Beam Test.....	37
23	Load versus Deflection Curve for LW4000 Flexural Beam Test.....	38
24	Load versus Deflection Curve for LW8000 6" by 12" Cylinder Static Compressive Strength Test.....	39
25	Load versus Deflection Curve for LW8000 Flexural Beam Test.....	40
26	Load versus Deflection Curve for NW4000 6" by 12" Cylinder Static Compressive Strength Test.....	42
27	Load versus Deflection Curve for NW4000 Flexural Beam Test.....	43
28	Load versus Deflection Curve for NW8000 6" by 12" Cylinder Static Compressive Strength Test.....	44
29	Load versus Deflection Curve for NW8000 Flexural Beam Test.....	45
30	Load versus Deflection Curve for HDM 6" by 12" Cylinder Static	

LIST OF FIGURES (CONTINUED)

Figure	Title	Page
	Compressive Strength Test.....	46
31	Load versus Deflection Curve for HDM Flexural Beam Test.....	47
32	Load versus Deflection Curve for VHDM 6" by 12" Cylinder Static Compressive Strength Test.....	49
33	Load versus Deflection Curve for VHDM Flexural Beam Test.....	50
34	Posttest Photographs of LW4000 and LW8000 Flexural Tests.....	51
35	Posttest Photographs of NW4000 and NW8000 Flexural Tests.....	52
36	Posttest Photographs of HDM and VHDM Flexural Tests.....	53
37	Target Strike Locations.....	54
38	Yaw versus Body Lengths of Travel for Shots 1, 2, 3, 15, 16, 17.....	57
39	Yaw versus Body Lengths of Travel for Shots 4, 5.....	58
40	Yaw versus Body Lengths of Travel for Shots 6, 18.....	59
41	Yaw versus Body Lengths of Travel for Shots 25, 26, 36.....	60
42	Yaw versus Body Lengths of Travel for Shots 37, 33, 30, 31, 32.....	61
43	Yaw versus Body Lengths of Travel for Shots 7, 8, 9, 13.....	63
44	Yaw versus Body Lengths of Travel for Shots 20, 22, 27, 28.....	64
45	Posttest Photographs of Shot 40.....	66
46	Posttest Photographs of Shot 42.....	67
47	Posttest Photographs of Shot 47.....	68
48	Posttest Photographs of shot 49.....	69
49	Posttest Photographs of Shot 53.....	70
50	Posttest Photographs of Shot 54.....	72
51	Unit Weight versus Total Yaw for Grid Type 16.....	73
52	Compressive Strength versus Total Yaw for Grid Type 16.....	74
53	Toughness versus Total Yaw for Grid Type 16.....	75
54	Material Property Comparison for Grid Type 16.....	76
55	Yaw versus Body Lengths of Travel for Grid Type 16.....	77
56	Posttest Photographs of Shot 39.....	78
57	Posttest Photographs of Shot 41.....	79
58	Posttest Photographs of Shot 45.....	81
59	Posttest Photographs of Shot 50.....	82
60	Posttest Photographs of Shot 52.....	83
61	Posttest Photographs of Shot 55.....	84
62	Yaw versus Body Lengths of Travel for Grid Type 20.....	85

LIST OF FIGURES (CONTINUED)

Figure	Title	Page
63	Unit Weight versus Total Yaw for Grid Type 20.....	86
64	Toughness versus Total Yaw for Grid Type 20.....	87
65	Material Property Comparison for Grid Type 20.....	88
66	Compressive Strength versus Total Yaw for Grid Type 20.....	89
67	Posttest Photographs of Shot 38.....	91
68	Posttest Photographs of Shot 43.....	92
69	Posttest Photographs of Shot 44.....	93
70	Posttest Photographs of Shot 46.....	94
71	Posttest Photographs of Shot 48.....	95
72	Posttest Photographs of Shot 51.....	96
73	Yaw versus Body Lengths of Travel for Grid Type 25.....	98
74	Unit Weight versus Total Yaw for Grid Type 25.....	99
75	Material Property Comparison for Grid Type 25.....	100
76	Unit Weight versus Toughness for JCI Test Method.....	104

LIST OF TABLES

Number	Title	Page
1	FY 91 Antipenetration Deflection Grid Test Matrix.....	21
2	FY 91 Deflection Grid Test Data.....	27
3	FY 92 Antipenetration Deflection Grid Test Matrix.....	29
4	FY 92 Deflection Grid Test Data.....	55

SECTION I INTRODUCTION

A. OBJECTIVE

In response to a letter dated 23 May 1991 from Headquarters United States Air Forces in Europe, the Air Force Civil Engineering Support Agency, Engineering Research Division stepped up an effort for a new layered protective system effective in defeating advanced penetrating weapons. The system consists of a reinforced concrete deflection grid and a burster slab to deflect and stop the penetrator. The objective of this subtask was to develop a design which would be cost effective and could be implemented in both new and retrofit construction.

B. BACKGROUND

Current protective construction practice in the USAFE and PACAF areas consists of heavily reinforced concrete, which requires massive amounts of materials and labor. This type of construction is designed to prevent breaching, and to reduce spall on the inside of exterior walls. Various combinations of soil layers, burster slabs, and rock rubble overlays have been used to trap penetrating weapons. Semihardened and hardened facilities are protected from aerial bombardment by a burster slab, designed for a particular threat. Weapon shape, weight, case material properties, charge-to-weight ratio, velocity, and fusing are the principal variables considered in the design of a burster slab. Its purpose is to break up or detonate the weapon at a sufficient distance to prevent serious damage to the target. With the increased accuracy of today's weapons, existing construction techniques do not provide guaranteed protection against weapon penetration, and the cost to do so could be prohibitive due to the shear mass required to defeat a deep penetrating weapon. In tests conducted by the Waterways Experiment Station (WES), it was found that yaw, the angle between the penetrator's center of gravity translational velocity vector and its geometric centerline, induced into the projectile prior to striking the burster slab, greatly affects its penetration capability (Reference 1). Stress levels generated in the weapon case during impact can trigger a variety of failure mechanisms.

Various antipenetration systems have been tested, using rock rubble as an overlay against various types of weapons (Reference 2), but rock rubble is not practical if the rock

is not readily available. Oblique impacts showed a tendency of the weapon to rotate in the boulder layer, revealing the importance of local impact conditions (Reference 3).

A yaw-inducing concept tested by WES using steel bars showed how effective a simple design could be in defeating low length to diameter, armor-piercing projectiles (Reference 4). The bars provided an unsymmetrical load on the projectile nose, which in turn caused a rotation of the projectile around its center of gravity.

Previous AFCESA tests at the Tyndall AFB Sky X Test Area had been conducted with deflection type devices constructed of cementitious materials. A basic deflection grid geometry was tested to observe the reaction between the deflection grid and the projectile. Data reduced from these exploratory tests showed a variance in induced projectile rotational rate as the physical properties of the concrete changed. The magnitude of the effect of each material variable, such as compressive strength, density, and toughness, was not determined, nor was the effect of impact point. Due to the irregular design of the deflection grid, projectile rotation was induced, at least in part, by unsymmetrical loading. The findings of this earlier work indicated the material properties of the concrete provide a significant contribution to projectile tumble rate. For a system to be effective, it must have an overall weight advantage over existing construction techniques, and provide the structural integrity to resist multiple strikes and maintain consistent performance.

C. SCOPE

A theoretical analysis of the ballistic penetration of a deflection grid is presented in Section II. Test procedures and laboratory setup are discussed in Section III. The test programs for FY 91 and FY 92 are presented in Section IV. Section V discusses the analysis of the test results for both test programs, based on geometry type, with conclusions and recommendations in Section VI.

SECTION II

BALLISTIC PENETRATION ANALYSIS

A. APPROACH

Many variables affect the behavior of dynamically loaded concrete. In the case of a deflection grid, the interaction of the projectile and the grid is very complex due to the grid's nonhomogeneous nature. Data from previous tests on concrete deflection grids made of normal steel-reinforced concrete showed a wide variation in induced projectile rotation rate. Figure 1 shows the projectile rotation in relation to body lengths of travel. The slope of the line is the projectile rotation rate. Figure 2 shows similar data for tests performed on grids constructed with a nylon fiber content of 10 pounds per cubic yard, and reduced conventional reinforcing steel. This tends to support the theory that the fibers create a more homogeneous structure and thereby produce more consistent, though not necessarily larger turning rates.

If the fibers add to the structural integrity of the concrete and delay the time to failure, an increased contact time between the penetrator and the deflection grid is achieved. Since reaction impulse is the key in determining the resultant projectile rotation rate, it might be beneficial to maximize the toughness of the grid material. By so doing, contact time for force application would be extended.

To demonstrate this effect, a simple impulse model has been developed with the following assumptions:

- Reaction force is not applied until one-fourth grid depth.
- Initial failure plane is tangent to the ogive at the projectile tip.
- Crack propagation through the remainder of the material starts immediately once the initial failure plane is established.

The impulse of a constant force is the product of the force and the time it is applied, and can be related to mass and velocity in the following equation;

$$F(t_2 - t_1) = m(v_2 - v_1)$$

where;

F = Force (lb) due to velocity of penetrator

t = Time (sec)

m = Mass of the projectile (lb sec²/in)

v = Projectile velocity (in/sec)

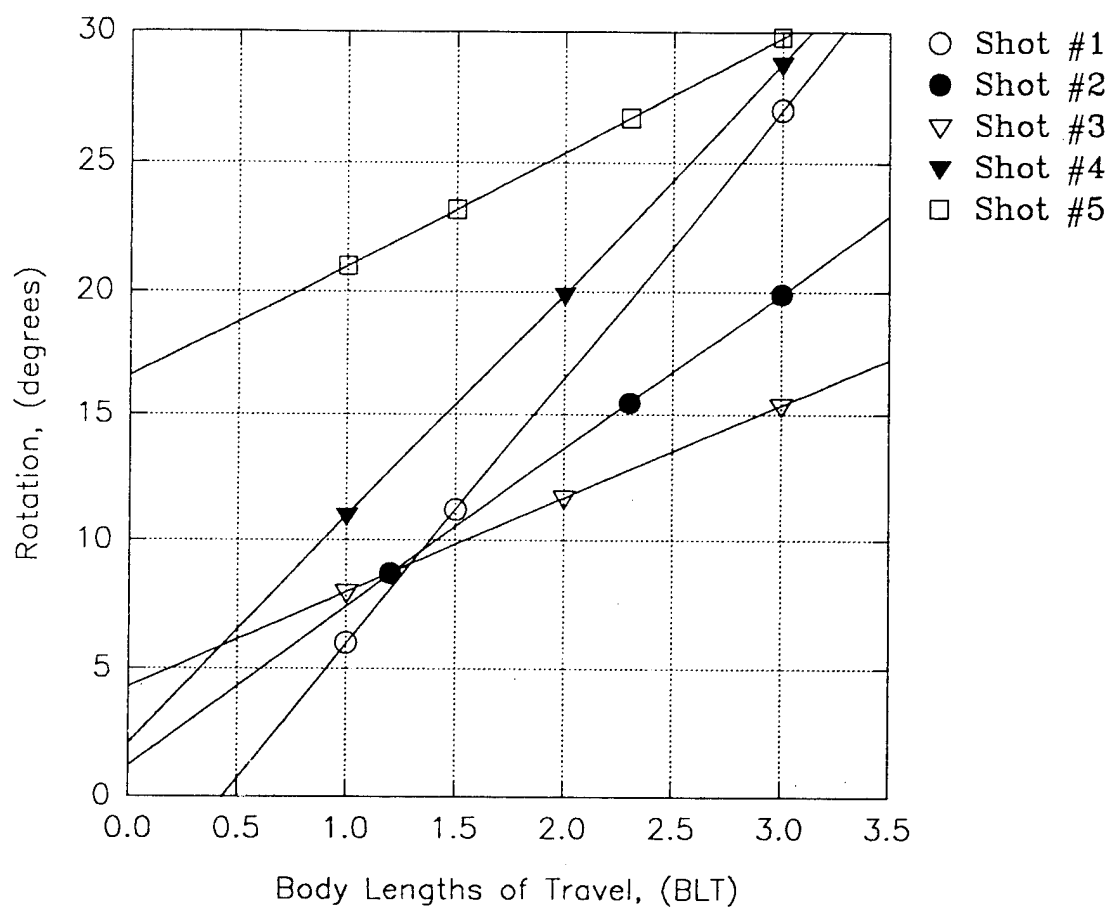


Figure 1. Projectile Rotation versus Body Lengths of Travel

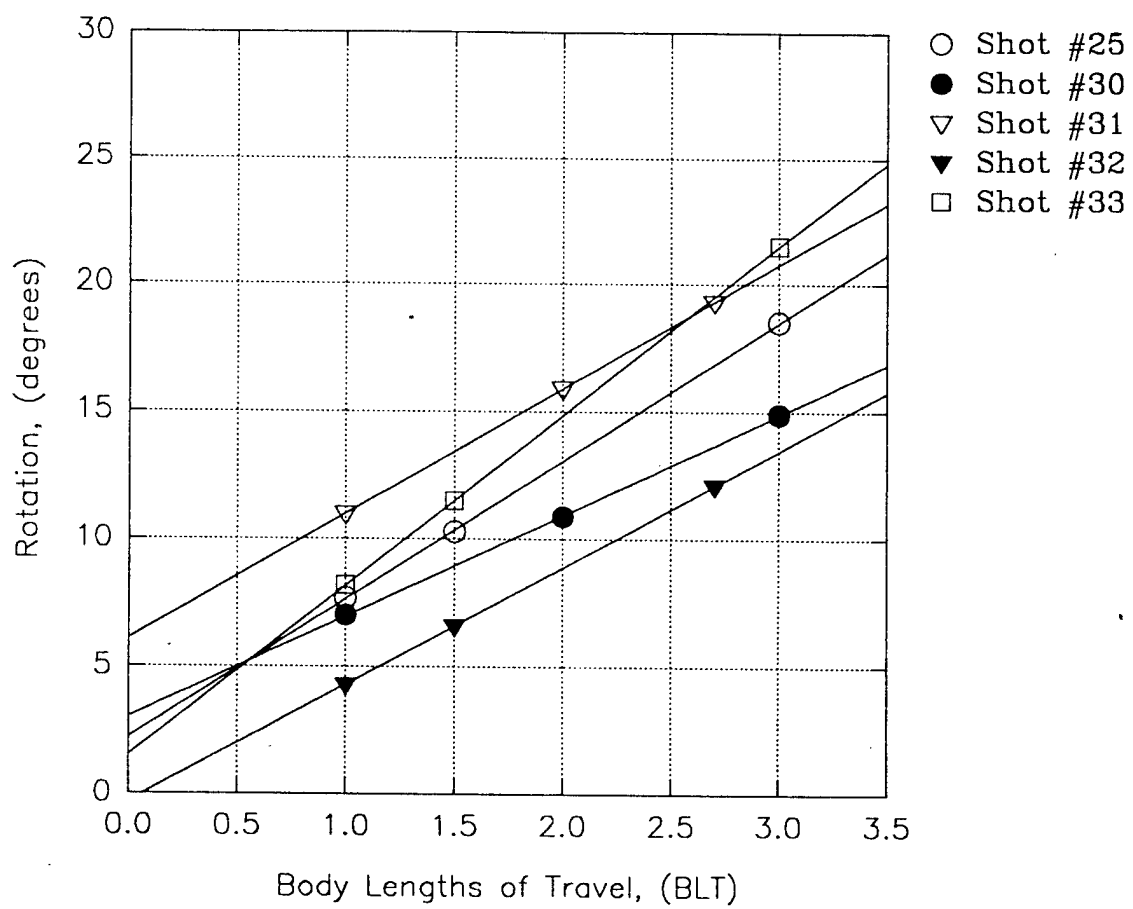


Figure 2. Projectile Rotation versus Body Lengths of Travel.

Since the values for time and velocity can be deduced from the acquired test data, the equation is rearranged to solve for the average reaction force.

$$F = m(v_2 - v_1) / (t_2 - t_1)$$

To solve for angular velocity, we must supplement the equation of linear impulse/momentum with an equation that says the net external moment on a body is equal to the product of the moment of inertia I and the angular acceleration \dot{W} of the body,

$$\Sigma M_{cg} = I_O * \dot{W}$$

where,

ΣM_{cg} = Sum of the moments about the center of gravity of the projectile (lb in)

I_O = Mass moment of inertia of the projectile (lb in sec²)

\dot{W} = Angular acceleration of the projectile (rad/sec²)

In this equation, $I_O * \dot{W}$ is the projectile's rate of angular momentum change, and is set equal to the sum of the moments due to the reactive forces. Another way to express this equation;

$$\Sigma M_{cg} = R * d = I_O * \dot{W}$$

where,

d = the moment arm of the reactive force (in)

R = reactive force (lbs) of the deflection grid

Integrating the above equation over the time period of interest yields the total angular impulse,

$$\int M_{cg} dt = I_O W$$

where,

W = Angular velocity (rad/sec)

I_O = Mass moment of inertia of the projectile (lb in sec²)

Contact time between the penetrator and the deflection grid is directly related to the time to failure of the material. Since toughness is a measure of the energy-absorption capability of the material, it seems reasonable to assume, that by maximizing the material toughness, contact time is increased, thereby increasing the rotational energy in the system and maximizing the yaw induced into the projectile. Appropriate forms of the forcing functions, taking into account density, compressive strength, and toughness, would require substantial development to validate the model. However, the limited number of tests performed in this subtask are not sufficient for that effort. The test plan was developed to find the system that would provide maximum deflection, consistent performance, survivability from multiple strikes and still provide a suitable cost trade off.

B. COMPUTER SIMULATION

Since the purpose of the deflection grid is to turn the projectile, computer simulation of the burster slab behind the grid was required for an initial design, to predict the grid's effectiveness. Using a two-dimensional penetration code PENCO2D (Reference 5) from Waterways Experiment Station, several runs were conducted to determine the effect of the angle of attack and the obliquity angle induced by the grid on penetration through the burster slab. Figure 3 shows the dimensions of the projectile and location of the center of gravity. Figure 4 shows the effect of a normal impact with an angle of attack of zero degrees as indicated by α . The plot has two horizontal lines, which indicate the front and rear surfaces of the burster slab. The projectile is displayed on the plot at impact and also at the end of the calculation, with a line connecting the two center of gravity (cg) positions. Perforation of the burster slab is indicated when the projectile cg falls below the horizontal line representing the rear of the burster slab. Figure 5 shows an impact where the velocity vector is normal to the burster slab surface, with a 4-degree projectile angle of attack. This establishes a 4-degree yaw at impact, simulating the effect of a deflection grid. In this case, the projectile perforates the burster slab. Figure 6 shows the effect when the angle of attack is increased to 8-degrees, still resulting in perforation. Figure 7 shows the projectile fails to perforate when the angle of attack is increased to 10-degrees. The plot shows the projectile trapped within the slab, as indicated by the location of the projectile cg. An angle of attack of 12 degrees, Figure 8, shows a substantial change in projectile orientation, with the cg located at mid-slab. Increased angles of attack were generated, indicating similar results. This process established a baseline for initial burster slab construction to be used in the FY 92 test program.

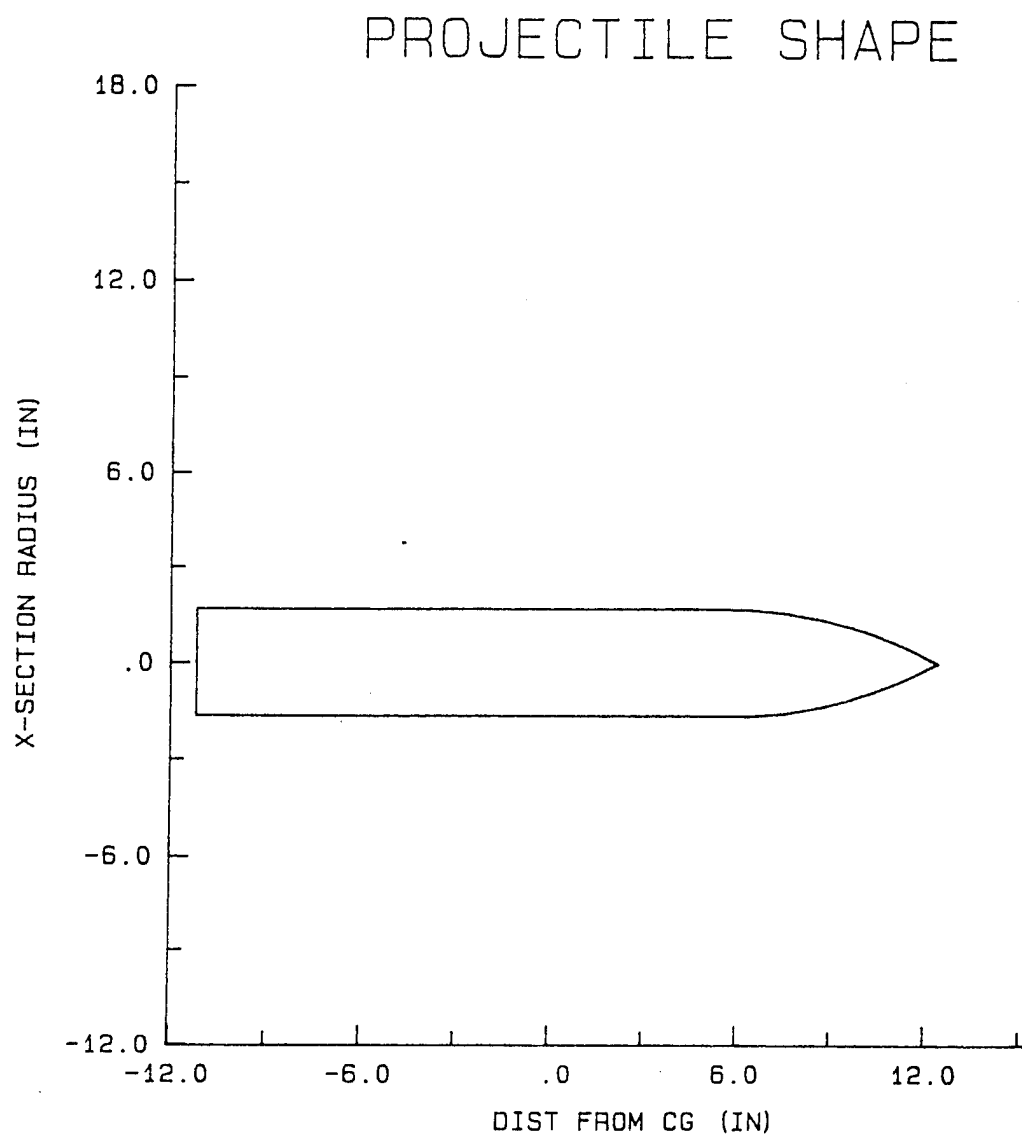


Figure3. Plot of Projectile Shape.

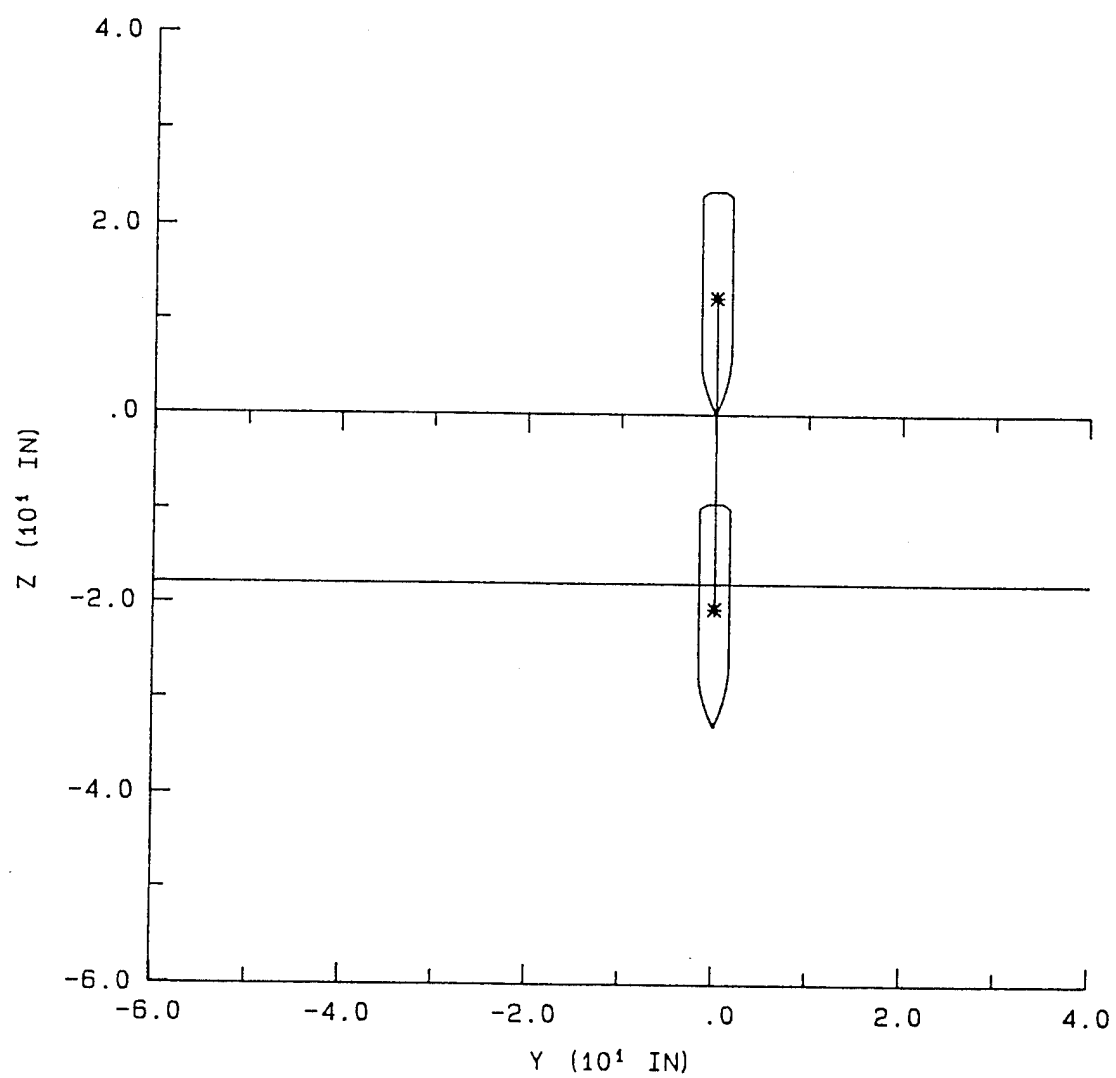


Figure 4. Plot of Projectile Penetration Depth at 0-degree Angle of Attack.

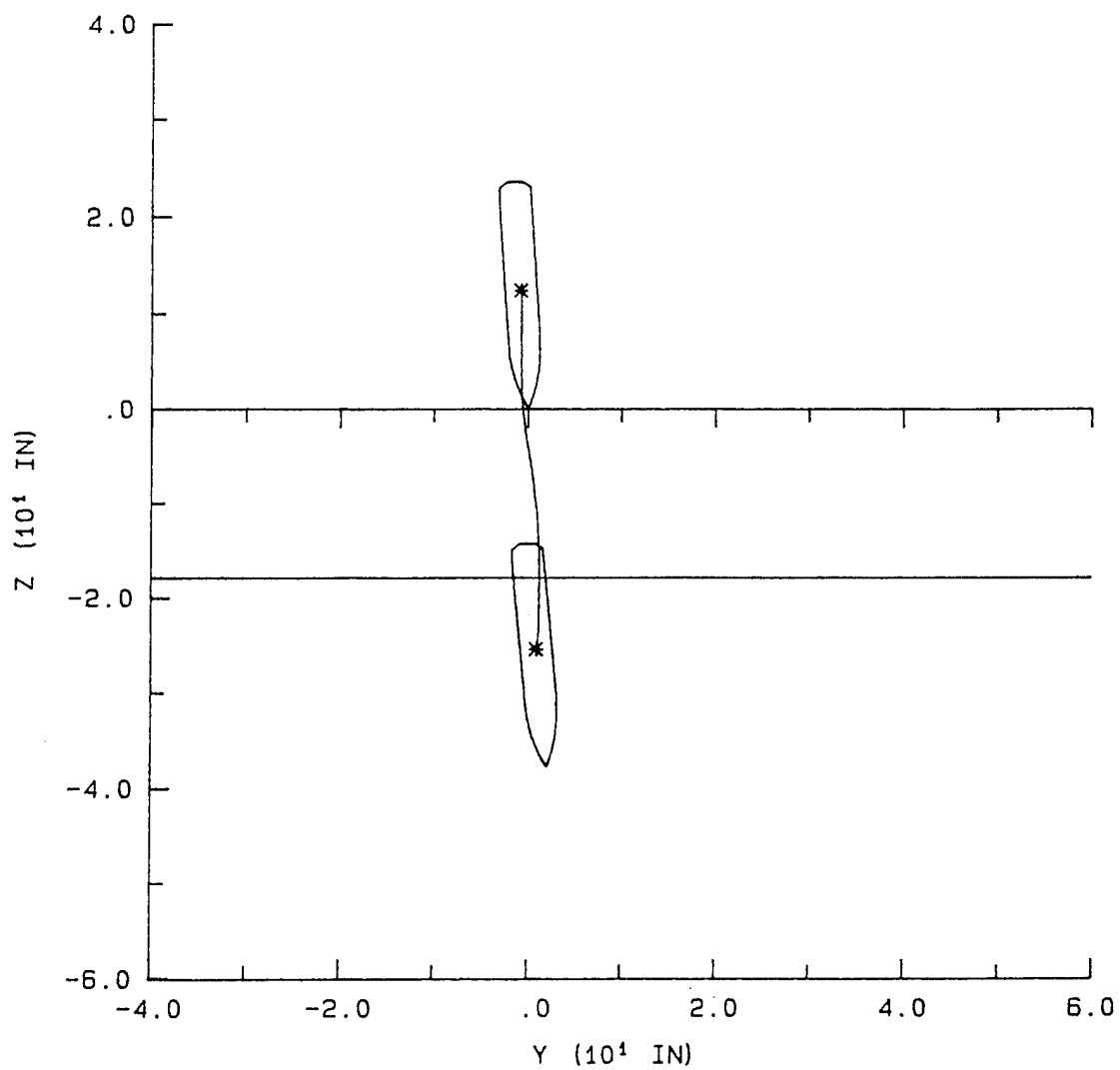


Figure 5. Plot of Projectile Penetration Depth at 4-degree Angle of Attack.

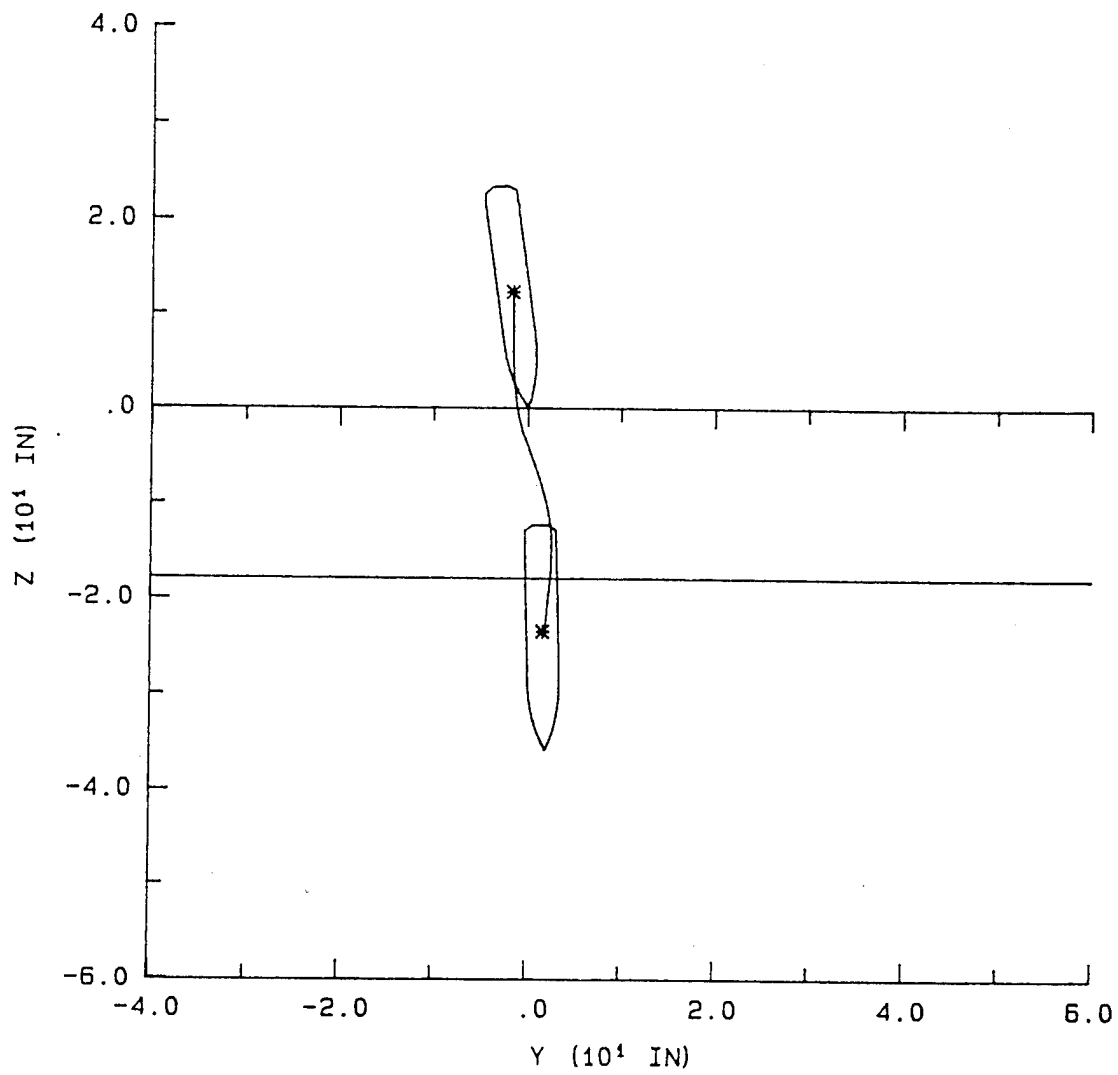


Figure 6. Plot of Projectile Penetration Depth at 8-degree Angle of Attack.

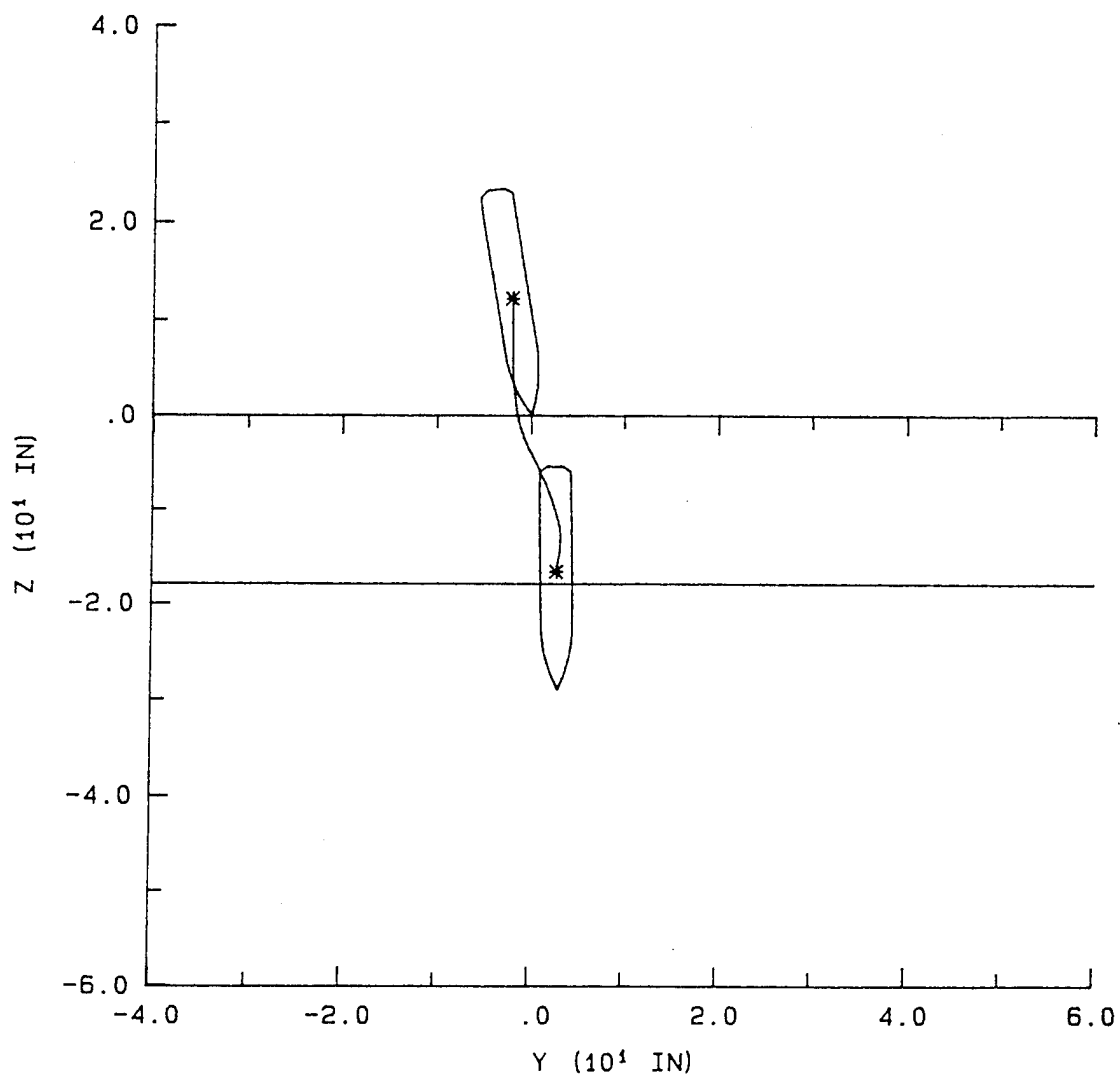


Figure 7. Plot of Projectile Penetration Depth at 10-degree Angle of Attack.

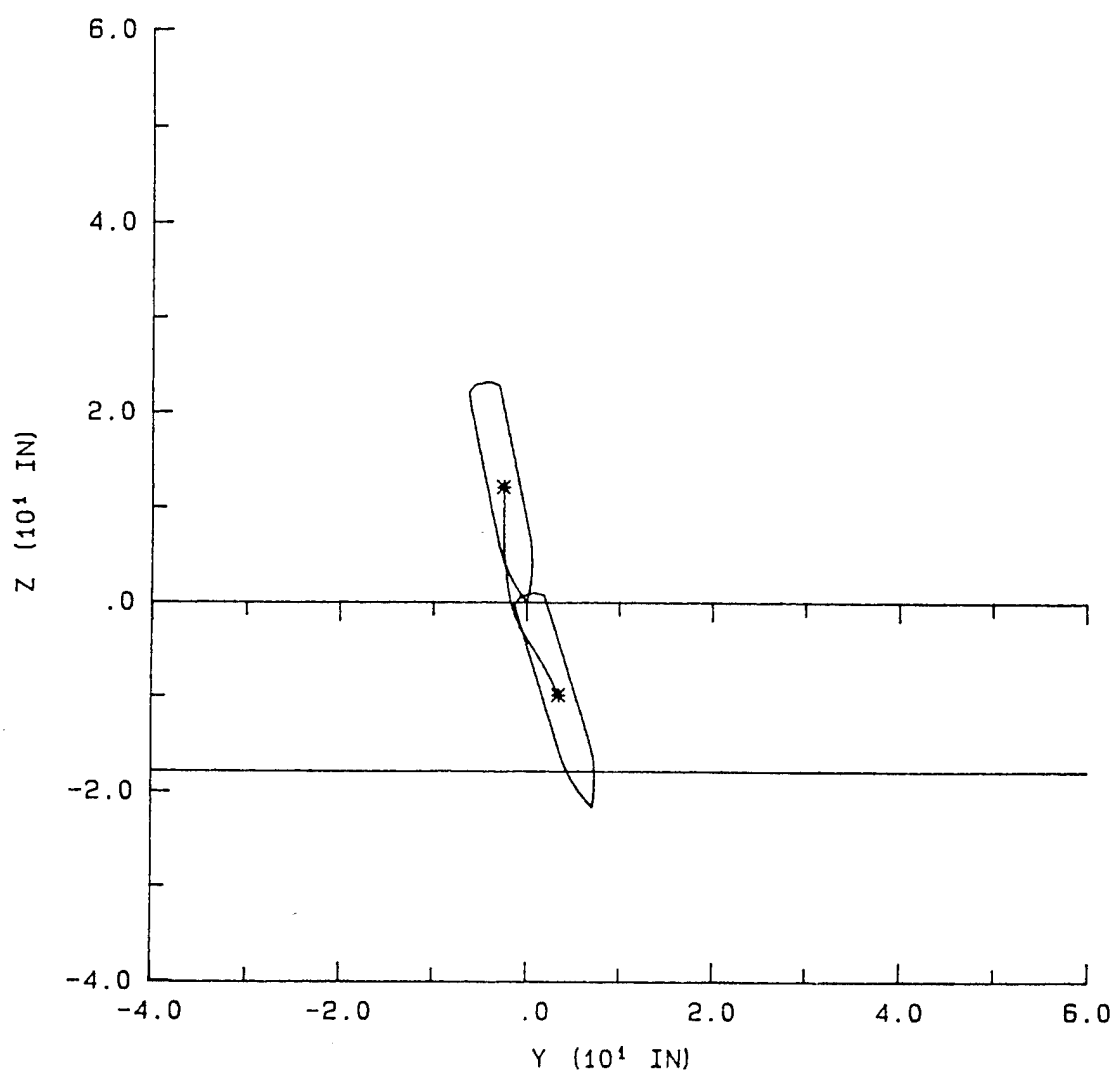


Figure 8. Plot of Projectile Penetration Depth at 12-degree Angle of Attack.

SECTION III

TEST SETUP

A. ANTIPENETRATION GUN FACILITY

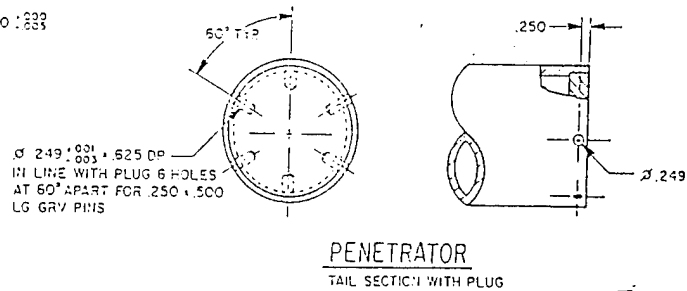
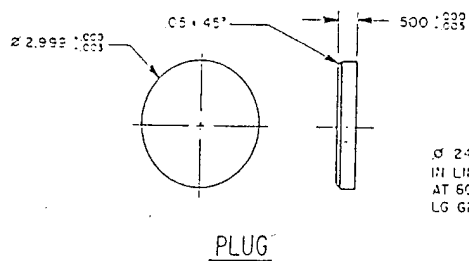
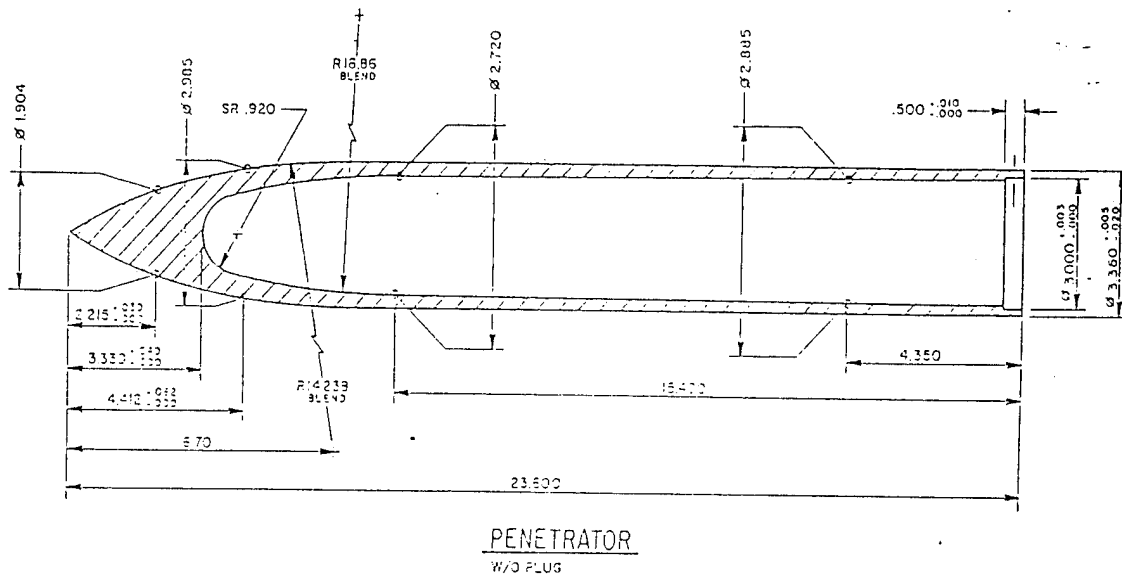
The antipenetration tests were conducted at the SKY X Structures and Pavements Test Area located at Tyndall AFB Florida. The gun facility consists of a Third-Generation Aircraft Shelter for housing the targets and data acquisition equipment, with a smooth bore 155 mm howitzer located at the entrance to the shelter to launch the projectiles.

The weapon being modeled is a generic design. The projectile's physical dimensions are shown in Figure 9. It is 23.6 inches long and 3.35 inches in diameter, with a body cavity to house an instrument package for in-flight telemetry, or an inert material to simulate the explosive charge. The case is forged from a single piece of 4130 steel. The projectile is propelled by an explosive charge placed in the breech of the howitzer. A sabot constructed of poly-isofoam holds the projectile centered in the barrel. A nylon pusher plug seals explosive gases generated for launching the projectile. Velocities can be varied by altering the weight of the propellant charge. The propellant charge consists of two materials. The base charge, which is 90 percent by weight of the total charge, is M3A1 Bulk Propellant. The initiating charge consists of Red Dot shotgun primer, which is 10 percent by weight of the total charge. The charge is initiated by an MK2 Percussion Primer and an electrically driven solenoid connected to the main firing system.

As the projectile exits the muzzle the sabot is stripped away, and the projectile passes through a series of screens to record its velocity as shown in Figure 10. Various recording devices are used to collect data; such as high-speed Photec 16 mm cameras, capable of 10,000 frames per second and a four-tube 300 KV Flash X-Ray unit, which provides orthogonal imagery.

Film rate for the high-speed cameras was set at 5000 frames per second, using Kodak Ektachrome Film SO-251, with an estar base. Triggering for the gun-firing sequence is initiated by the high-speed cameras. Once the film rate has reached 5000 frames per second, a signal is passed from the camera to the main firing circuit, and within milliseconds, the projectile is launched.

As the projectile passes through the last velocity screen attached to the face of the deflection grid, a signal is sent to the flash X-ray trigger unit, which incorporates a delay to fire the first set of X-ray tube heads as the projectile just exits the grid. The second set of tube heads fire 3.28 milliseconds later, x-raying the projectile prior to impacting the burster slab. The X-ray unit is charged to 220,000 volts for optimum performance. Film



• ALL DIMENSIONS GIVEN IN INCHES
SCALE: 1/3
UNLESS OTHERWISE SPECIFIED, LIMITS ARE .020

Figure 9. Schematic of Penetrator used in AFCEA Tests.

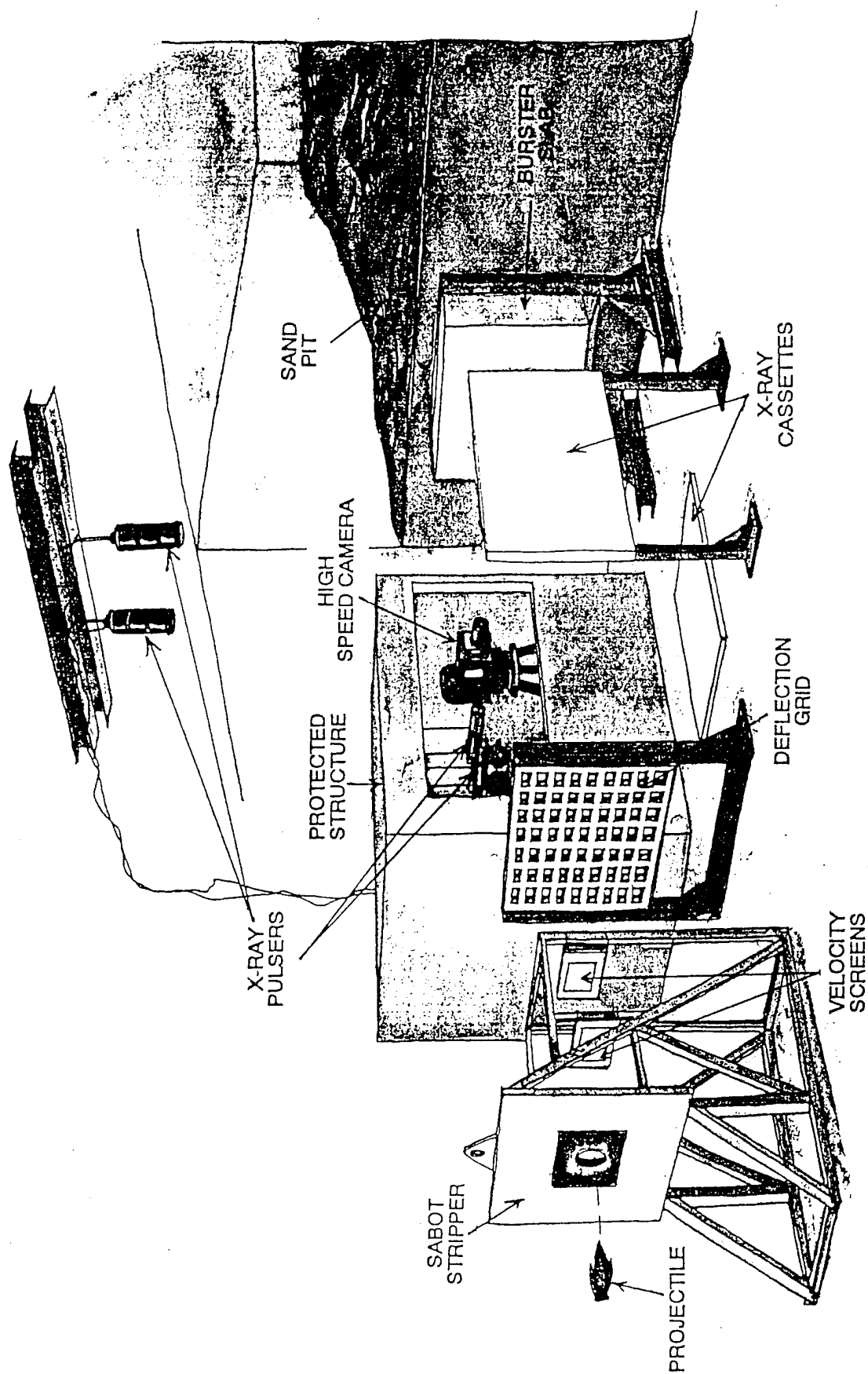


Figure 10. Equipment layout antipenetration laboratory

used for all tests consists of Kodak T-Mat H, using Lanex intensifying screens. Films are processed immediately after every test using a Kodak X-Omat 35 Medical X-Ray Processor. Once processed, angles are resolved from the orthogonal projections using the following formula:

θ = Resolved Angle

α = Angle measured from vertical view

β = Angle measured from horizontal view

$$\theta = \arccos \left[1 / \sqrt{ (1 / \cos^2 \alpha + 1 / \cos^2 \beta) - 1 } \right]$$

B. MATERIAL TEST LABORATORY

All material tests were conducted in the AFCESA Structural Materials Laboratory in the 9700 Area at Tyndall AFB Florida. Data on static compressive strength, flexural strength, and toughness were obtained with a Forney Static Compression Test Apparatus and a Forney System 2000 controller, Figure 11, capable of a maximum load of 400,000 lbs. The System 2000 controller is a digital display and microprocessor-controlled system comprised of a digital display, data input terminal and an RS-232C interface. The system monitors force generated by the test machine, computes test results, stores test data in memory, and transmits data through an RS-232C serial port to a 286-based personal computer. Information on load, deflection, and time are recorded for static compressive strength tests for cylinders and flexural tests for beams. Flexural tests were conducted using third point loading, with a 12 inch support span. Due to the presence of the nylon fibers, deflections were expected to be extremely high. To ensure accurate measurements, deflections for the beams were kept to .5 inches, so as not to exceed the linear range of the LVDT. Toughness indices for the flexural tests were calculated in accordance with ASTM C1018 and the Japanese Standard JCI-SF4 (Reference 6). In the ASTM standard, toughness indices I-5 and I-10 are calculated using deflections at 3δ and 5.5δ , where δ is the deflection at the first crack. These toughness indices are dimensionless numbers that represent the ratio of two areas under the load deflection curve. Another method for describing the energy absorbed a material in flexure is the Japanese Standard JCI-SF4,

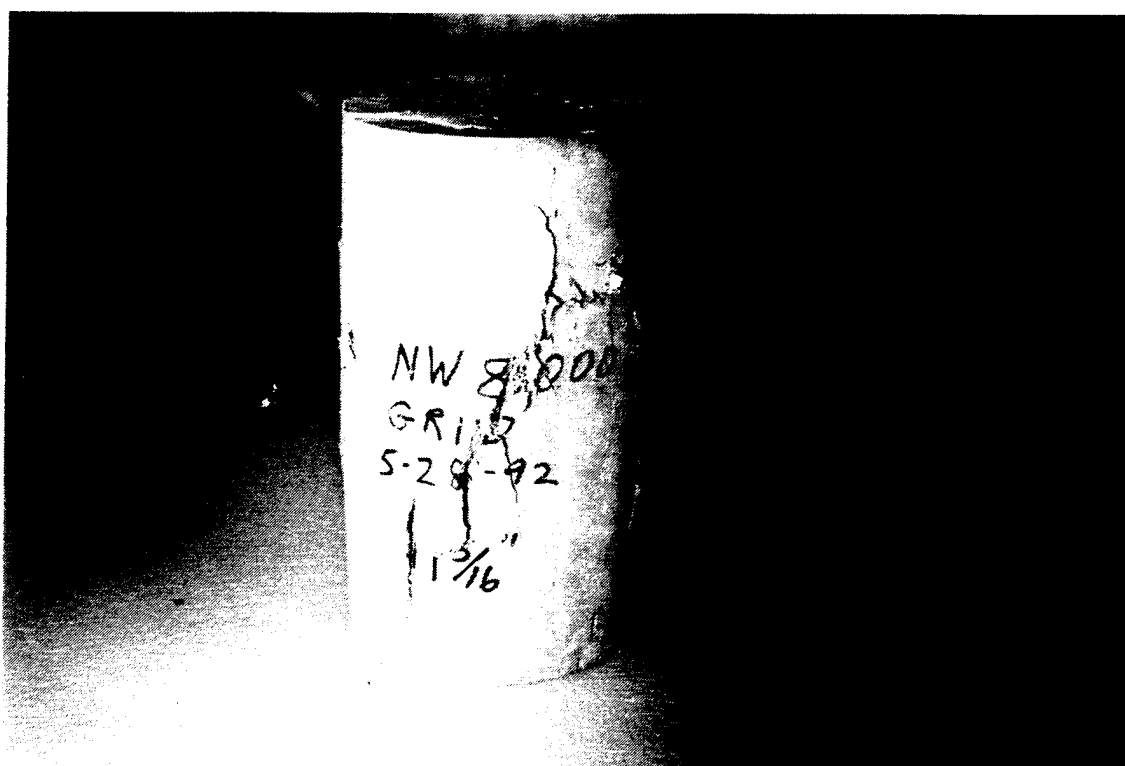
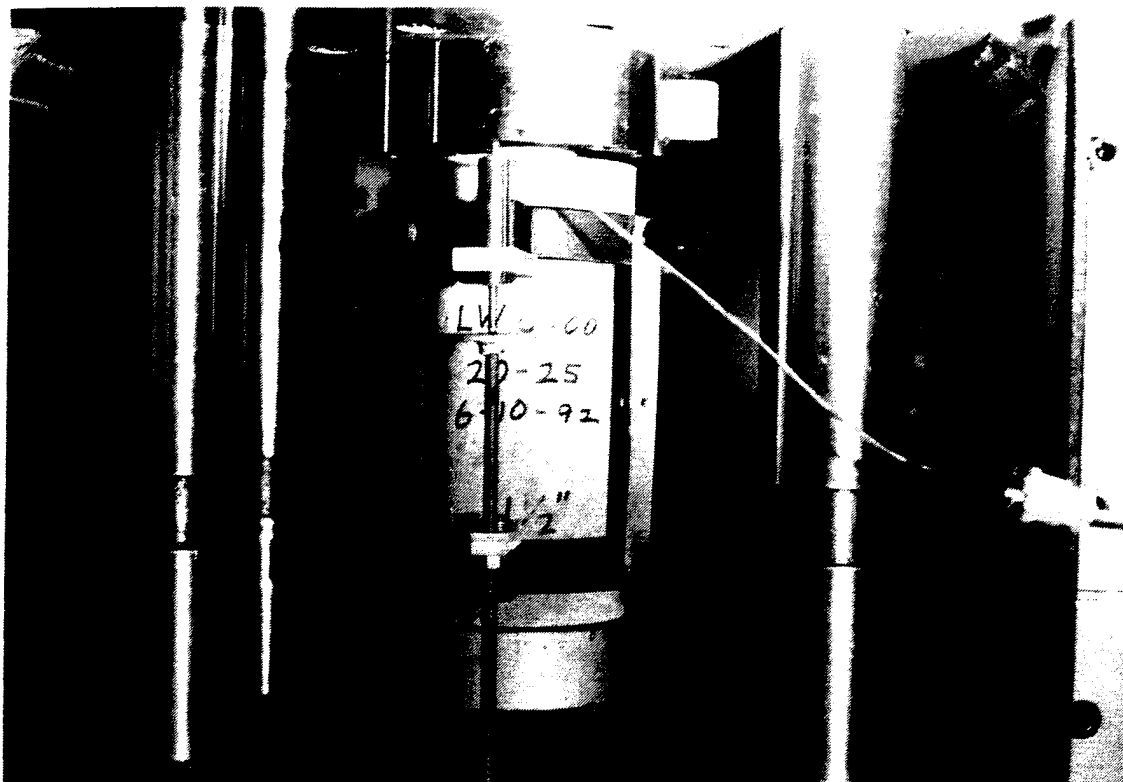


Figure 11. Pretest and Posttest Photographs of Static Compression Tests.

which calculates the area under the curve up to the deflection equal to 1/150 of the span. This yields a value in inch-pounds, and is a reliable indicator of absorbed energy. For the compressive strength tests, a Chinese standard test method was implemented, in which the critical load point of 85 percent of the ultimate load replaces the first flexural crack point in defining the compressive toughness index (Reference 7). This method was selected because ASTM has no method for determining the toughness index for a cylinder in static compression. Durability tests were conducted using a Logan Freeze-Thaw Chamber with periodic measurement of sonic velocity, using a James Electronics V-Meter Model C-4899.

SECTION IV TEST PROGRAMS

A. INTRODUCTION

The following section discusses the FY 91 and FY 92 deflection grid test programs. The FY 91 test program was an exploratory experimental effort to determine the effect of perforated concrete slab sections on the stability of an advanced penetrating weapon. This effort, in its early stages, focused on the geometry of the concrete deflection grid, and the influence of compressive strength. Due to a wide variance in projectile rotational rates, and the catastrophic damage to the deflection grids at high compressive strengths, steel and nylon fibers were added to the mix designs. Burster slabs were not incorporated into the tests until FY 92, since observation of the projectile's induced rotation was the objective of the FY 91 tests. The projectile was allowed to travel freely for 20 feet after striking the deflection grid, to obtain sufficient high speed photography of the event. Based on the FY 91 test results, the FY 92 test program systematically varied deflection grid and burster slab configuration parameters to obtain response data from which to develop an antipenetration system design procedure. For each fiscal year program, the test schedule, test item configuration, material properties, and field test results are presented.

B. FY 91 TEST PROGRAM

1. Test Schedule

A test matrix was developed to determine the effects of geometry, compressive strength, impact angle, amount of steel reinforcement, and fibers. Table 1 shows the test schedule.

2. Test Item Configuration

Molds for three geometric deflection grid patterns were constructed from marine grade plywood. Grid type 01 was a square hole perforation design as shown in Figure 12. Grid type 02 was a staggered circular hole configuration to accommodate a higher percentage of reinforcing steel as shown in Figure 13. Grid type 03, shown in Figure 14, was a waffle style design which eliminated the grid perforations, reduced the amount of steel reinforcement, and reduced the deflection grid thickness to four inches. Simplicity of construction was a major factor in these earlier designs, to minimize labor and construction costs for the full-scale systems.

TABLE 1. FY91 ANTIPENETRATION DEFLECTION GRID TEST MATRIX

TEST NO.	GRID TYPE	CONCRETE MIX DESIGN VALUES						IMPACT ANGLE, deg
		f'c, psi		STANDARD REBAR	REINFORCEMENT TYPE		FIBERS	
					NYLON	STEEL		
		4,000	8,000					
1	01	X		X			0	
2	01	X		X			0	
3	01	X		X			0	
4	01	X		X			30	
5	01	X		X			30	
6	01	X		X			45	
15	01	X		X			0	
16	01	X		X			0	
17	01	X		X			0	
18	01	X		X			45	
25	01	X	X			X	0	
26	01		X			X	0	
36	01		X			X	0	
30	01		X	X		X	30	
31	01		X	X		X	30	
32	01		X	X		X	30	
33	01		X	X		X	45	
37	01		X	X		X	0	
7	02		X	X			45	
8	02		X	X			0	
9	02		X	X			0	
13	02		X	X			0	
20	03		X		X		0	
22	03		X		X	X	0	
27	03		X			X	0	
28	03		X			X	0	

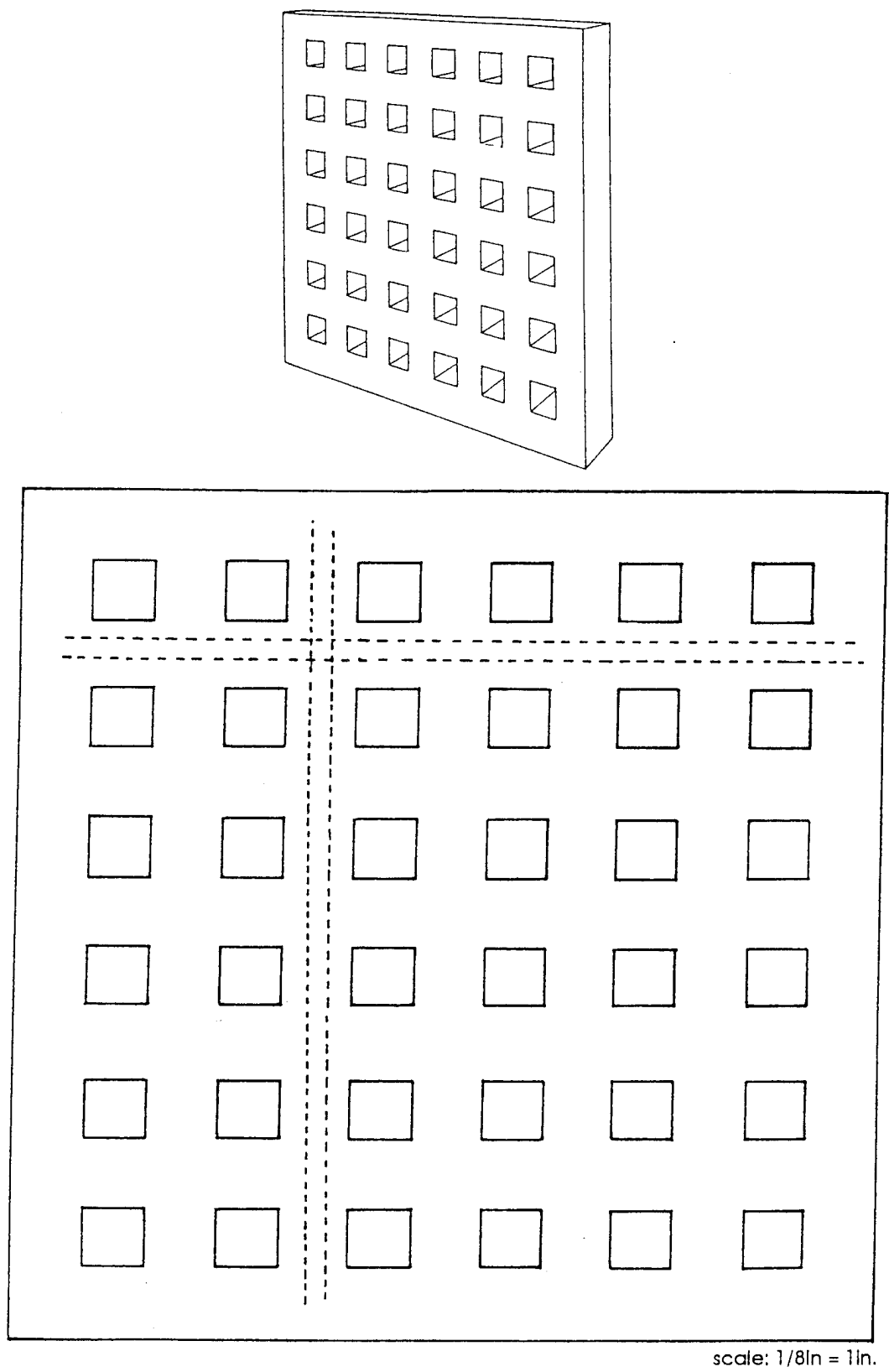


Figure 12. Deflection Grid Type 01.

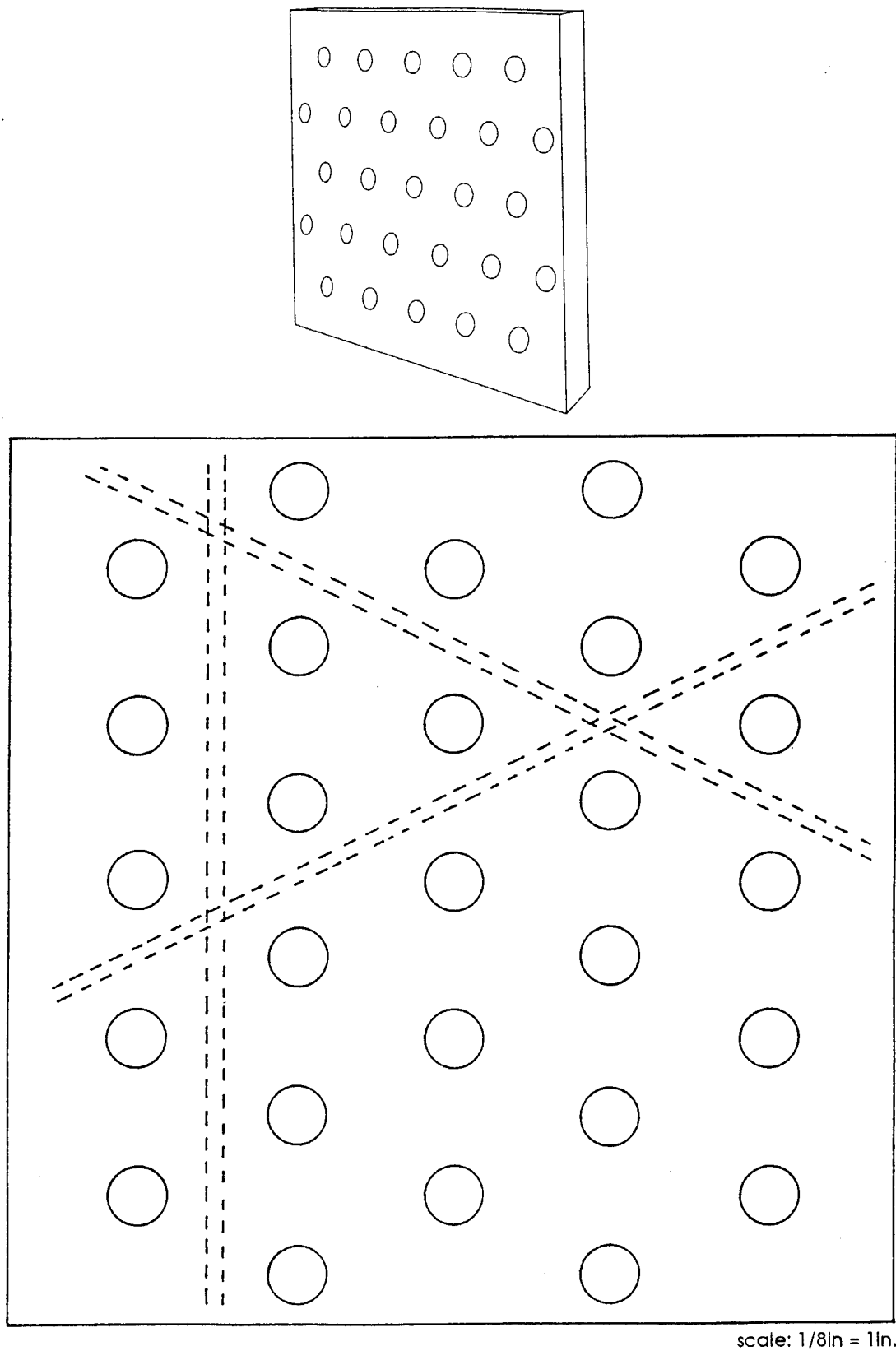
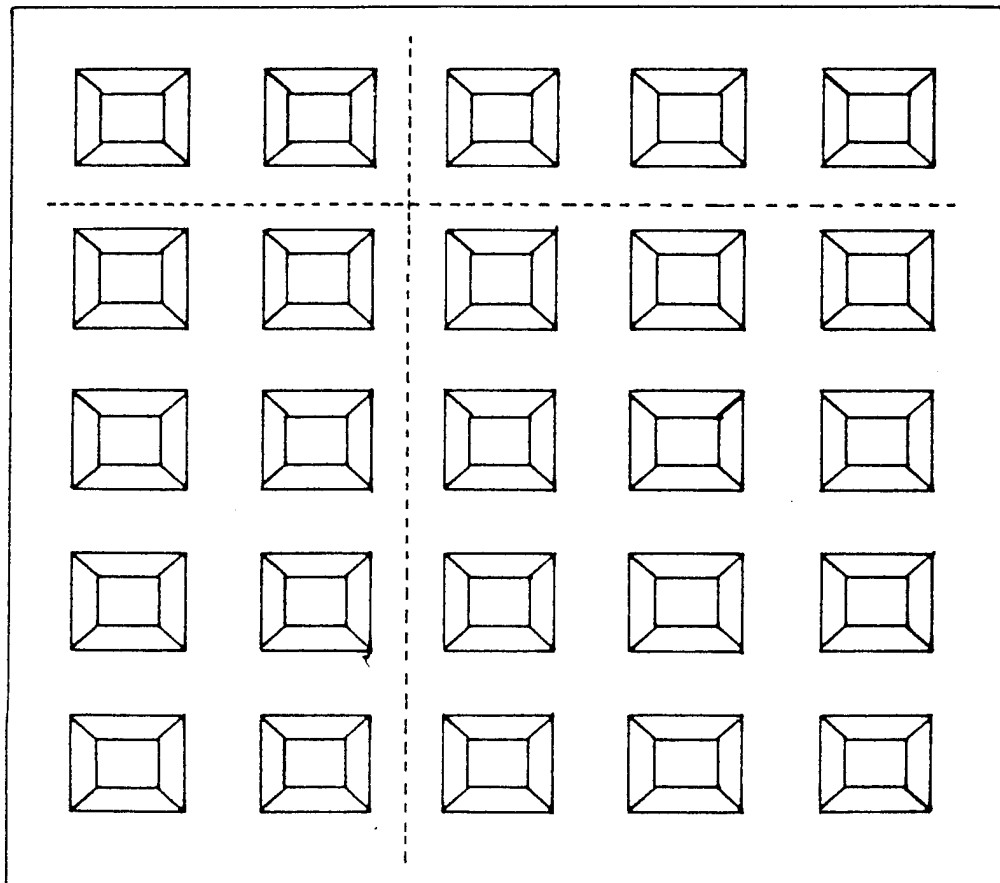
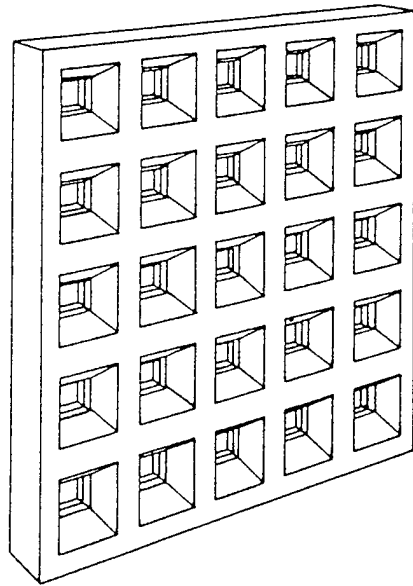


Figure 13. Deflection Grid Type 02.



scale: 1/8in = 1in.

Figure 14. Deflection Grid Type 03.

3. Material Properties

To achieve the target compressive strengths shown in the test matrix, four mix designs were developed. Low strength is classified as 4,000 psi and high strength as 8,000 psi. Designs for the mixes had the following material quantities per cubic yard:

Low Strength

<u>Material</u>	<u>Quantity/CY</u>
Type I Portland Cement	588 lb
Coarse Aggregate (1)	1790 lb
Fine Aggregate (2)	1146 lb
Water	352 lb

High Strength

<u>Material</u>	<u>Quantity/CY</u>
Type I Portland Cement	760 lb
Coarse Aggregate (1)	1400 lb
Fine Aggregate (2)	1150 lb
Force 10,000 (3)	7 gal
Water	295 lb

High Strength with Nylon Fibers

<u>Material</u>	<u>Quantity Lbs/CY</u>
Type I Portland Cement	789 lb
Coarse Aggregate (1)	1,870 lb
Fine Aggregate (2)	972 lb
Force 10,000 (3)	7.9 gal
Nylon Fibers (4)	10 lb
Water	260 lb
WRDA-79 (5)	90 fl oz

High Strength with Steel Fibers

<u>Material</u>	<u>Quantity Lbs/CY</u>
Type I Portland Cement	752 lb
Coarse Aggregate (1)	1,330 lb
Fine Aggregate (2)	1,440 lb
Force 10,000 (3)	7.5 gal
Water	195 lb
1" Carbon Steel Fibers	80 lb

Notes:

- (1) Limestone Coarse Aggregate (SSD), .75 inch maximum size
- (2) Silica Sand (SSD), 2.07 Fineness Modulus
- (3) W.R. Grace Force 10,000 Slurry @ 1 gallon/100 lb of cement
- (4) .75 inch Nycon Nylon Fibers
- (5) W.R. Grace Water Reducer/Retarder

4. Field Test Results

Table 2, contains data on the tests conducted in FY 91, including shot number, impact angle, exit angle out of the grid, rotation rate in degrees per body length of travel, total yaw at three body lengths of travel, and remarks on the material composition of the deflection grid.

TABLE 2. FY 91 DEFLECTION GRID TEST DATA

Shot No.	Impact Angle degrees	Exit Angle degrees	Yaw Rate DBLT	Total Yaw degrees	Remarks
1	0	6.0	10.5	27	SH/DR/LS
2	0	7.5	6.2	19.9	SH/DR/LS
3	0	8.0	3.7	15.4	SH/DR/LS
4	30	11.0	8.9	28.8	SH/DR/LS
5	30	21.0	4.4	29.8	SH/DR/LS
6	45	.2	3.7	7.6	SH/DR/LS
15	0	6.8	2.9	12.7	SH/DR/LS
16	0	6.4	1.5	9.4	SH/DR/LS
17	0	14.2	2.5	19.1	SH/DR/LS
18	45	11.1	3.4	17.9	SH/DR/LS
25	0	7.7	5.2	18.5	SH/NR/HS/NF
26	0	6.2	7.4	21.0	SH/NR/HS/NF
36	0	2.9	.7	4.3	SH/NR/HS/NF
30	30	7.0	3.9	14.9	SH/SR/HS/NF
31	30	11.0	4.9	20.8	SH/SR/HS/NF
32	30	4.3	4.6	13.6	SH/SR/HS/NF
33	45	8.2	6.6	21.5	SH/SR/HS/NF
37	0	2.5	1.8	6.2	SH/SR/HS/NF
7	45	6.5	8.2	22.9	RH/DR/LS
8	0	7.5	5.4	18.3	RH/DR/LS
9	0	0	5.7	11.4	RH/DR/LS
13	0	14.3	7.7	28.9	RH/DR/LS
20	0	1.8	.5	2.9	WT/SR/HS/SF
22	0	3.5	1.5	6.6	WT/SR/HS/SF
27	0	5.7	5.5	16.7	WT/NR/HS/NF
28	0	5.7	5.3	16.3	WT/NR/HS/NF

Remarks:

SH - Square hole grid design

RH - Round hole grid design

WT - Waffle style grid design

DR - Double layer of reinforcement steel

SR - Single Layer of reinforcement steel

NR - No steel reinforcement

LS - Low compressive strength mix design (3500psi to 4500psi)

HS - High compressive strength mix design (7500psi to 8500psi)

NF - Nylon fibers

SF - Steel Fibers

C. FY 92 TEST PROGRAM

1. Test Schedule

Based on observations during the FY91 program, a test matrix was developed to investigate the effects of geometry, density, and compressive strength for a series of eighteen experiments, as shown in Table 3. Four densities and two compressive strengths were selected, resulting in six concrete mix designs. Initially, strike points were selected at locations that would produce conservative rotation rates, with all shots conducted at normal impact.

2. Test Item Configuration

The test matrix shows three grid types tested for the FY 92 program. To conserve materials and reduce the test specimen weight, the grid dimensions were reduced to three foot square, with a thickness of four inches. Reinforcing steel was reduced to a single layer of #3 rebar. Figure 15 shows the details of Grid Type 16, named for the number of perforations. Figure 16 shows Grid Type 20 with rectangular openings in an offset pattern to enhance irregular fracture lines upon impact. This design had the least volume of all six geometries. Figure 17 shows Grid Type 25 which still maintains the same size hole perforation but has a reduction in spacing. The purpose was to retain the symmetry but decrease the mass in the web areas. Actual photographs of the three geometries prior to testing are shown in Figures 18 through 20.

3. Material Properties

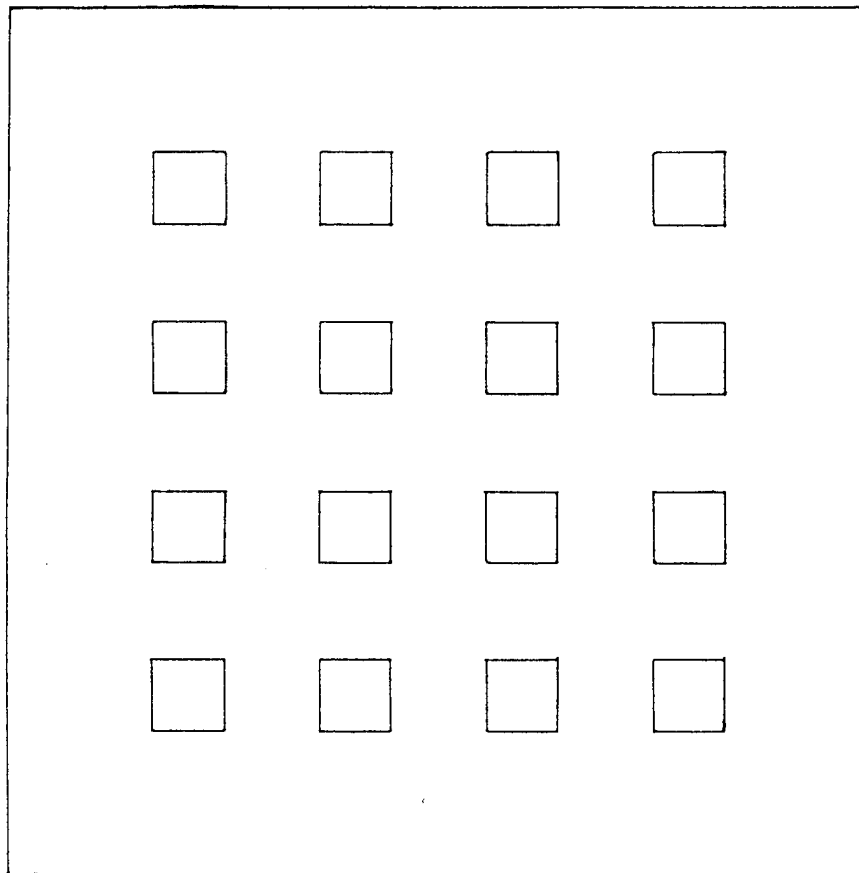
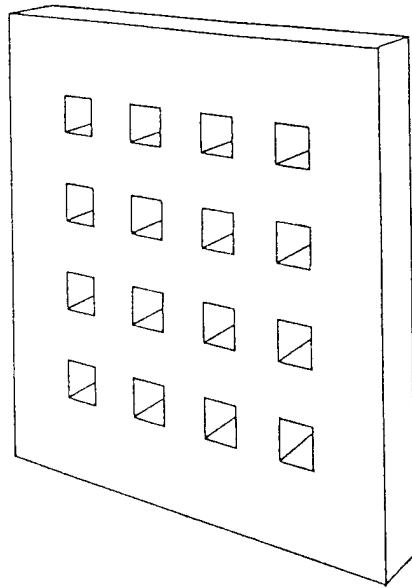
Six concrete mixes were designed to achieve the target values in the test matrix. To maintain precise control during construction of the deflection grids, a single rubber mold was cast for each geometry type, and concrete mixes were poured in batches of three. The two light weight mixes were designed for a unit weight of 110 pcf and a static compressive strength of 4,000 and 8,000 psi, designated LW4000 and LW8000, respectively. Designs for the two mixes had the following material quantities per cubic yard:

LW4000

<u>Material</u>	<u>Quantity/CY</u>
Type I Portland Cement	640 lb
Solite aggregate	837 lb
Sand	1226 lb
WRDA-79	30 oz
Nylon Fibers	10 lb
Water	365 lb

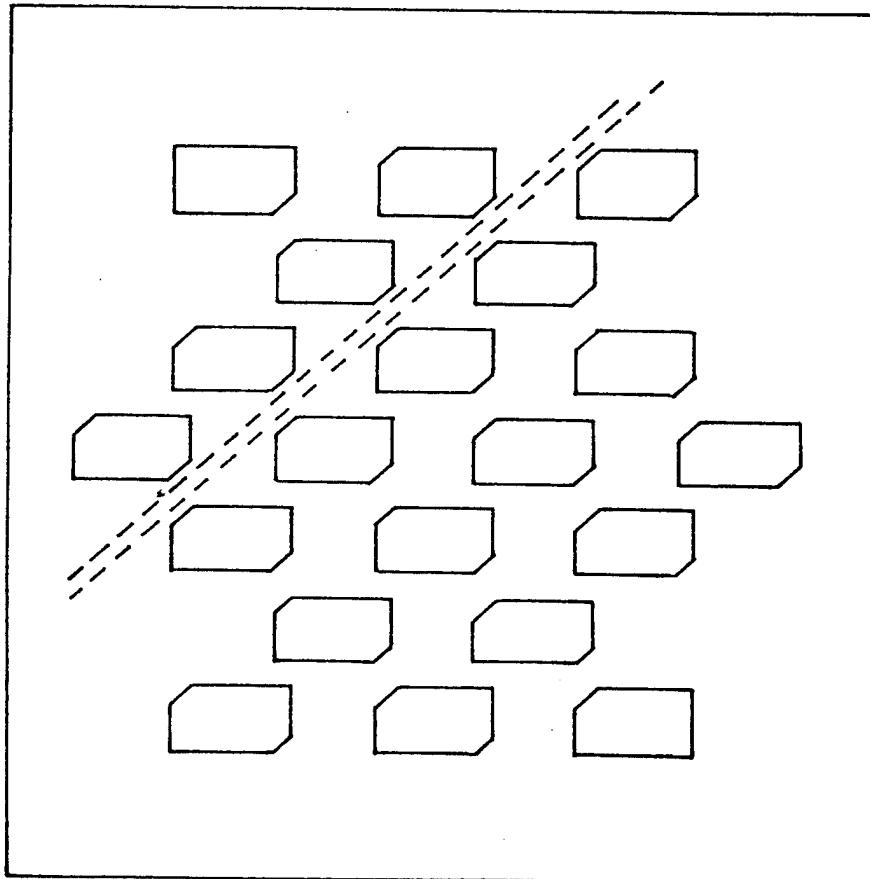
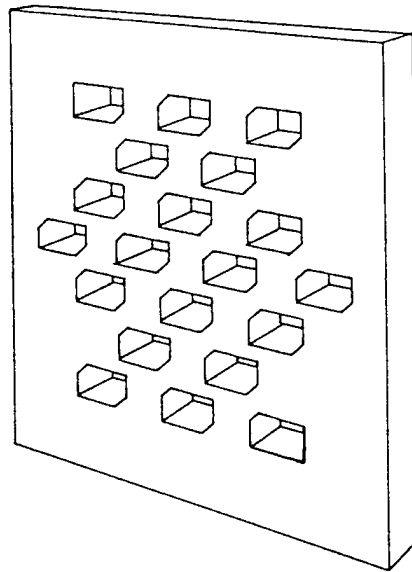
TABLE 3. FY92 ANTIPENETRATION DEFLECTION GRID TEST MATRIX

TEST NO.	GRID TYPE	CONCRETE MIX DESIGN VALUES					
		UNIT WEIGHT, pcf				f'c, psi	
		110	150	210	325	4,000	8,000
47	16	X				X	
42	16	X					X
53	16		X			X	
49	16		X				X
54	16			X	X		X
40	16						
45	20						
41	20	X				X	X
52	20	X				X	
50	20						X
55	20			X			X
39	20				X		X
46	25						
43	25	X				X	X
51	25	X					
48	25						X
44	25			X			X
38	25				X		X



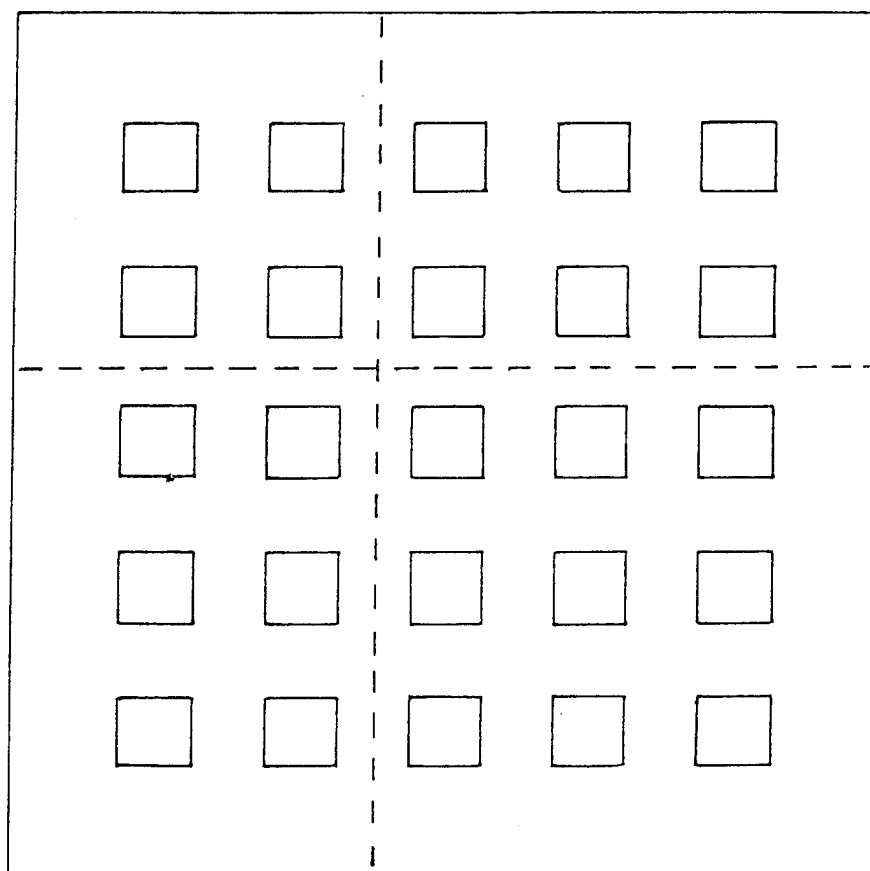
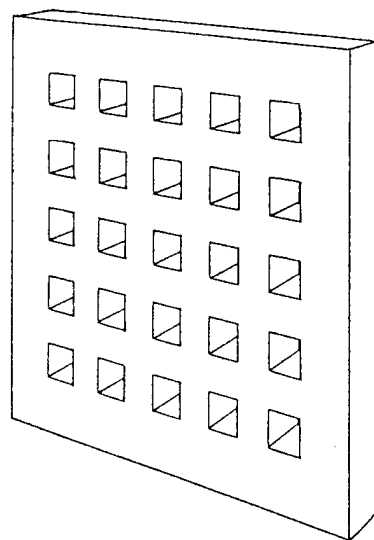
scale: $1/8\text{in} = 1\text{in}$.

Figure 15. Deflection Grid Type 16.



scale: 1/8in = 1in.

Figure 16. Deflection Grid Type 20.



scale: 1/8in = 1in.

Figure 17. Deflection Grid Type 25.

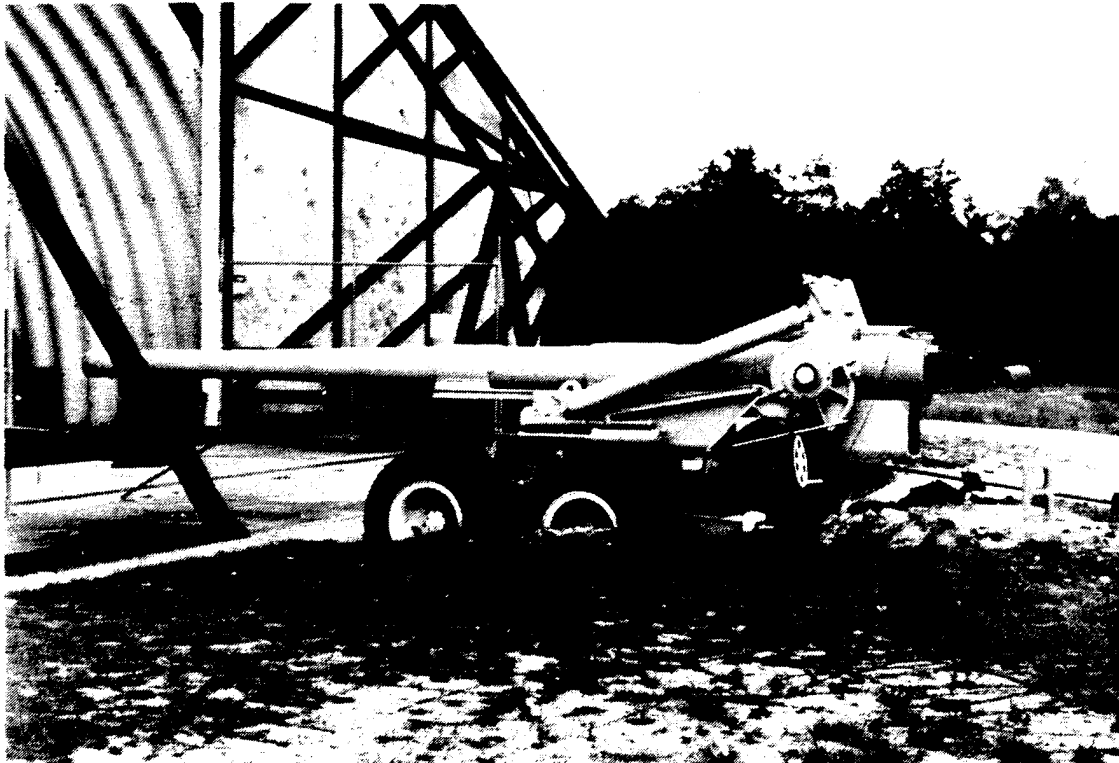


Figure 18. Pretest Photographs of 155 mm Howitzer and Grid Type 20.

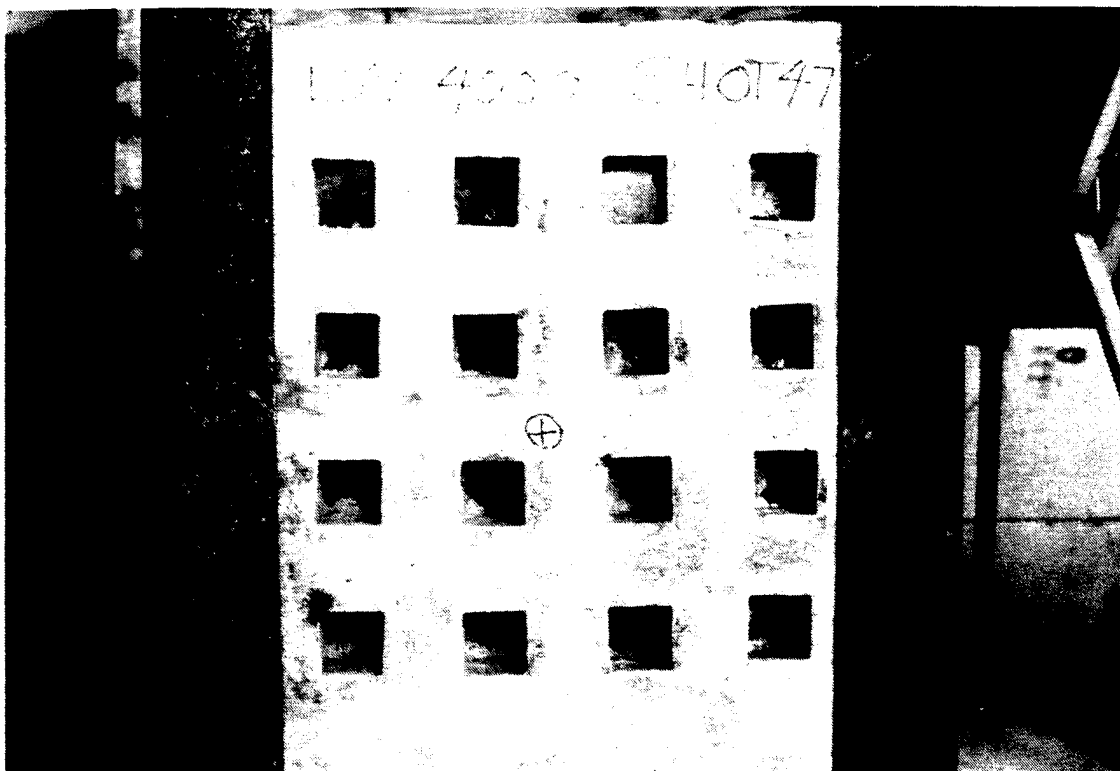


Figure 19. Pretest Photograph of Grid Type 16.

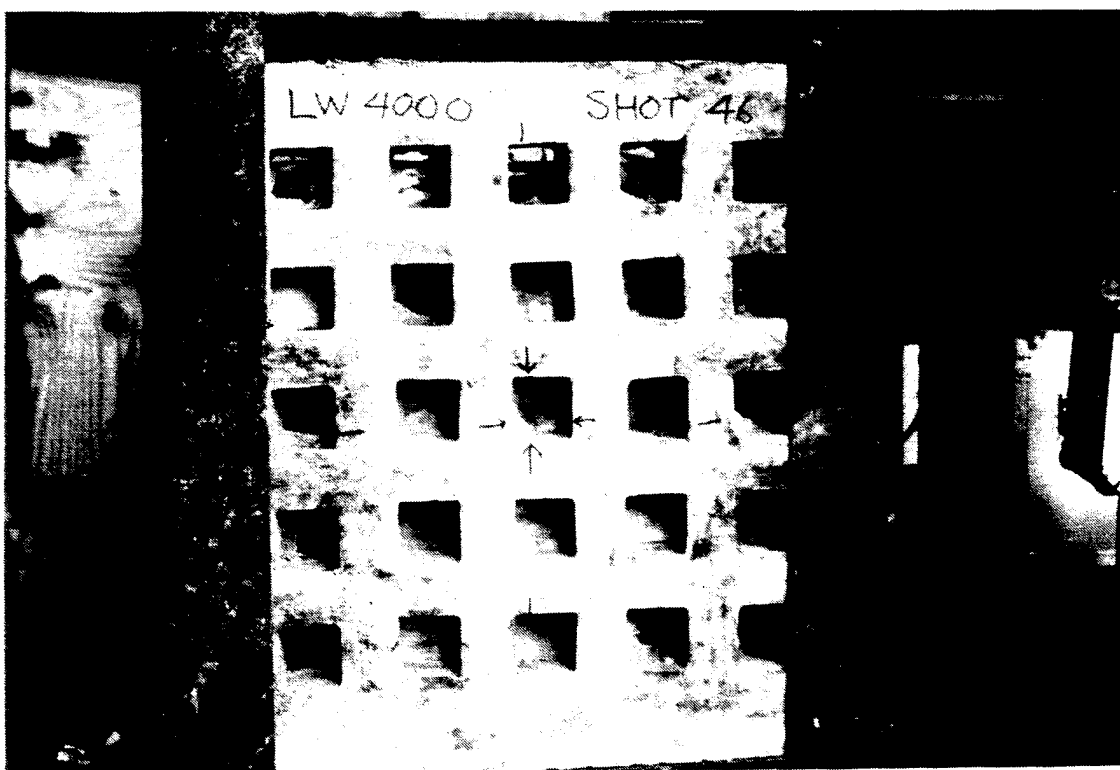


Figure 20. Pretest Photograph of Grid Type 25.

LW8000

<u>Material</u>	<u>Quantity/CY</u>
Type I Portland Cement	940 lb
Solite aggregate	1100 lb
Sand	1110 lb
Force 10,000	215 lb
WRDA-79	50 oz
Nylon Fibers	10 lb
Water	210 lb
WRDA-19 (1)	55 oz

Notes:

(1) W.R. Grace Superplastisizer @ 6oz per 100 pounds of cement

Results of laboratory tests conducted on an LW4000 6 inch by 12 inch cylinder yielded a maximum load of 94,648 pounds, as shown in Figure 21. The cylinder held together throughout the test. Visual cracks as wide as 1/4 inch were observed, but with no catastrophic failure. A flexural test was conducted on an LW4000 beam at an initial deflection rate of .00024 in/sec as shown in a Figure 22. Figure 23 shows the flexural load-deflection relationship and toughness indices for the same beam, computed in accordance with ASTM and JCI standards. Results of the LW8000 cylinder test showed a maximum compressive load of 159,392 pounds, which equated to 5,639 psi compressive strength, well short of the desired 8,000 psi. Figures 24 and 25 show a 50 percent increase in absorbed energies over the LW4000 cylinder and beam.

The design mixes for the normal weight concrete were to achieve a unit weight of 150 pcf, and compressive strengths of 4,000 and 8,000 psi, and are designated NW4000 and NW8000 respectively. Designs for these mixes had the following material quantities per cubic yard:

NW4000

<u>Material</u>	<u>Quantity/CY</u>
Type I Portland Cement	609 lb
Limestone (3/4 inch)	1850 lb
Sand	1116 lb
Nylon Fibers	10 lb
WRDA-79 (5oz/100lb)	30 oz
Water	335 lb

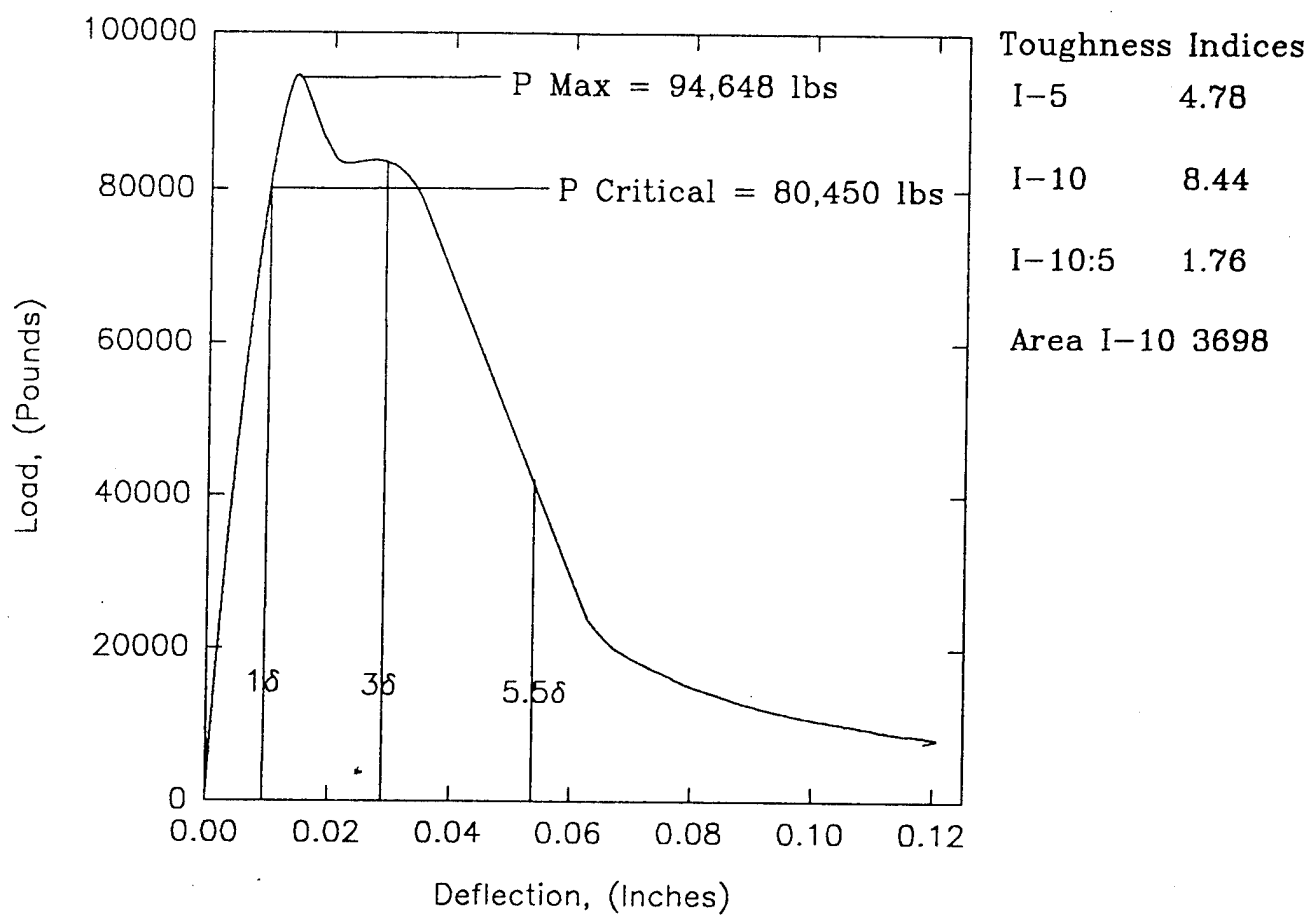


Figure 21. Load versus Deflection Curve for LW4000 6" by 12" Cylinder Static Compressive Strength Test.

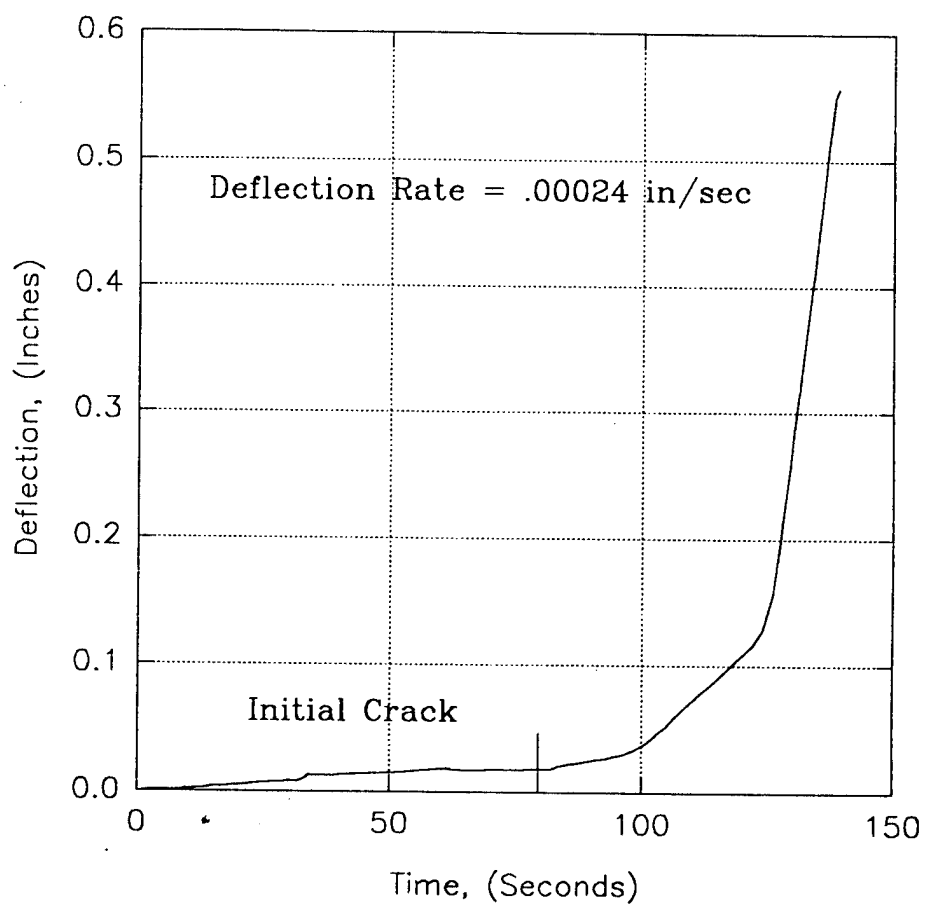


Figure 22. Deflection versus Time Curve for LW4000 Flexural Beam Test.

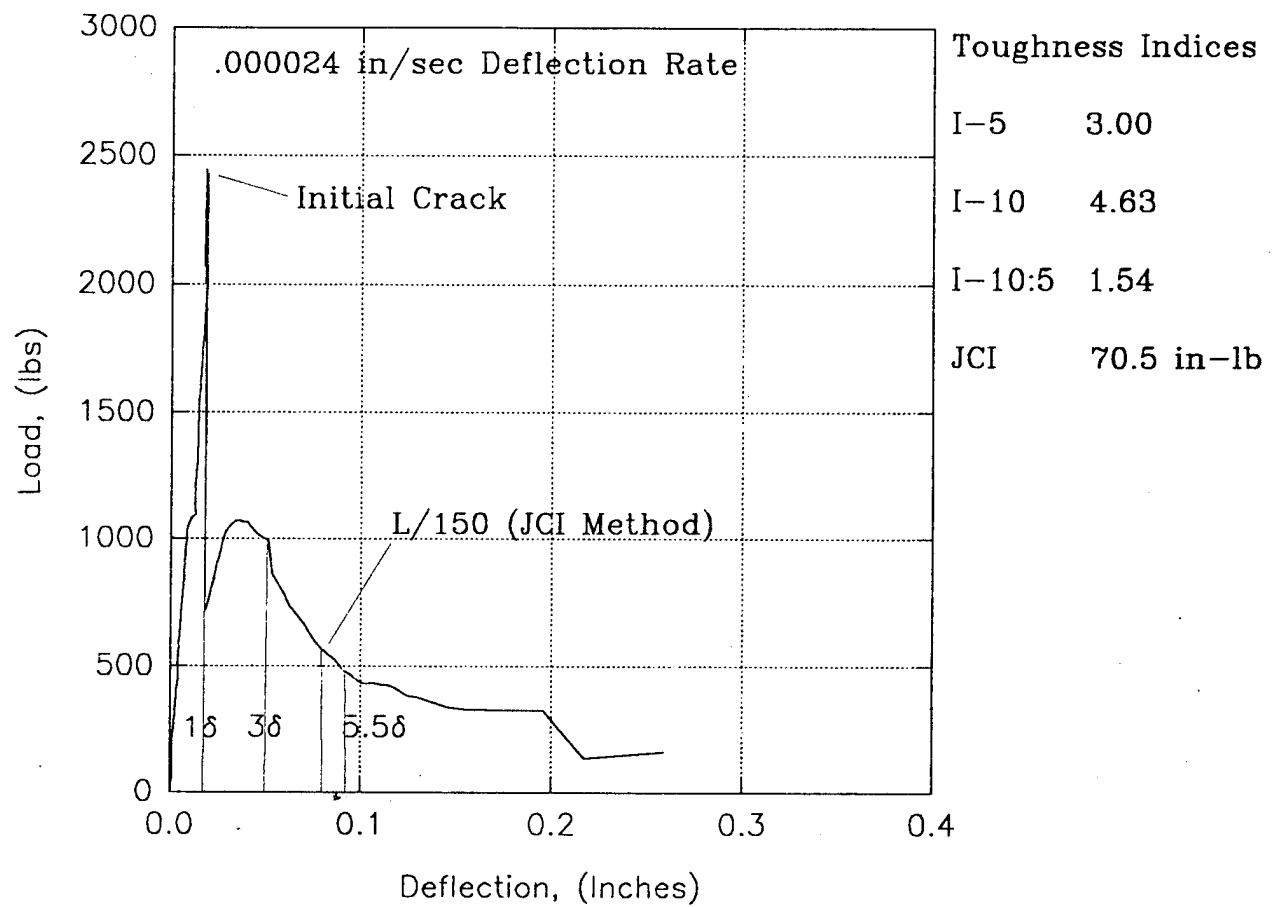
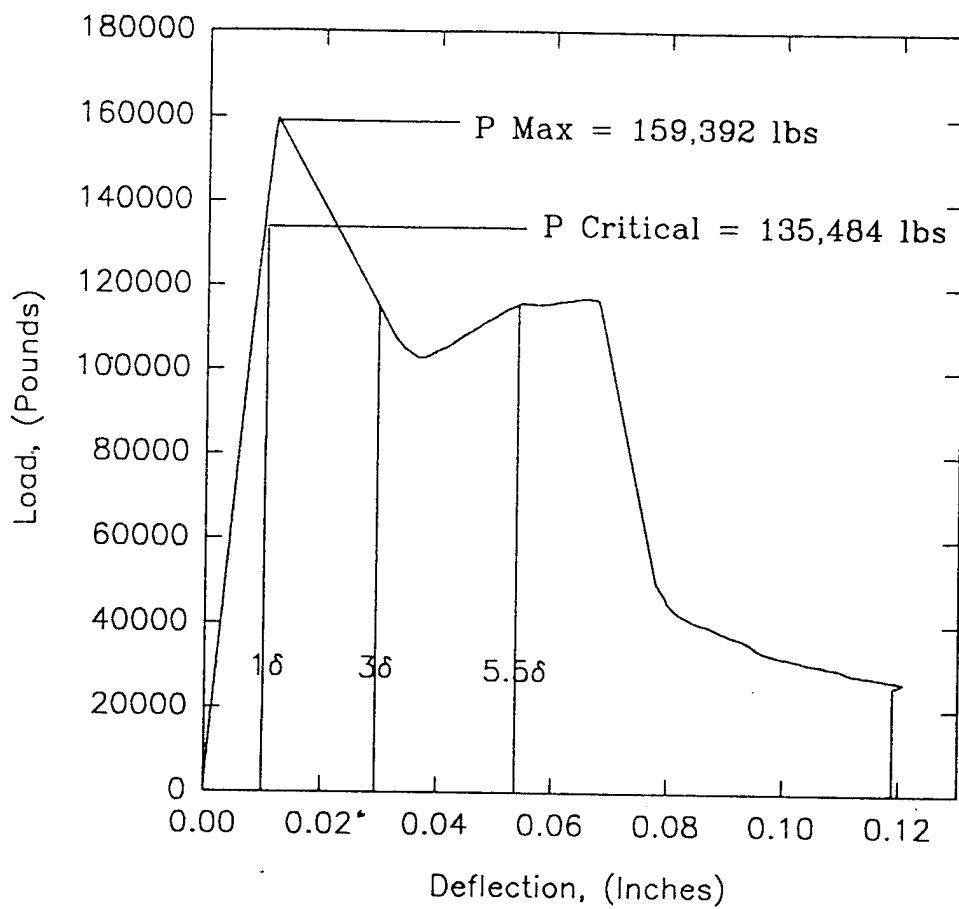


Figure 23. Load versus Deflection Curve for LW4000 Flexural Beam Test.



Toughness Indices

I-5 4.98

I-10 8.90

I-10:5 1.78

Area I-10 6057

Figure 24. Load versus Deflection Curve for LW8000 6" by 12" Cylinder Static Compressive Strength Test.

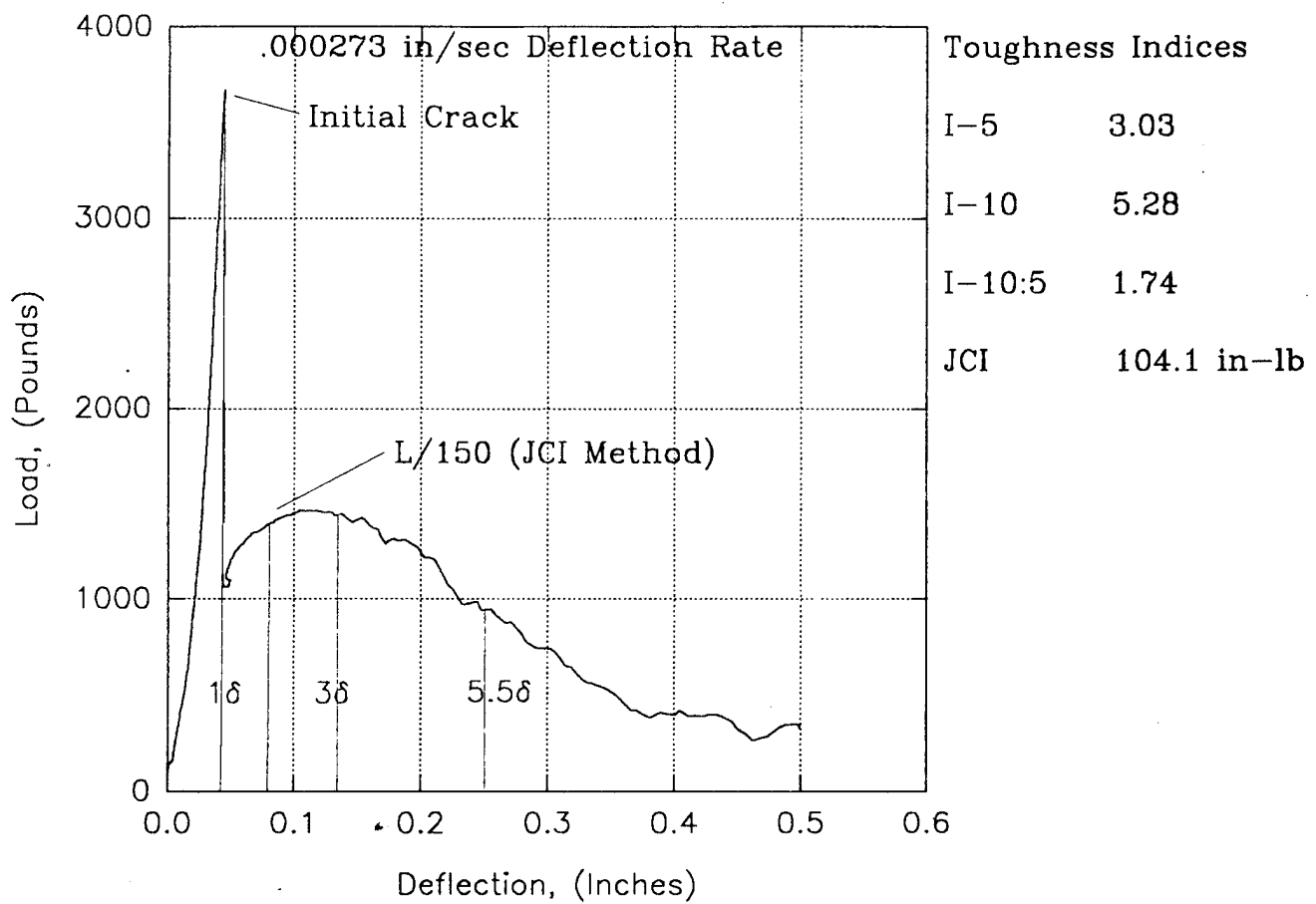


Figure 25. Load versus Deflection Curve for LW8000 Flexural Beam Test.

NW8000

<u>Material</u>	<u>Quantity/CY</u>
Type I Portland Cement	752 lb
Limestone (3/4 inch)	1790 lb
Sand	1145 lb
Nylon Fibers	10 lb
WRDA-79	40 oz
WRDA-19	45 oz
Water	300 lb

Figure 26 shows a peak load of 151,288 pounds for the NW4000 cylinder, resulting in a 5,351 psi static compressive strength. Figure 27 shows the load-deflection curve for a standard flexural test on an NW4000 beam, using an initial deflection rate .000177 in/sec, which yielded a JCI toughness index of 135.2 in-lb. The NW8000 cylinder load-deflection curve in Figure 28 showed a sharp drop at ultimate load due to a malfunction in the LVDT. Compressive strength was exceptionally high at 9,853 psi. The NW8000 flexural test yielded a small increase in toughness over the NW4000 flexural test as shown in Figure 29.

The design of the 210 pcf unit weight weight mix, was limited to a single compressive strength, due to the nature of the design. A compressive strength of 8000 psi was desired, and designated HDM for high density mortar. The mix design is based on a standard 94-pound sack of cement.

HDM

<u>Material</u>	<u>Quantity/sack</u>
Type I Portland Cement	94 lb
Hematite SN	400 lb
WRDA-79	5 oz
WRDA-19	12 oz
Nylon Fibers	15 oz
Water	42 lb

Figure 30 shows an ultimate load for an HDM cylinder of 170,418 lb, for a compressive strength of 6,028 psi. Workability of the mix was acceptable, and good consolidation of the materials was obtained. Figure 31 shows a JCI toughness value of 143.1 in-lb at a deflection rate of .000192 in/sec.

To reach a unit weight of 325 pcf it was necessary to use graded steel slag. The mix design was designated VHDM for very high density mortar. The following

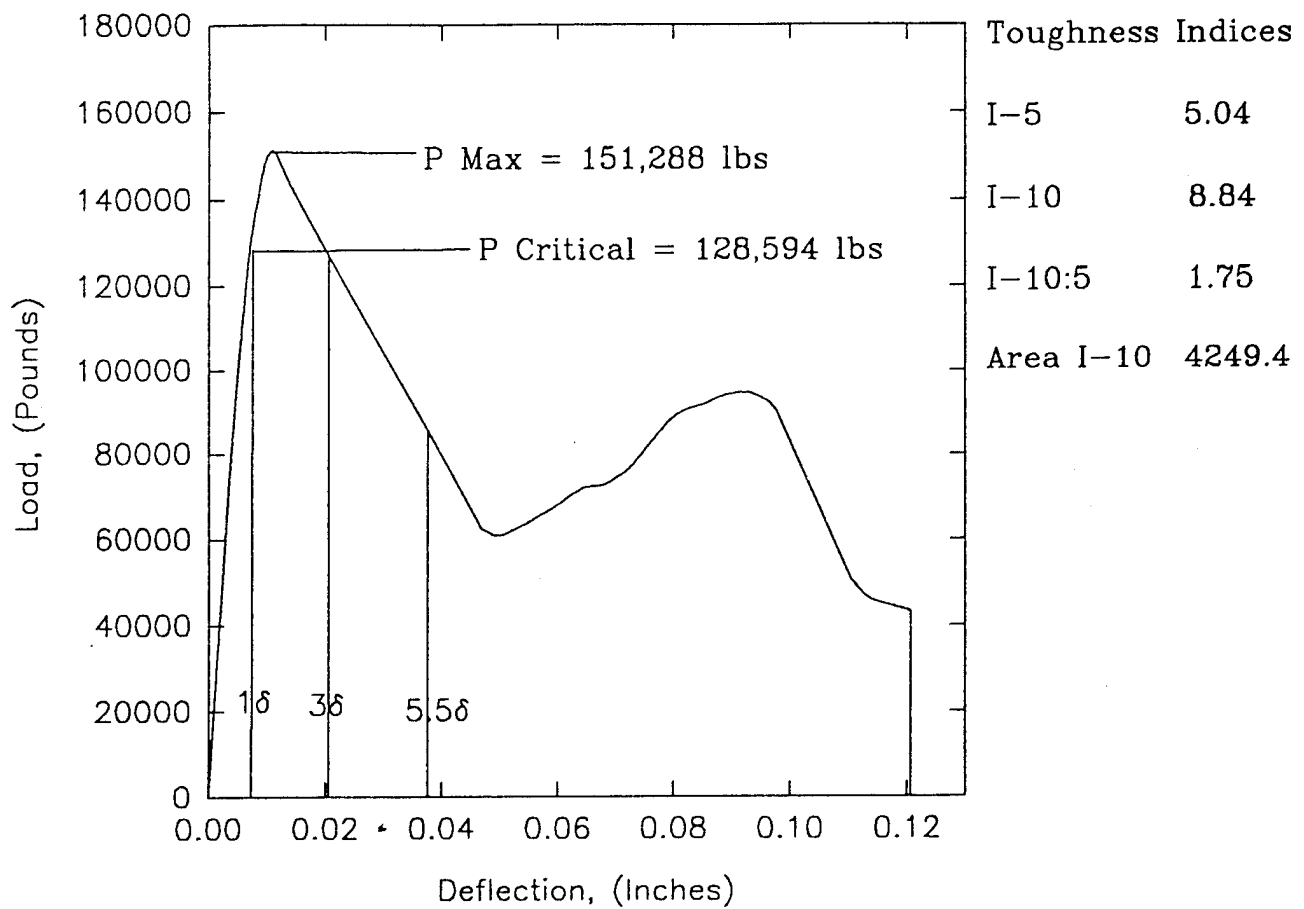


Figure 26. Load versus Deflection Curve for NW4000 6" by 12" Cylinder Static Compressive Strength Test.

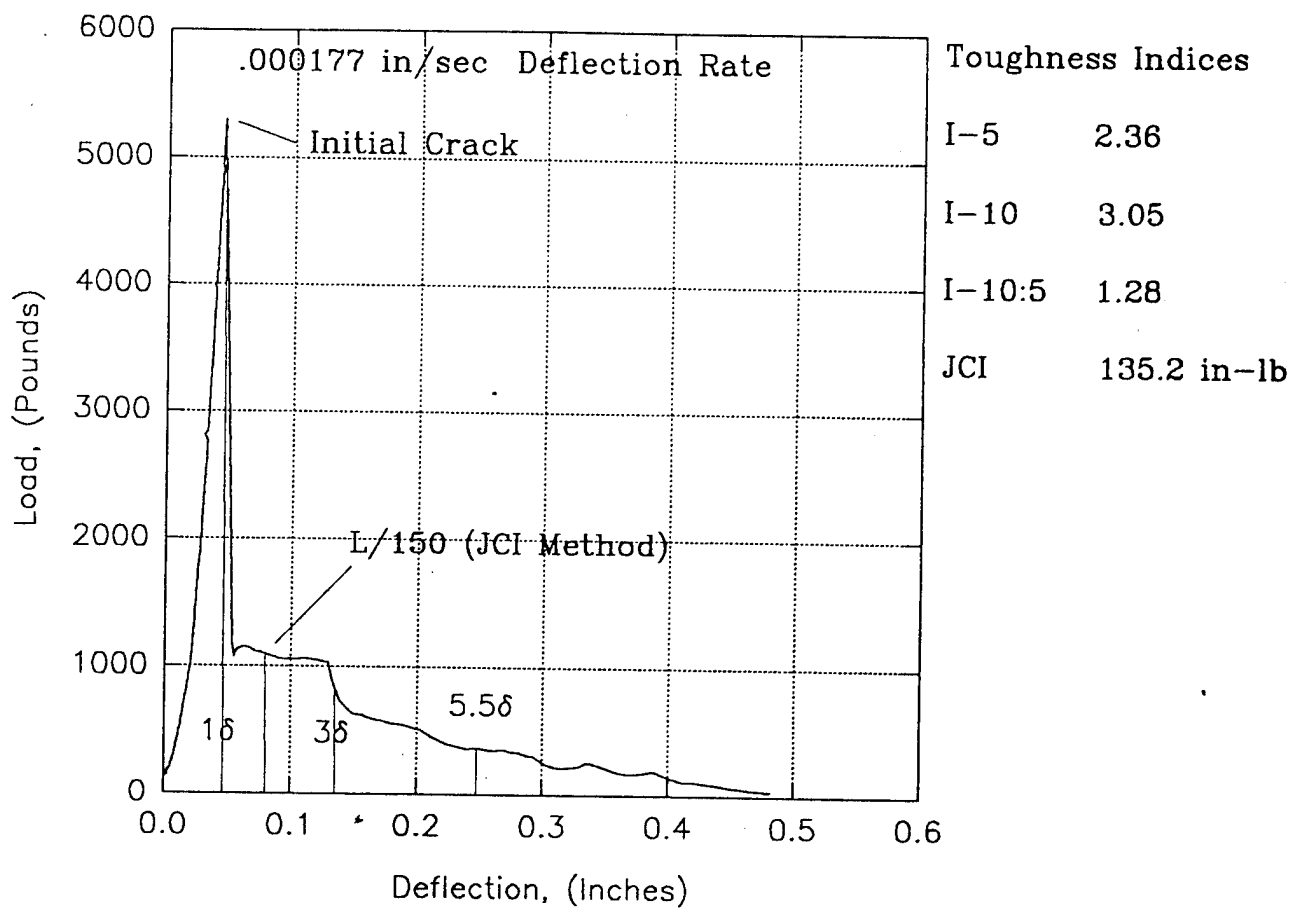


Figure 27. Load versus Deflection Curve for NW4000 Flexural Beam Test.

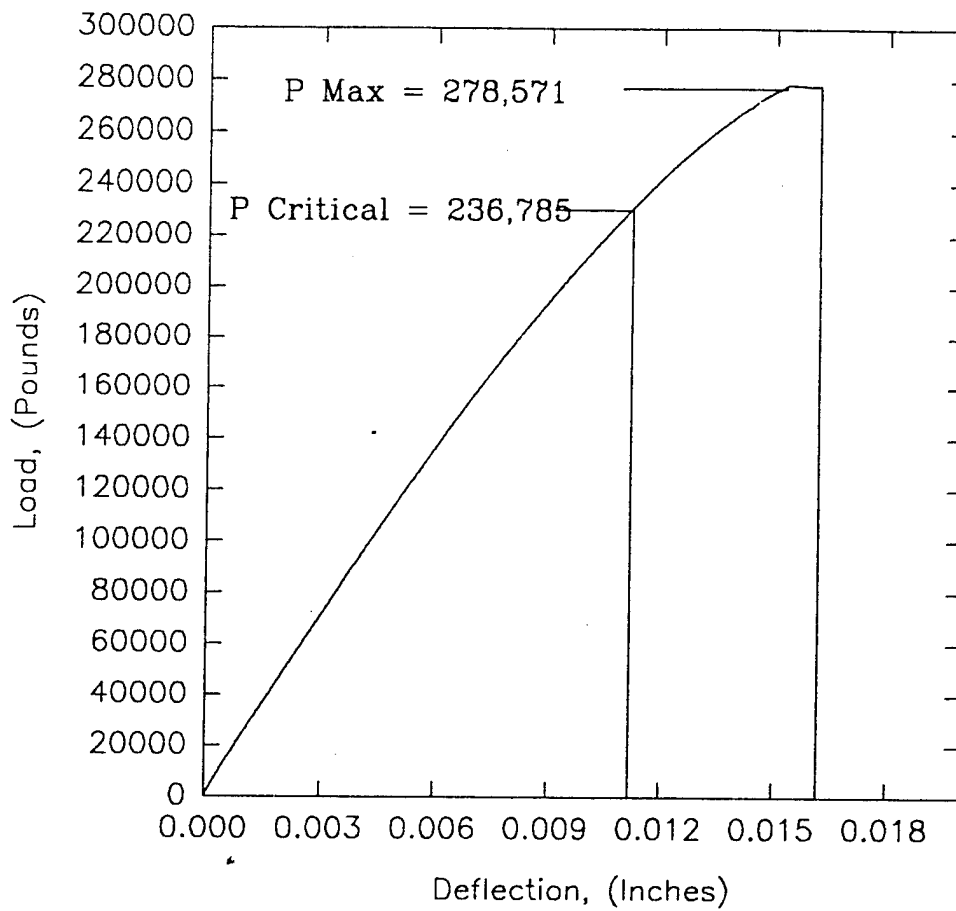


Figure 28. Load versus Deflection Curve for NW8000 6" by 12" Cylinder Static Compressive Strength Test.

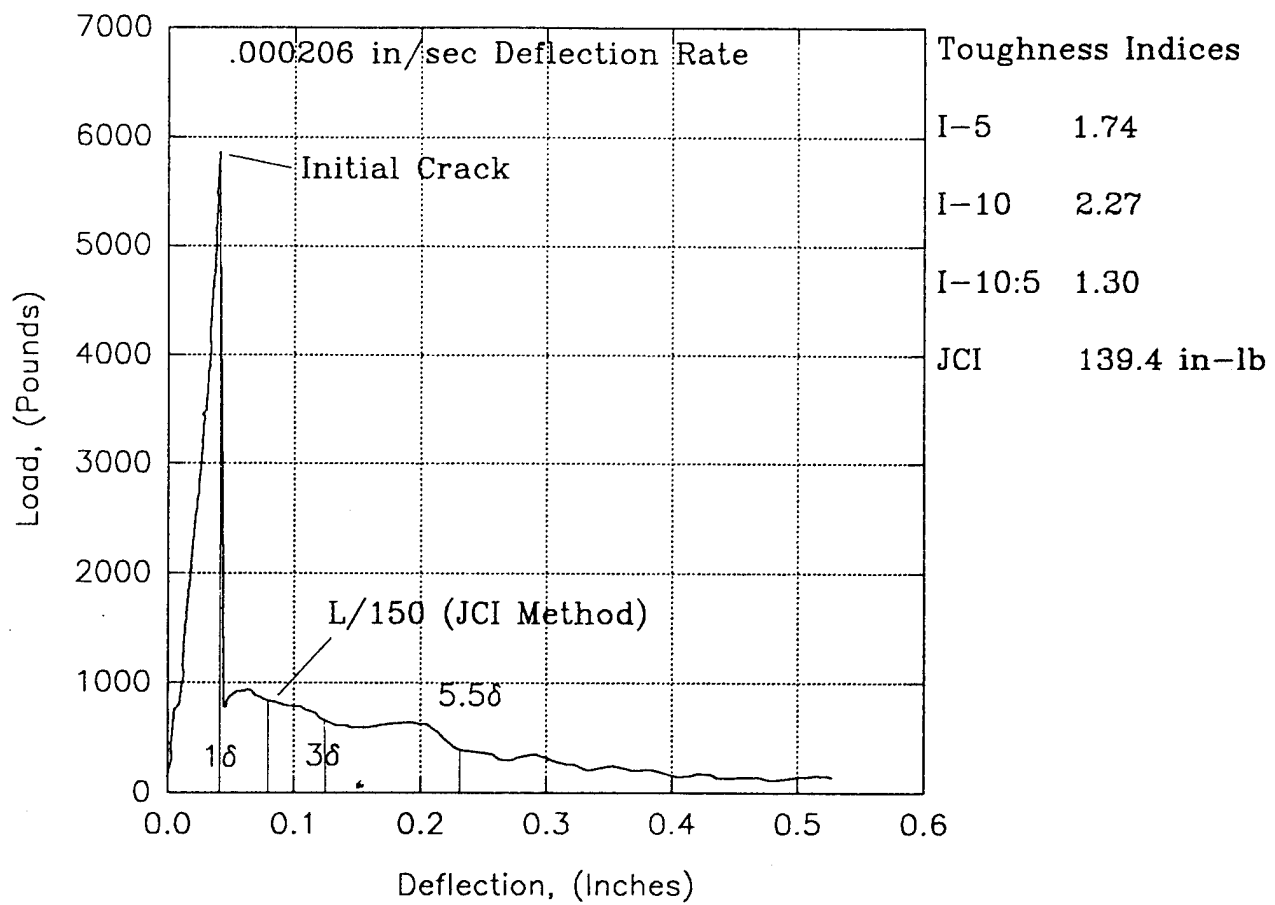


Figure 29. Load versus Deflection Curve for NW8000 Flexural Beam Test.

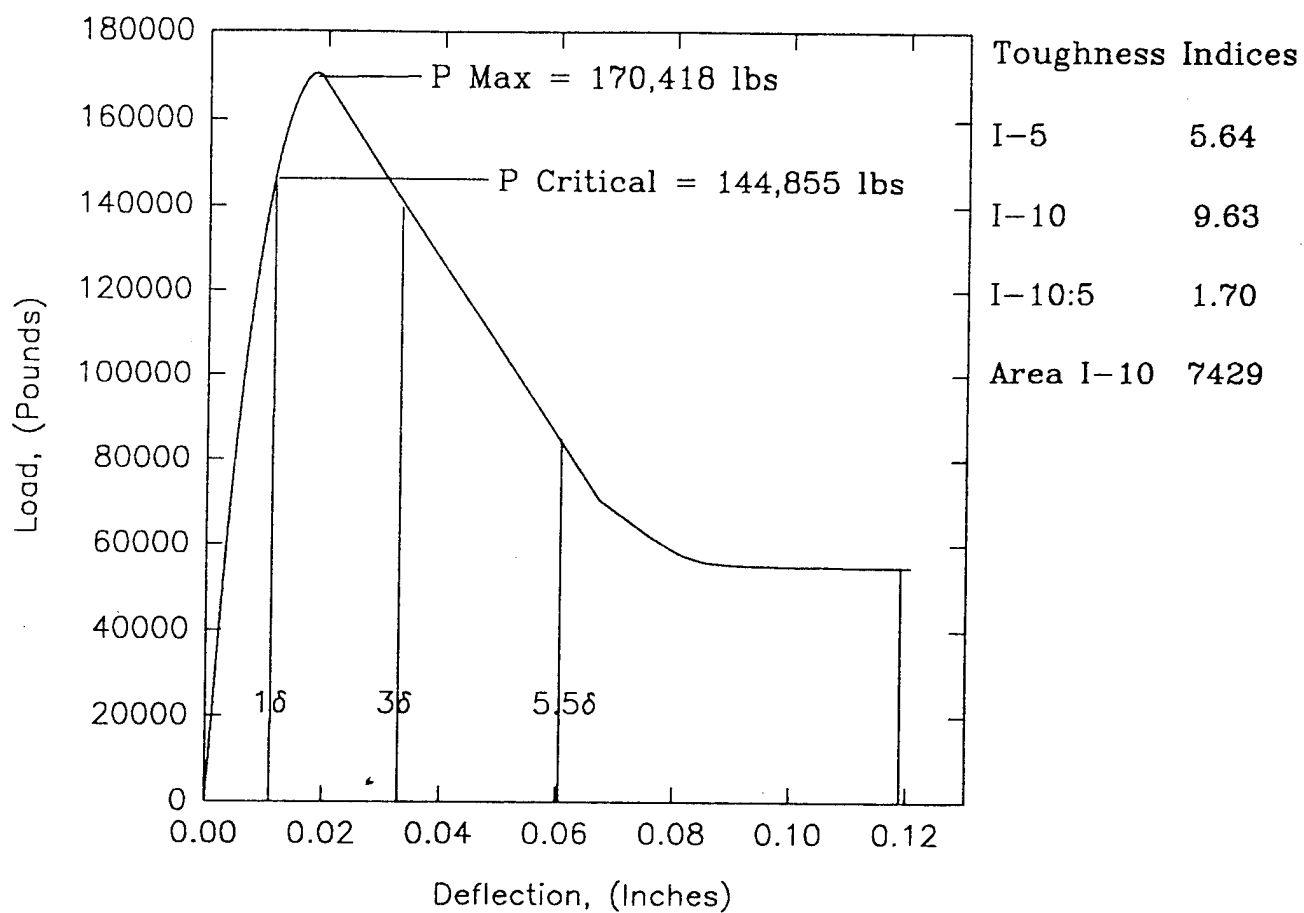


Figure 30. Load versus Deflection Curve for HDM-6" by 12" Cylinder Static Compressive Strength Test.

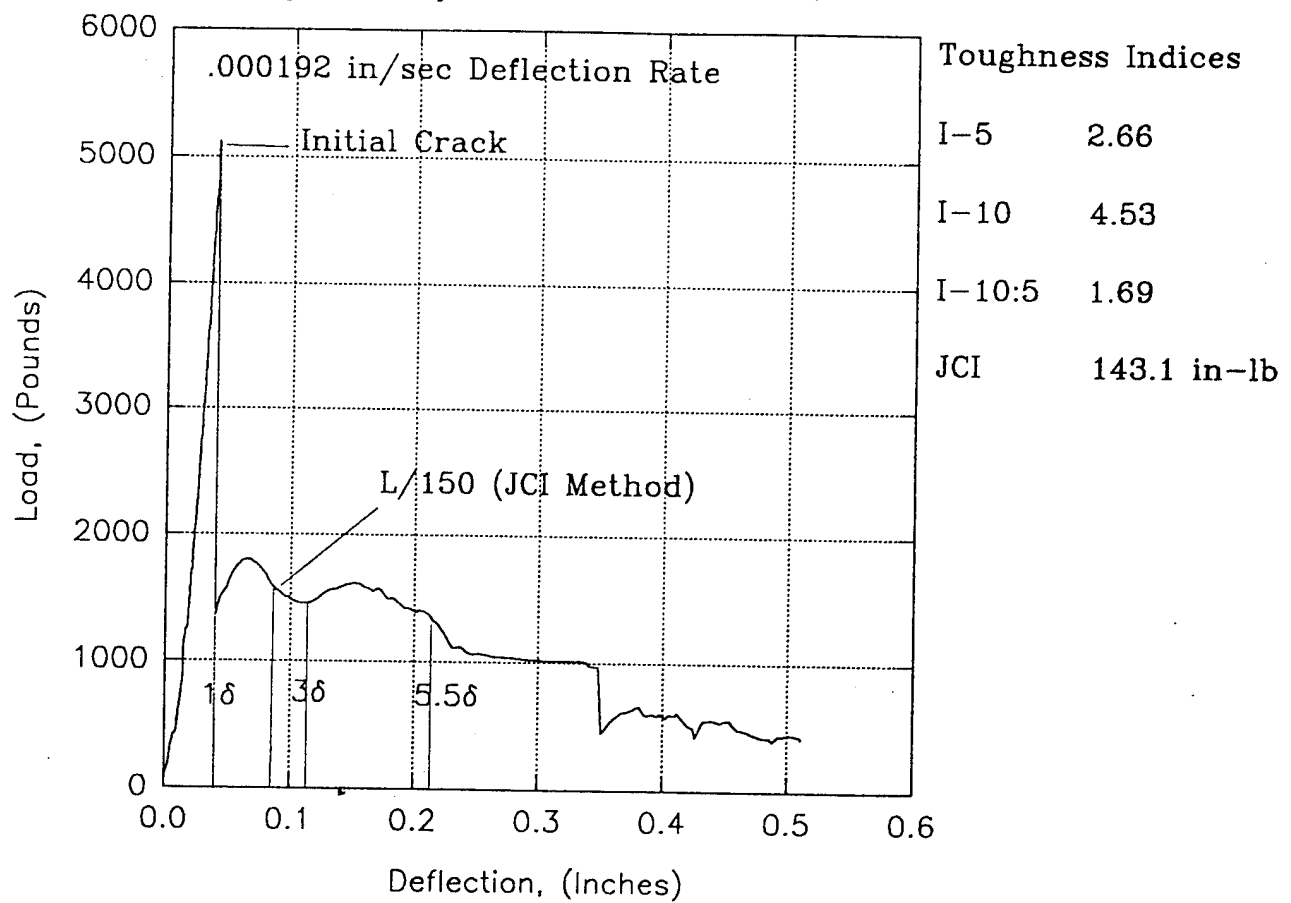


Figure 31. Load versus Deflection Curve for HDM Flexural Beam Test.

material quantities are based on a standard 94-pound sack of cement, as in the previous design.

VHDM

<u>Material</u>	<u>Quantity/sack</u>
Type I Portland Cement	94 lb
Steel slag	690 lb
WRDA-79	5 oz
Nylon Fibers	15 oz
Water	42 lb

The VHDM cylinder reached a maximum load of 243,550 pounds for a compressive strength of 8,615 psi as shown in Figure 32. The VHDM flexural test, Figure 33, yielded a JCI toughness index of 201.1 in-lb, which was the highest level achieved of the six samples.

Posttest conditions of the beams tested in flexure are shown in Figures 34 through 36. Due to the high fiber content, the beams held together even at severe deflections. Data recording was stopped at 0.5 inches of deflection due to the limitations of the LVDT.

4. Field Test Results

Eighteen deflection grid tests were performed on the three basic geometries. With the exception of four targets, impact points were generally confined to the center of a web where theoretical modeling had shown the resulting weapon rotation would be least. Actual strike points for the tests are shown in Figure 37.

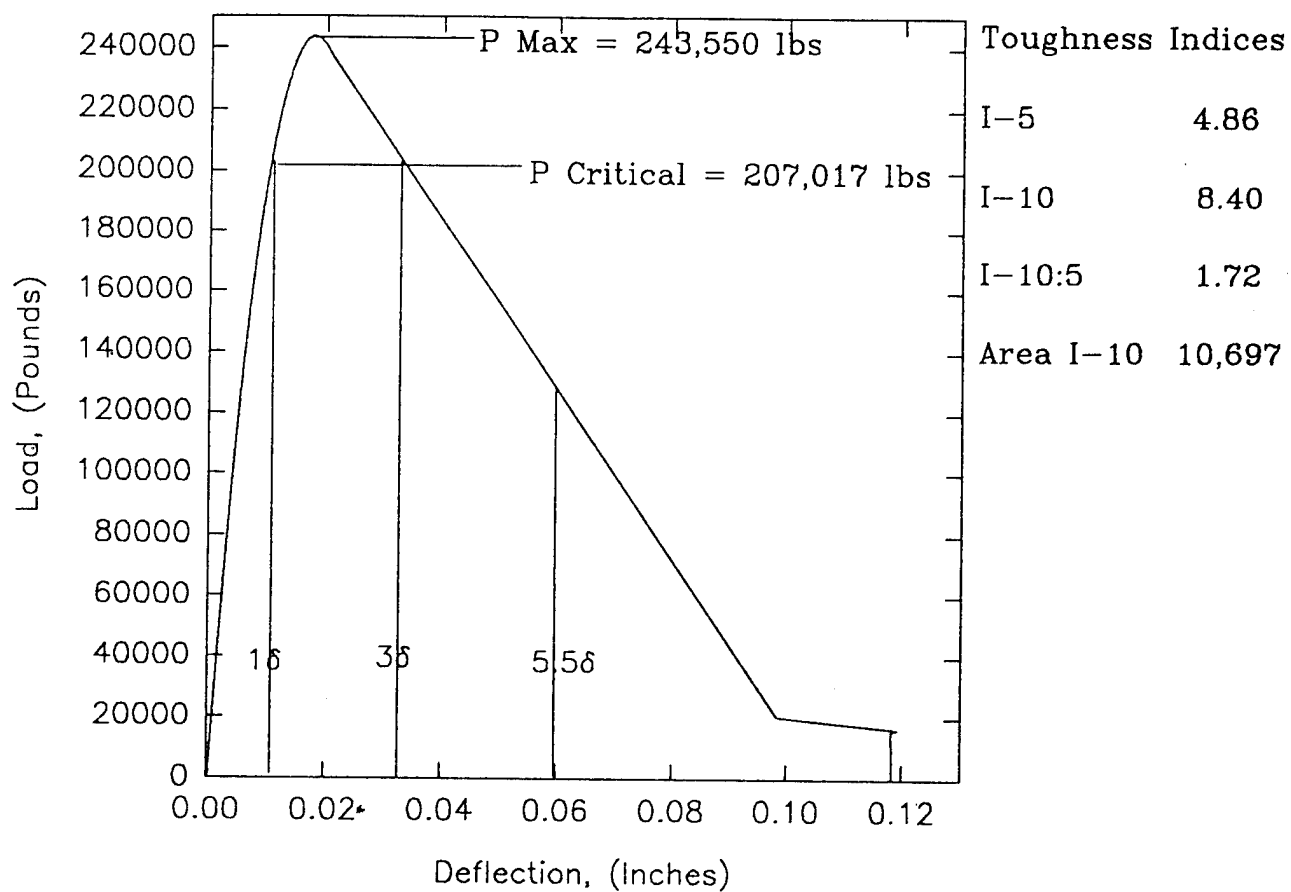


Figure 32. Load versus Deflection Curve for VHDM 6" by 12" Cylinder Static Compressive Strength Test.

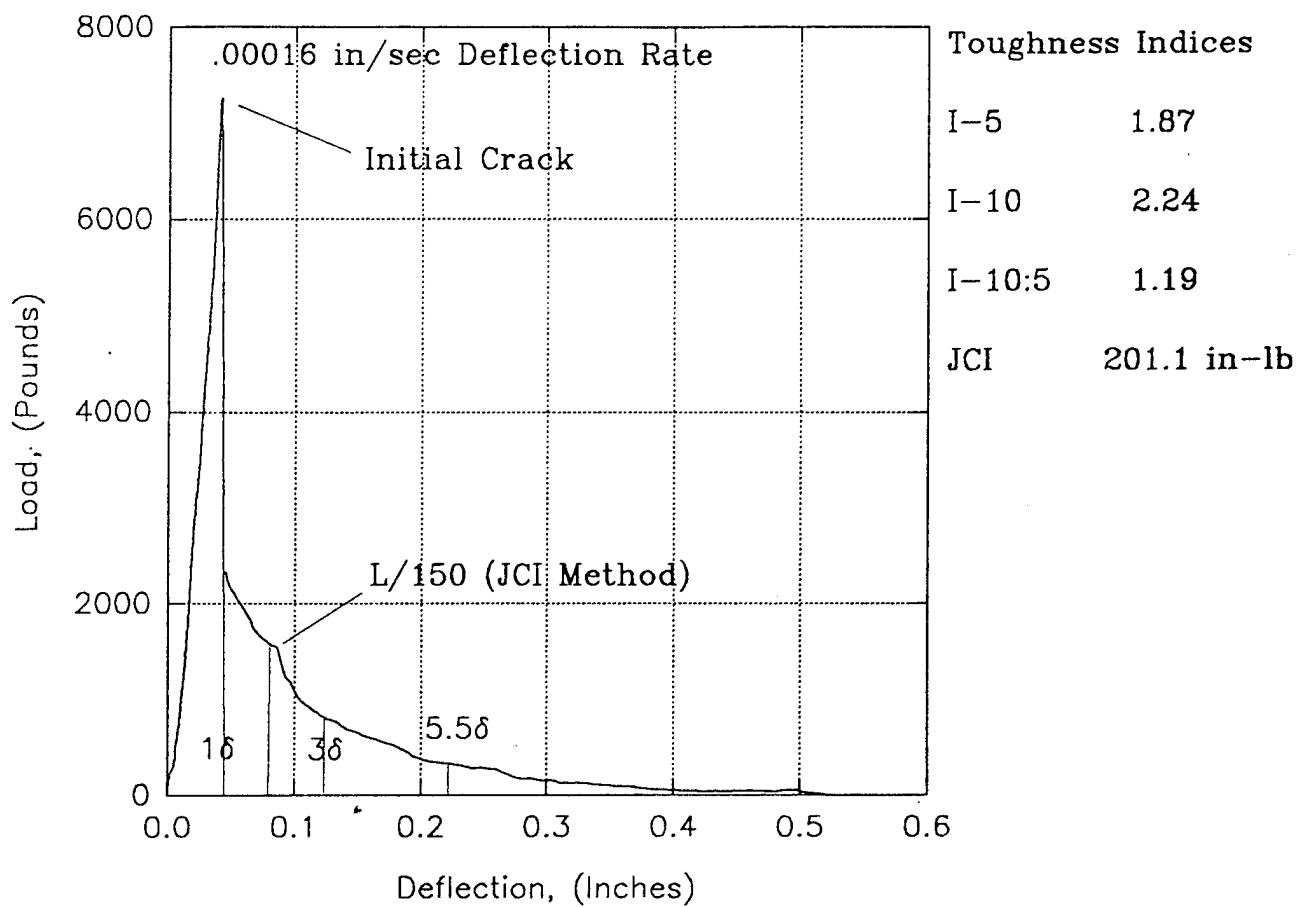


Figure 33. Load versus Deflection Curve for VHDM Flexural Beam Test.

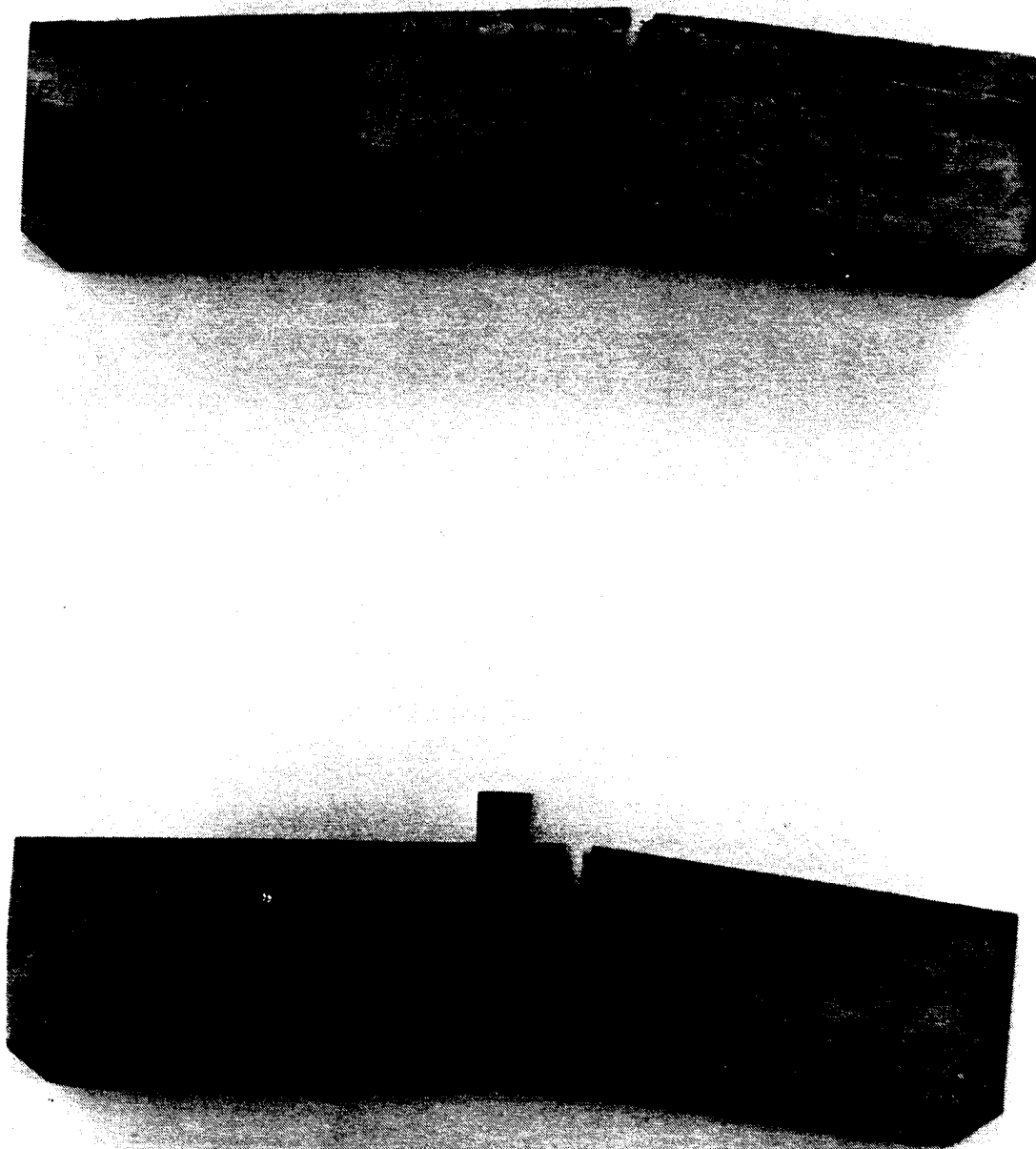


Figure 34. Posttest Photographs of LW4000 and LW8000 Flexural Tests.

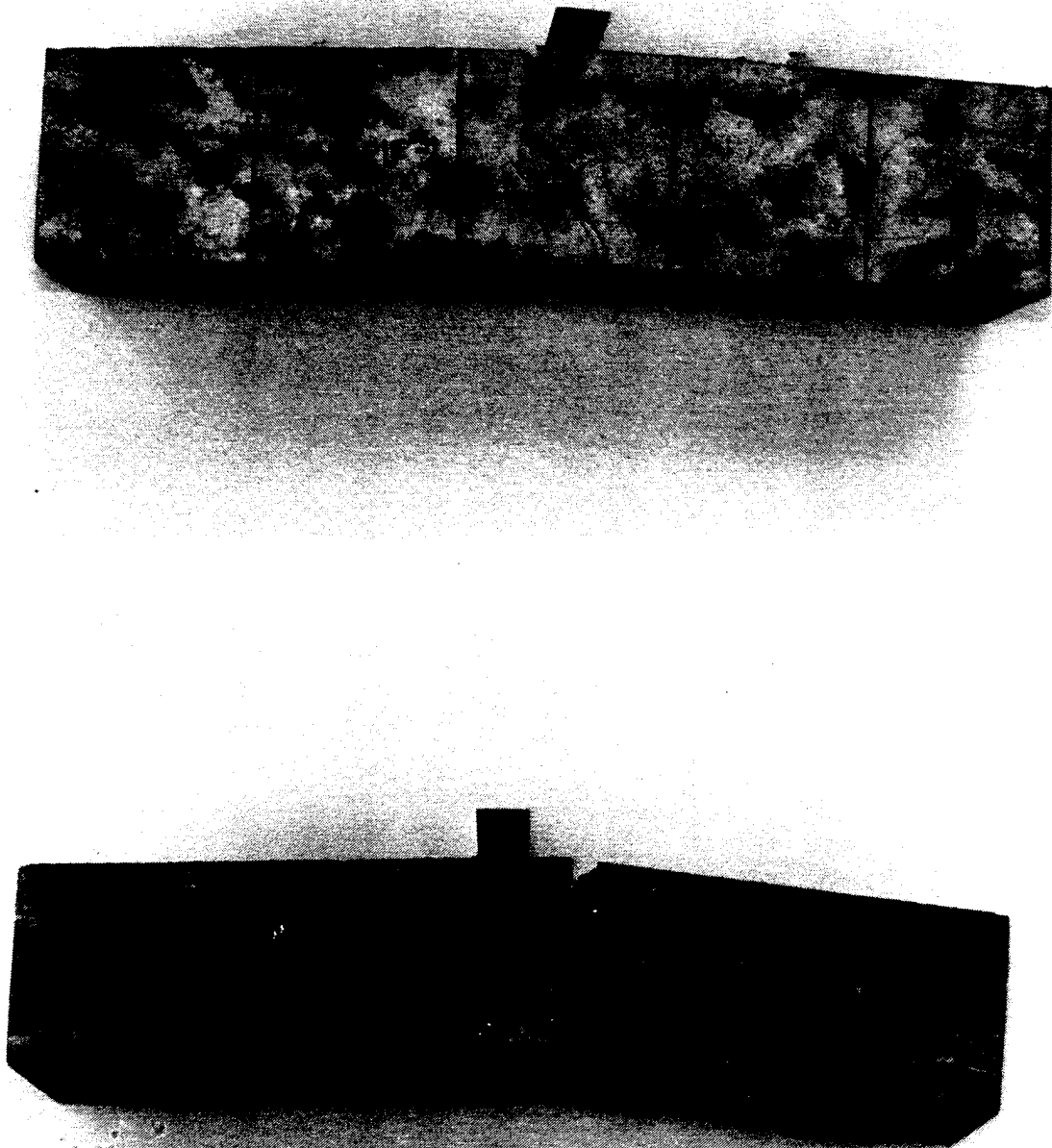


Figure 35. Posttest Photographs of NW4000 and NW8000 Flexural Tests.

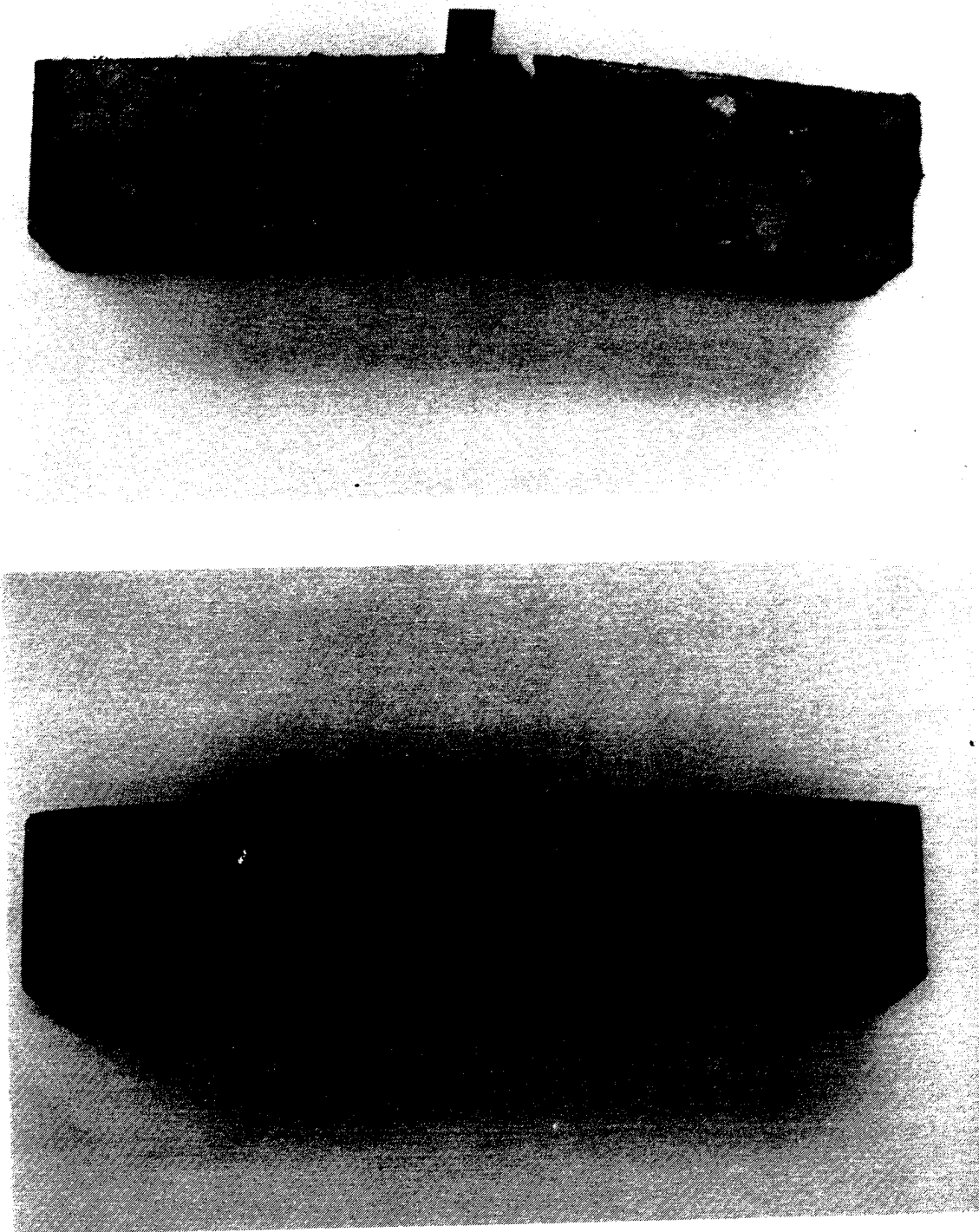


Figure 36. Posttest Photographs of HDM and VHDM Flexural Tests.

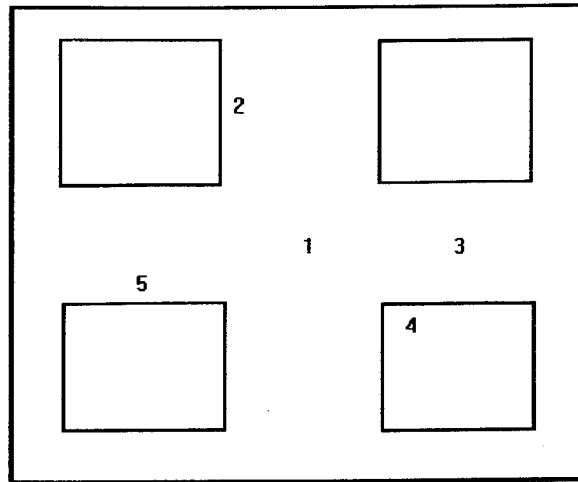


Figure 37. Target Strike Locations

Table 4 provides data by shot number, including grid type designation, target material unit weight in pounds per cubic foot, static compressive strength in pounds per square inch, exit angle in degrees, rotation rate in degrees per body lengths of travel (DBLT), total yaw in degrees at three body lengths of travel (the distance between the deflection grid and the burster slab), velocities before and after impact in feet per second, and strike point. Early in the testing series, the impact point was chosen to align with the center of a web to achieve the most conservative amount of rotation. As the light weight mix designs were tested, rotations of the projectile were not as high as expected, and the impact point was changed so as not to waste the possibly useful data that could be obtained for off-center impacts. These exceptions have been annotated in Section V, Analysis of Test Results.

TABLE 4. FY 92 DEFLECTION GRID TEST DATA

Shot No.	ρ pcf	fc psi	Exit Angle degrees	Yaw Rate DBLT	Total Yaw degrees	Vel _{in} fps	Vel _{out} fps	Impact Point
47	116	3348	2.9	3.5	9.9	1146	1118	1
42	121	5638	.2	2.3	4.8	1081	1054	1
53	151	5351	3.9	1.9	7.7	1102	1041	1
49	153	9853	41.2	13.0	67.2	1134	660	1
54	207	6028	9.3	5.8	20.9	1045	863	1
40	305	8615	7.6	5.4	18.4	1150	1067	1
45	116	3348	1.4	.7	2.8	1147	1143	1
41	121	5638	2.9	1.8	6.5	1130	1092	1
52	151	5351	5.4	3.5	12.4	1140	1092	1
50	153	9853	7.5	2.5	12.5	1132	1118	1
55	207	6028	6.6	3.8	14.2	1107	1016	1
39	305	8615	5.6	5.3	16.2	1152	1118	1
46	116	3348	5.2	4.4	14.0	1173	1143	4
43	121	5638	9.0	4.5	18.0	1127	1118	3
51	151	5351	3.1	2.7	8.5	1140	1118	1
48	153	9853	4.3	1.7	7.7	1165	1143	5
44	207	6028	10.6	8.0	26.6	1093	1054	1
38	305	8615	12.1	7.7	27.5	1111	1067	2

SECTION V

ANALYSIS OF TEST RESULTS

A. FY 91 ANALYSIS

The analysis of the deflection grid test data is presented by grid geometric type, with comparisons of induced yaw to body lengths of penetrator travel. A major portion of the tests were conducted on Grid Type 01, with variances in grid reinforcing type and penetrator angle of impact. Experiments on Grid Types 02 and 03 were limited to four tests each.

1. Grid Type 01

Figure 38 compares the rotation rates for Shots 1, 2, 3, 15, 16, and 17. These grids were made of 4,000 psi concrete with standard reinforcing steel. Angles of impact were maintained at zero degrees, with a random selection for strike location. Rotation rates ranged from 1.5 degrees per body length of travel (DBLT) to 10.5 DBLT. The data exhibit a wide scatter, with total yaw at three body lengths, ranging from 9 to 27 degrees. Although significant rotations were achieved, a lack of consistency is evident.

For Shots 4 and 5, the angle of impact was changed to 30 degrees, but the material composition was the same as for the previous tests. Rotation rate and total yaw both showed a significant increase as shown in Figure 39. This can be attributed to the oblique impact angle, which enhanced the probability of an unsymmetrical load application on the nose of the projectile during the penetration process.

Figure 40 shows the effect of a 45 degree impact angle for Shots 6 and 18. Material composition was maintained as in the previous tests. Rotation rates were less with a significant difference in total yaw achieved.

Shots 25, 26, and 36 were conducted with 8,000 psi concrete, with only nylon fibers for reinforcement. Angle of impact was zero degrees, with a random strike location. Figure 41 shows the effect of the nylon fibers in providing a more consistent rotation rate. Shot 36 showed poor performance characteristics, which was later attributed to severe air voids in the deflection grid.

Figure 42 compares the rotation rates for Shots 30, 31, 32, 33, and 37. The grid material was 8,000 psi concrete with reinforcing steel and nylon fibers. The rotation rates ranged from 1.8 DBLT to 6.6 DBLT, with minimal damage to the deflection grid. Radial cracking was eliminated, and breach damage was confined within a 1.5 projectile-diameter circle. Divergence of the data can probably be attributed to the random strike location of the penetrator.

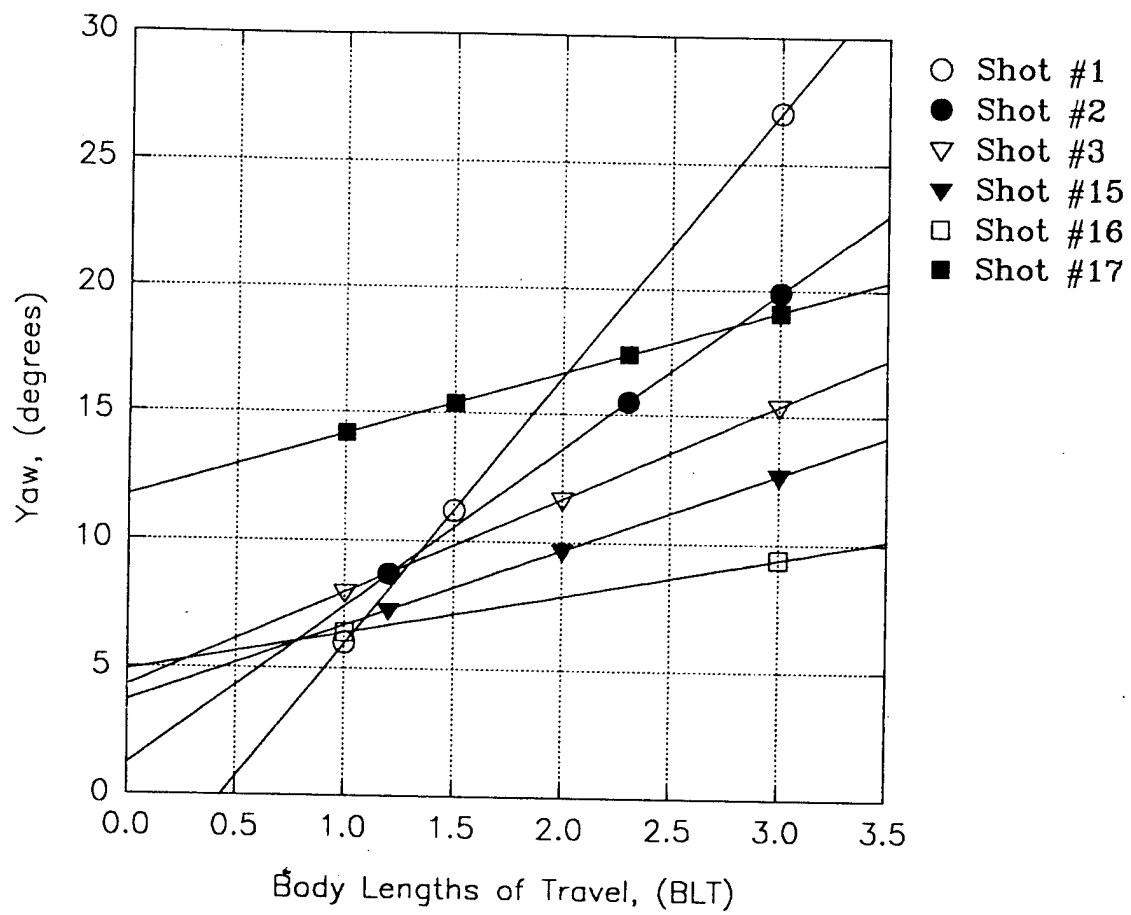


Figure 38. Yaw versus Body Lengths of Travel for Shots 1, 2, 3, 15, 16, 17.

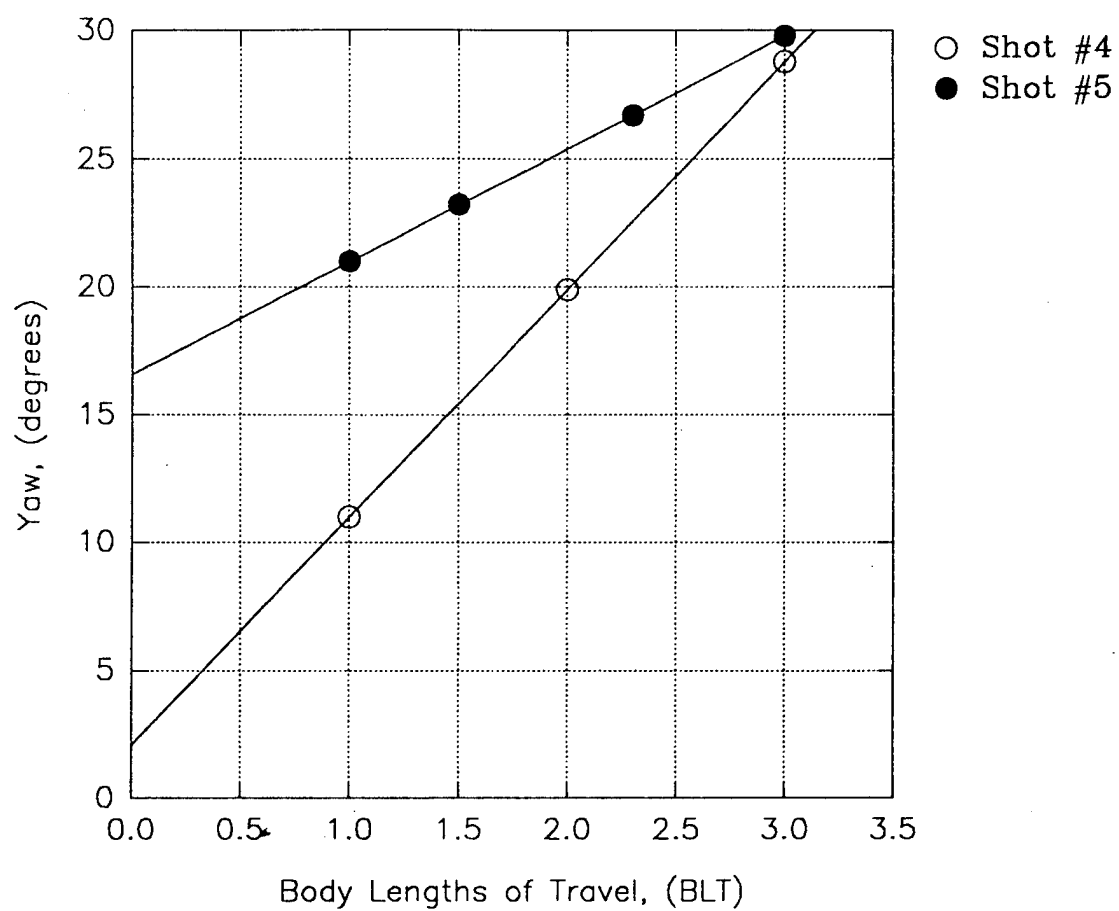


Figure 39. Yaw versus Body Lengths of Travel for Shots 4, 5.

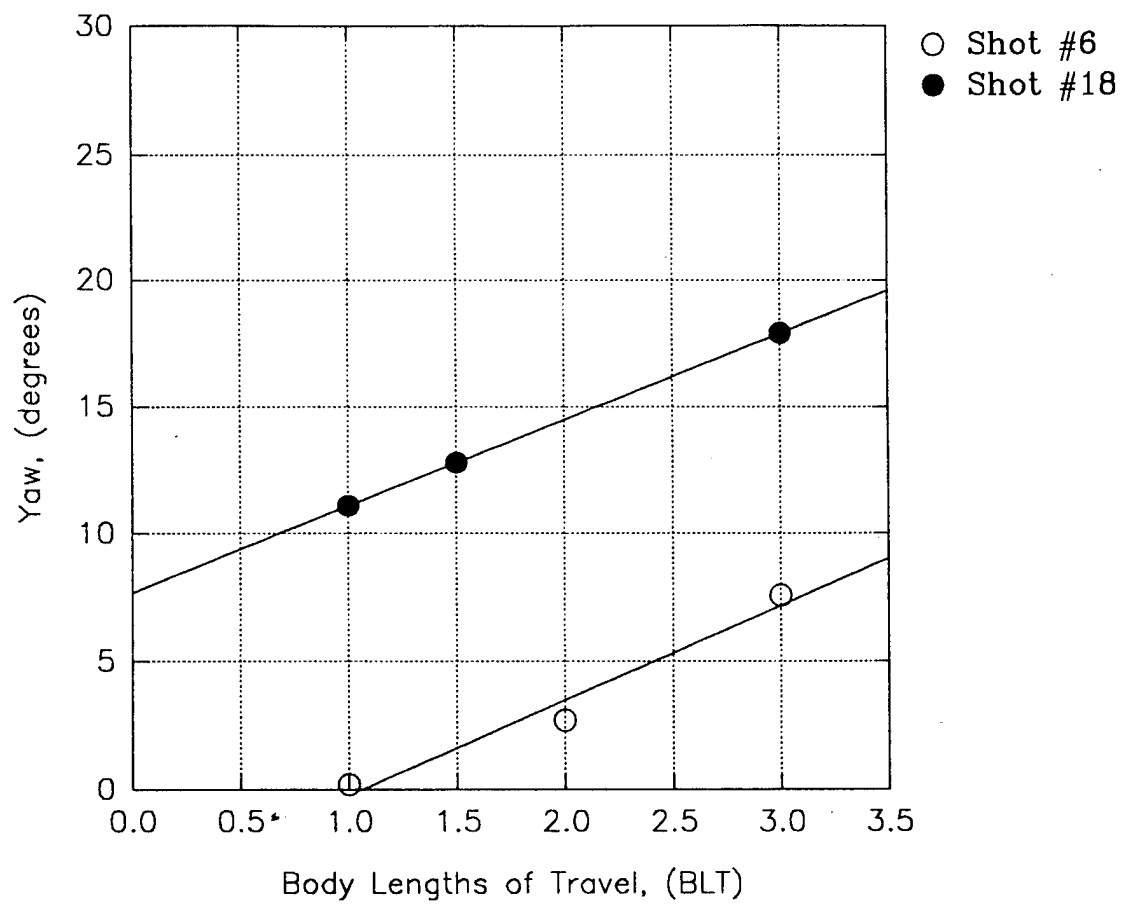


Figure 40. Yaw versus Body Lengths of Travel for Shots 6, 18.

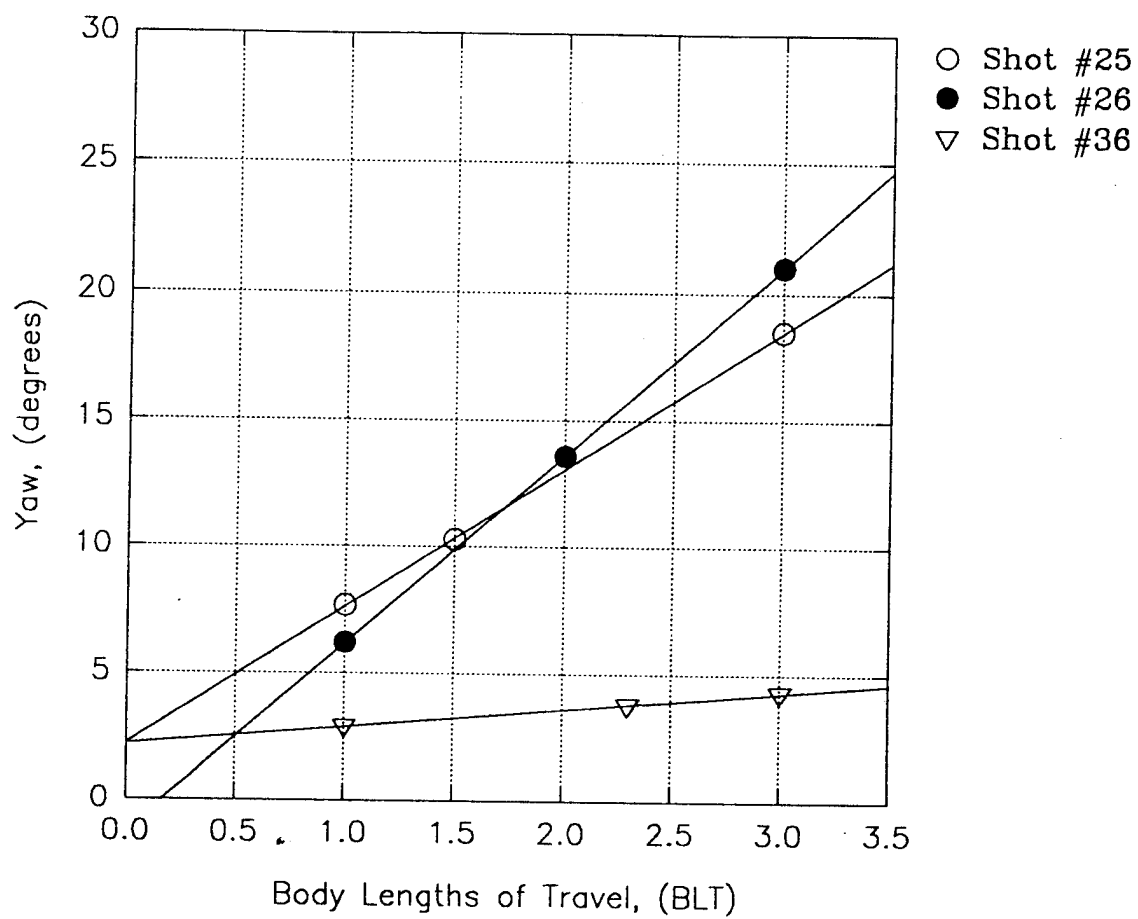


Figure 41. Yaw versus Body Lengths of Travel for Shots 25, 26, 36.

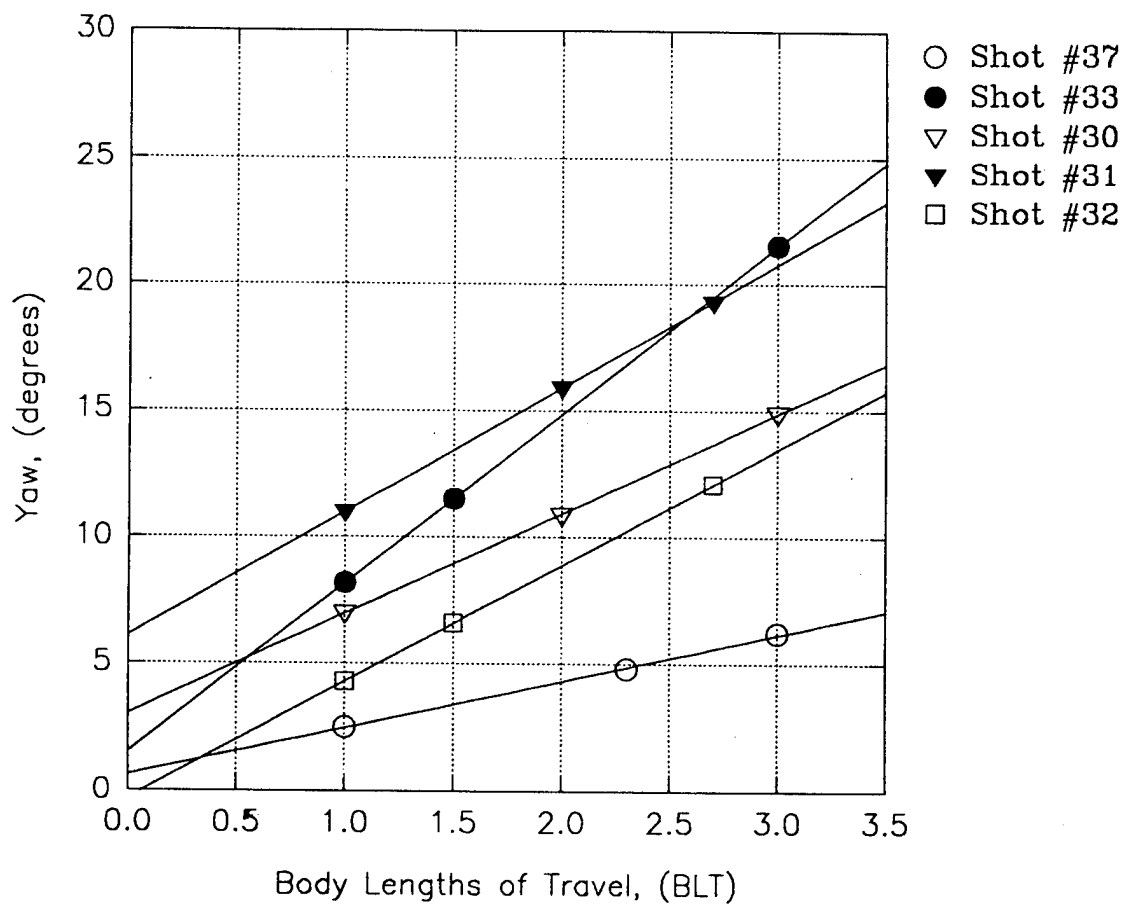


Figure 42. Yaw versus Body Lengths of Travel for Shots 37, 33, 30, 31, 32.

2. Grid Type 02

Shots 7, 8, 9, and 13 used 4,000 psi concrete with standard steel reinforcement. Shot 7 had a 45-degree impact angle, while the rest were set at zero degrees. Comparisons in Figure 43 show rotation rates ranging from 5.4 DBLT to 8.2 DBLT, with a wide scatter in total yaw at three body lengths of travel. This lends support to the premise that the nonhomogeneous nature of concrete produces random results. The yaw induced in these four tests is probably sufficient to defeat the weapon with a burster slab placed at three body lengths, but not with 100 percent reliability.

3. Grid Type 03

Shots 20 and 22 used 8,000 psi concrete with a single layer of reinforcing steel and also steel fibers. Shots 27 and 28 used a single deflection grid composed of 8,000 psi concrete with a single layer of reinforcing steel and also nylon fibers. Figure 44 compares the performance of steel to nylon fibers. Higher rotation rates were achieved with the nylon fibers. Upon posttest inspection, it was determined the steel fiber reinforced concrete suffered from fiber pull-out, leading to a shorter time to failure for the deflection grid. The nylon reinforced grids were able to maintain contact with the projectile for a longer period of time, thereby increasing the penetrator's induced yaw.

From the FY 91 tests, it was concluded that the nylon fibers were a key element in extending the contact time with the penetrator. Damage to the grid was reduced significantly through the use of nylon fibers and rotation rates achieved were more consistent.

B. FY 92 ANALYSIS

Defining the forcing functions involved with the interaction of a penetrator and a complex concrete target is extremely difficult, due to the nonhomogeneous nature of the target. It was necessary to design the tests to control as many independent variables as possible, to investigate the relationship of material properties to the induced projectile rotation rate. The controlled key variables were impact point, concrete compressive strength, concrete unit weight, grid geometry, and projectile velocity. The analysis of the data is presented by grid geometric type, with comparisons of compressive strength, toughness, and density to total induced yaw.

1. Grid Type 16

The six tests using Grid Type 16 were Shots 40, 42, 47, 49, 53, and 54. Shot number 40 used Very High Density Mortar (VHDM) with a unit weight of 305 pcf and a static compressive strength of 8,615 psi. The strike point was centered on the web,

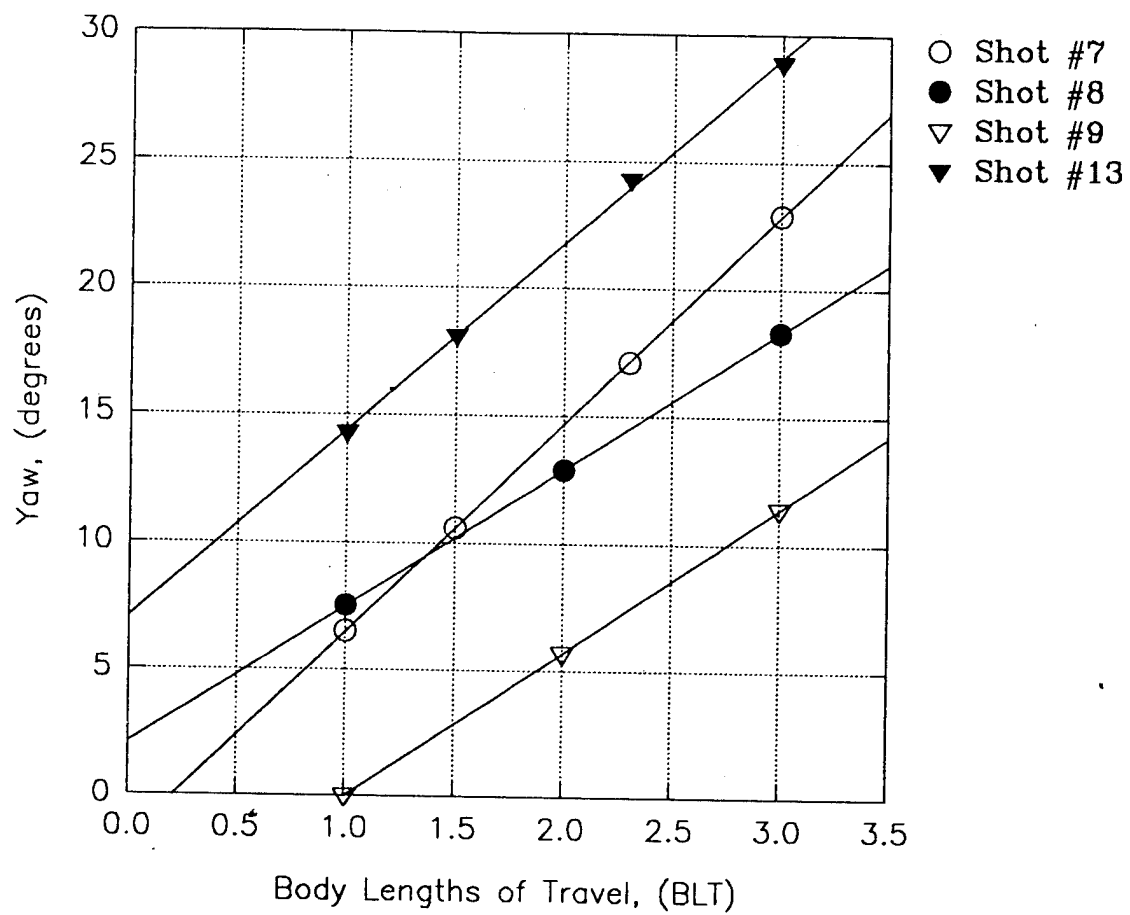


Figure 43. Yaw versus Body Lengths of Travel for Shots 7, 8, 9, 13.

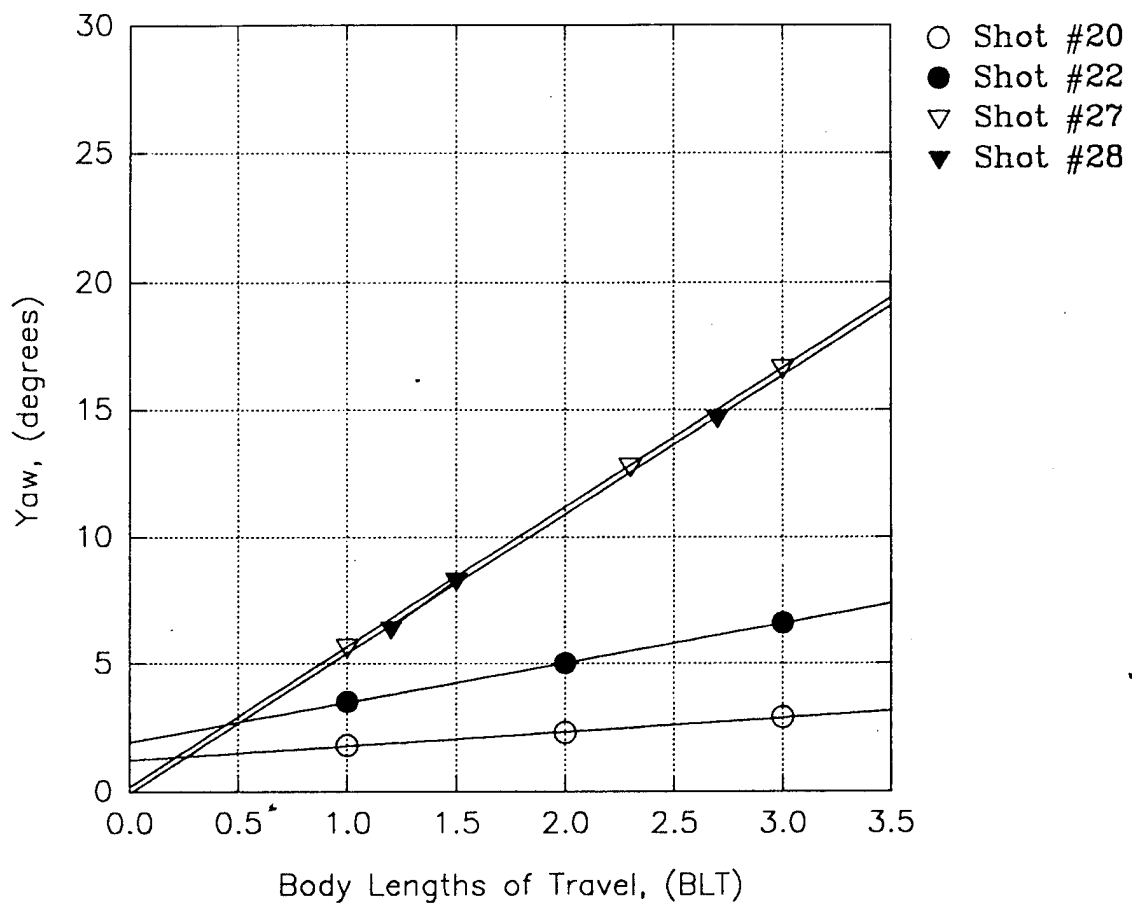


Figure 44. Yaw versus Body Lengths of Travel for Shots 20, 22, 27, 28.

and resulted in massive damage to the projectile after striking the burster slab. Damage to the burster slab was limited to a two foot square area approximately 4 inches deep, with the projectile rebounding off the face of the burster slab and landing 40 feet back towards the howitzer. Posttest photographs of the projectile and the grid are shown in Figure 45. Yaw impact angle at the burster slab was determined to be 18.3 degrees.

Shot 42 used the Light Weight 8000 (LW8000) mix design, with a unit weight of 121 pcf and a static compressive strength of 5,634 psi. The strike point was 0.25 inches to the left of center of the web and resulted in 4.5 degrees of rotation upon impact with the burster slab. The projectile perforated the burster slab and 8 feet of sand before coming to rest. Damage to the projectile was minor and the end cap was still in place on the penetrator. Posttest photographs are shown in Figure 46.

Shot 47 used the Light Weight 4000 (LW4000) mix design, with a unit weight of 116 pcf with a static compressive strength of 3,346 psi. The strike point was 0.25 inches to the left of center of the web, and resulted in 9.8 degrees of rotation upon impact with the burster slab. The top left corner of the burster slab was obliterated, with the projectile continuing for several feet into the sand bank. Damage to the projectile was minor, as shown in Figure 47.

Shot 49 used the Normal Weight 8000 (NW8000) mix design, with a unit weight of 153 pcf with a static compressive strength of 9,853 psi. The strike point was centered on the web. As the projectile exited the grid, an angle of 41.2 degrees of rotation was measured by the flash x-ray, and 67.3 degrees were achieved prior to striking the burster slab. Damage to the deflection grid was extensive due to rotation of the projectile as it passed through. The burster slab showed evidence of a side-on impact. Figure 48 displays the posttest condition of the projectile and the deflection grid. Due to the large rotation of the projectile, these data were excluded from many of the comparisons and graphs, so as not to distort the presentation of data. A review of the high speed camera film showed no irregularities in the flight path of the penetrator prior to impact of the deflection grid. This test displayed the highest rotation rate and total yaw of any test.

Shot 53 used the Normal Weight 4000 (NW4000) mix design, with a unit weight of 151 pcf with a static compressive strength of 5,350 psi. The strike point was centered on the web, and the projectile showed only 7.6 degrees of rotation upon impact of the burster slab. Damage to the projectile was minimal, as shown in Figure 49.

Shot 54 used the High Density Mortar (HDM) mix design, with a unit weight of 207 pcf with a static compressive strength of 6,028 psi. The strike point was centered on the web, and a yaw angle of 20.7 degrees was observed prior to striking the burster slab. The end cap was missing from the projectile, and cracks were observed near

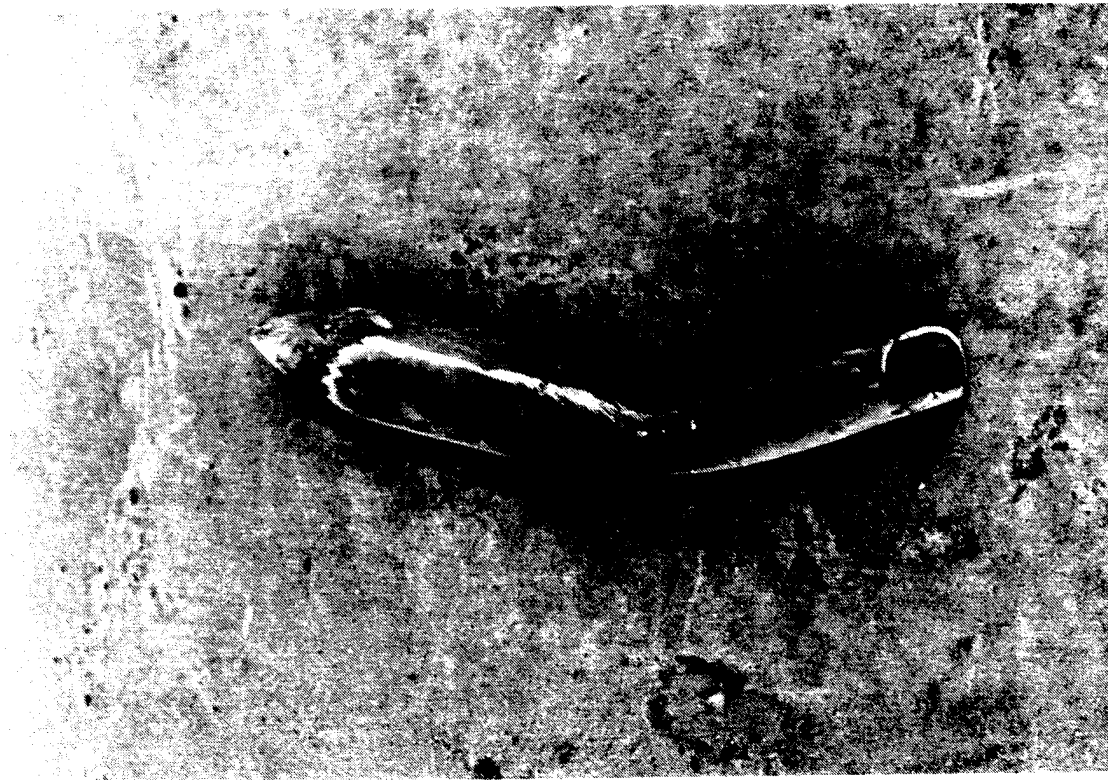


Figure 45. Posttest Photographs of Shot 40.

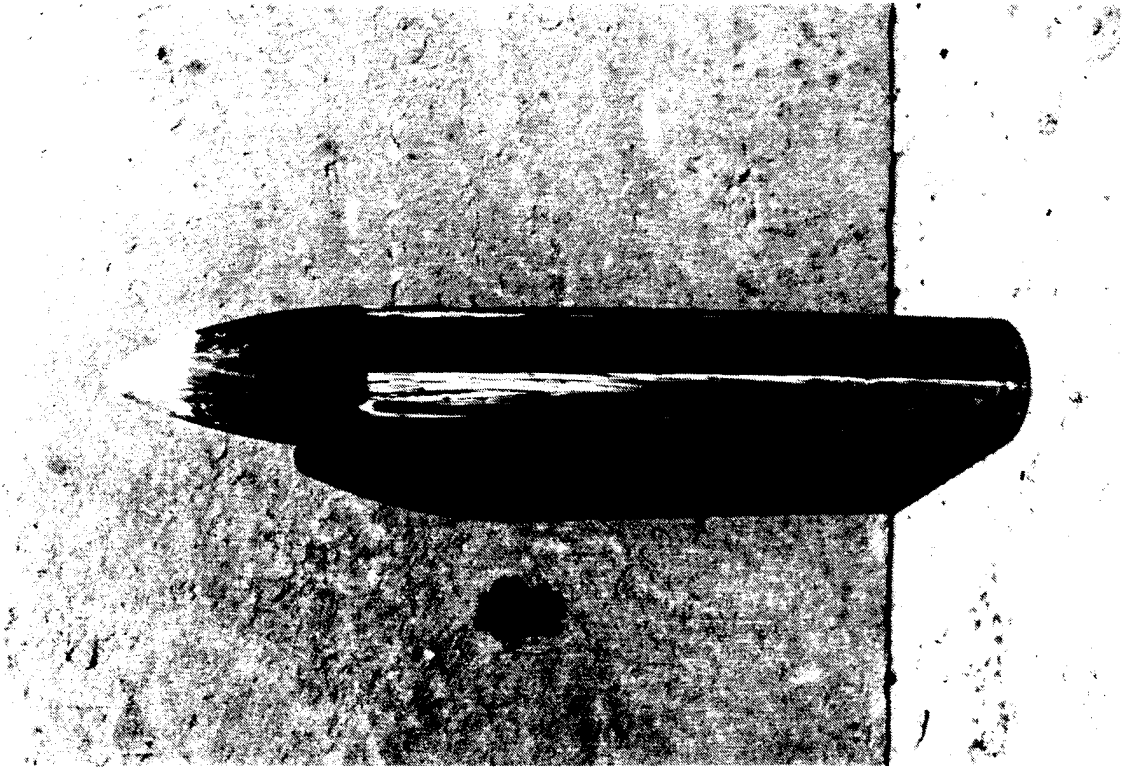


Figure 46. Posttest Photographs of Shot 42.

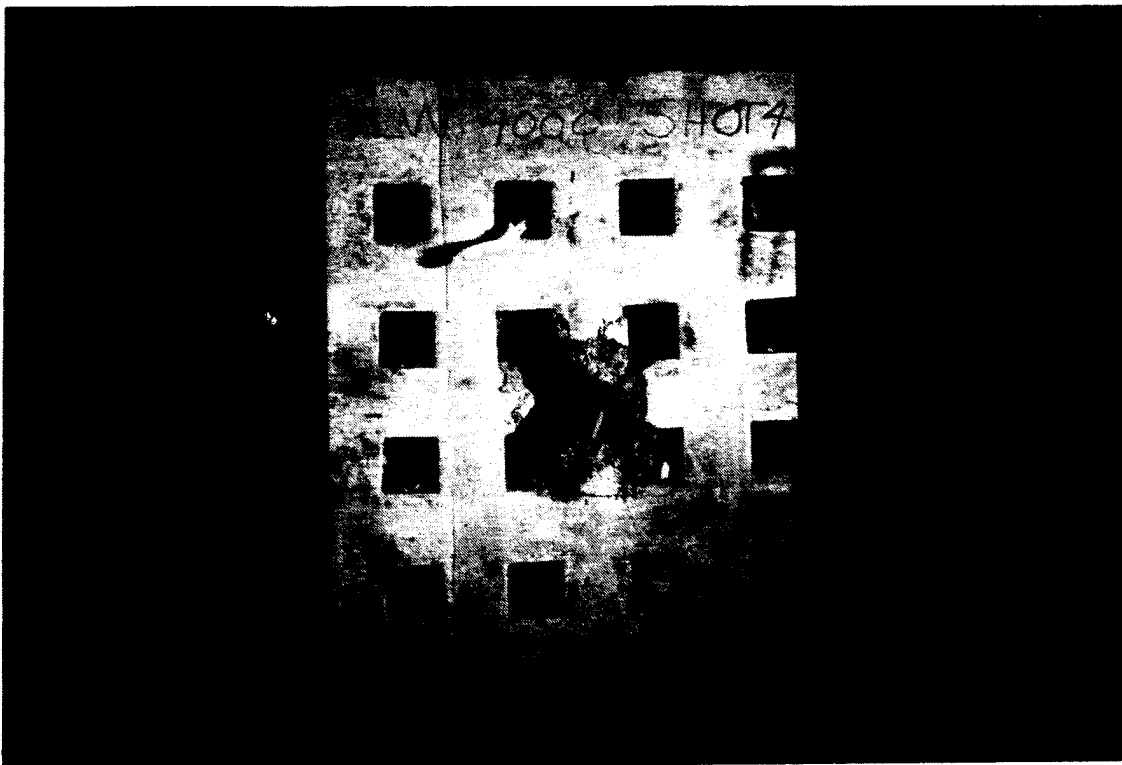


Figure 47. Posttest Photographs of Shot 47.

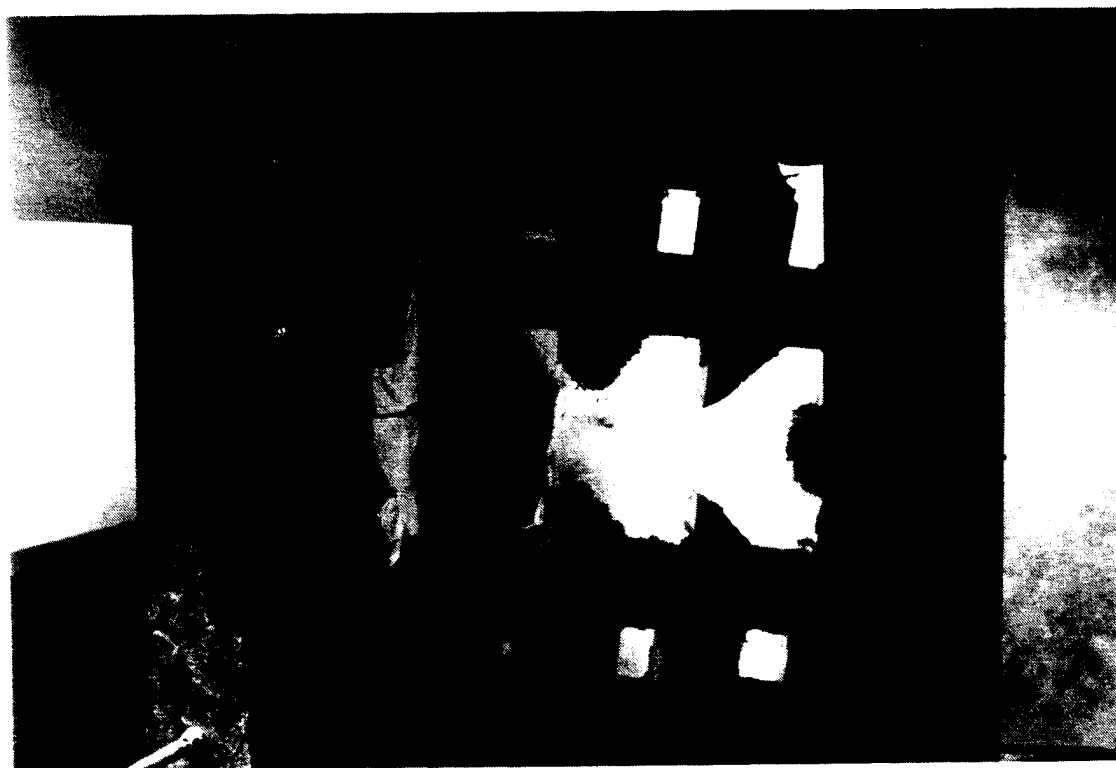


Figure 48. Posttest Photographs of Shot 49.



Figure 49. Posttest Photographs of Shot 53.

the end of the casing. The projectile was found severely bent, lying in front of the burster slab after having failed to penetrate, as shown in Figure 50.

Of the six tests, the projectile was unable to penetrate the burster slab in three cases: Shots 40, 49, and 54. By eliminating Shot 49 as an outlier, those deflection grids which had a unit weight greater than 200 pcf were capable of stopping the penetrator in three body lengths of travel. Figure 51 demonstrates that as unit weight increases, total yaw also increases. The comparison of static compressive strength and total yaw in Figure 52 shows poor correlation for the 16 hole geometry. For those concretes with static compressive strength above 6,000 psi, compressive strength appears to have a significant impact. Since toughness is closely related to the amount of energy absorbed by the material, a comparison between toughness and total yaw was performed, as shown in Figure 53, which shows a striking similarity to the unit weight versus total yaw data in Figure 51. In addition, a material property comparison was performed, treating unit weight and compressive strength as independent variables, and total yaw as the dependent variable. The result is shown in Figure 54. The data indicate a general trend of increasing yaw as compressive strength and unit weight increase. A comparison was also made between body lengths of travel of the projectile and the yaw induced for the six shots, as shown in Figure 55. For those concretes with unit weight above 200 pcf, a minimum of 5 DBLT was observed, which was a factor of 2 to 3 greater than the lighter weight mix designs. Shot 49's rotation was so large that the data point fell beyond the range of the chart.

2. Grid Type 20

The six tests using Grid Type 20 were Shots 39, 41, 45, 50, 52, and 55. Shot 39 used the VHDM mix design, with a unit weight of 305 pcf and a static compressive strength of 8,615 psi. The strike point was centered on the web, and resulted in 16.3 degrees of yaw upon impact with the burster slab. The projectile struck the burster slab and rebounded back towards the howitzer, causing severe damage to the penetrator case. Delamination of the burster slab and the posttest condition of the penetrator are shown in Figure 56.

Shot 41 used the LW8000 mix design, with a unit weight of 121 pcf and a static compressive strength of 5,634 psi. The strike point was centered on the web, and resulted in 6.5 degrees of yaw upon impact with the burster slab. The penetrator continued through the 18 inch burster slab and seven feet of sand before coming to rest. The projectile was still intact and showed minor case damage, as shown in Figure 57.

Shot 45 used the LW4000 mix design, with a unit weight of 116 pcf and a static compressive strength of 3,346 psi. The impact point was centered on the web, and

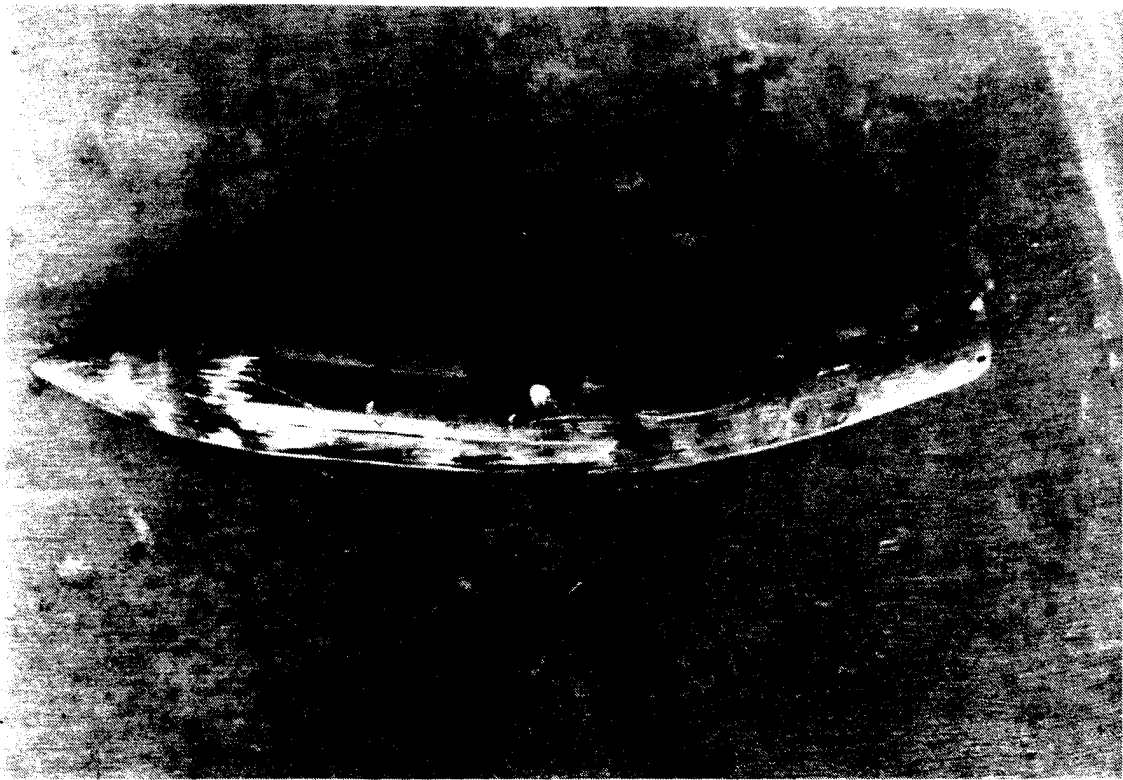


Figure 50. Posttest Photographs of Shot 54.

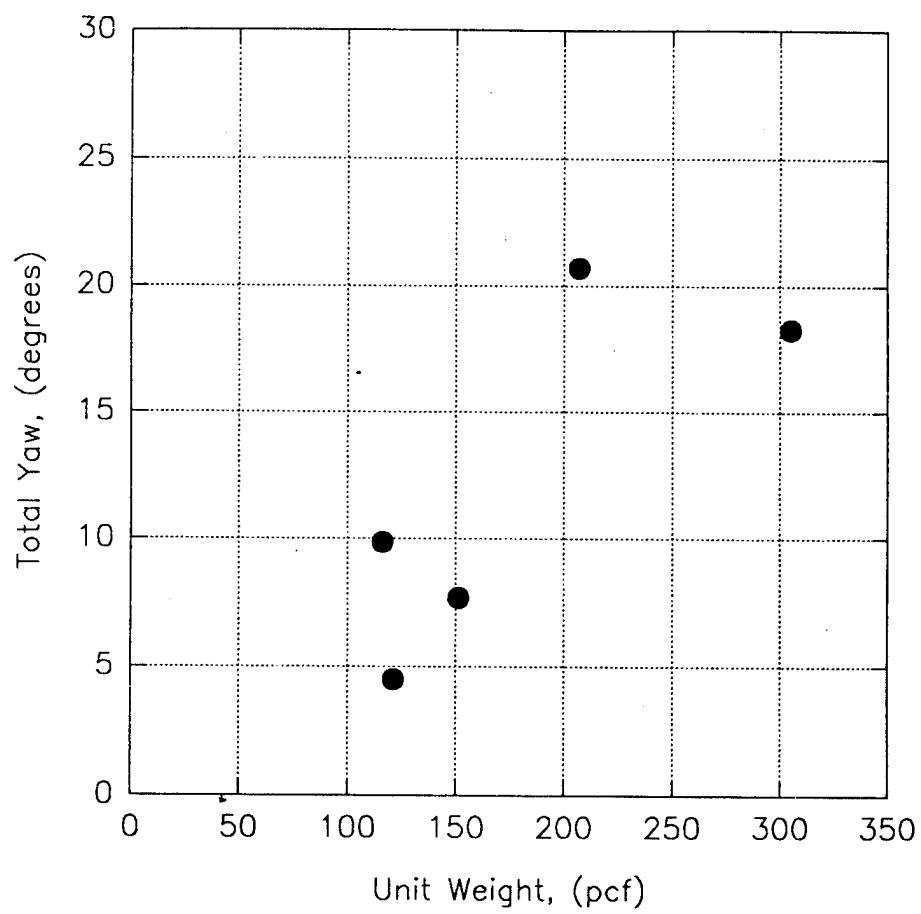


Figure 51. Unit Weight versus Total Yaw for Grid Type 16.

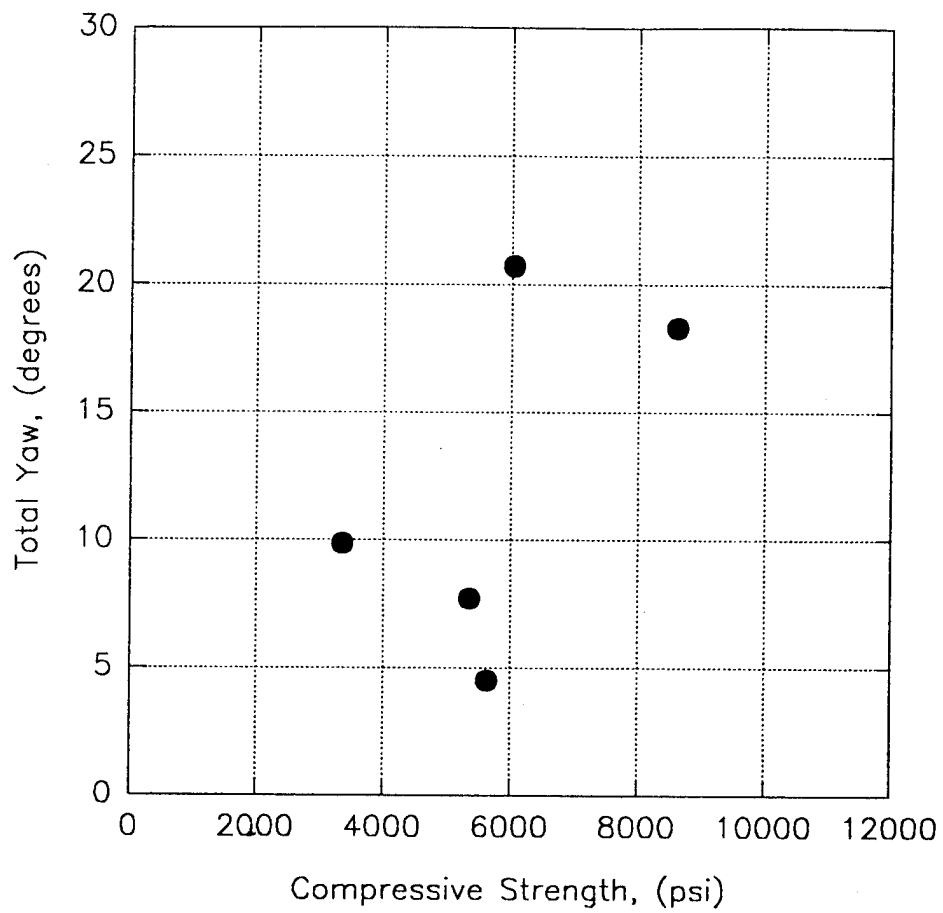


Figure 52. Compressive Strength versus Total Yaw for Grid Type 16.

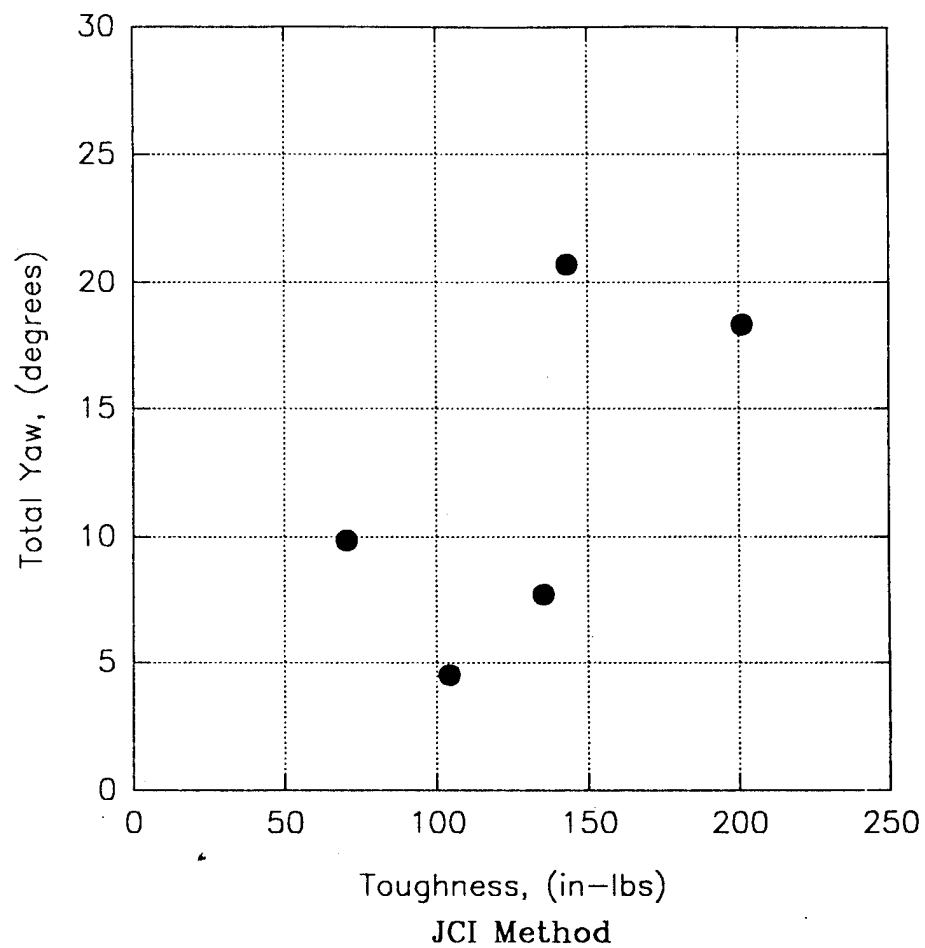


Figure 53. Toughness versus Total Yaw for Grid Type 16.

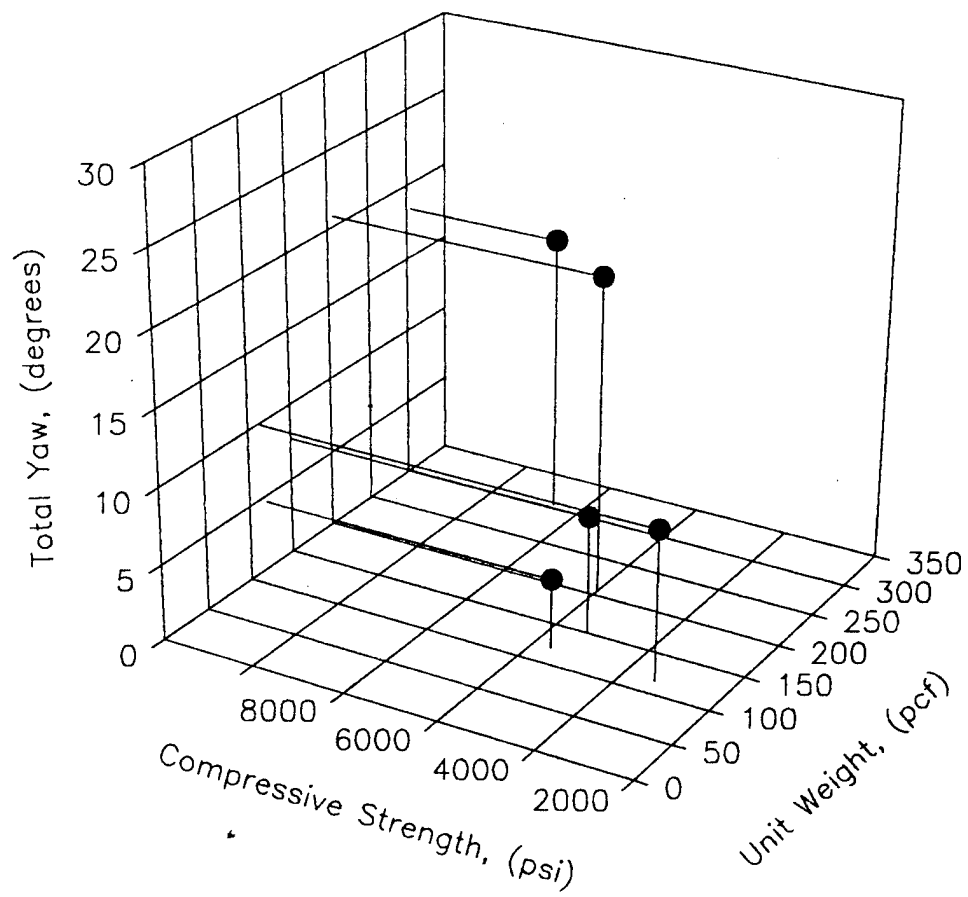


Figure 54. Material Property Comparison for Grid Type 16.

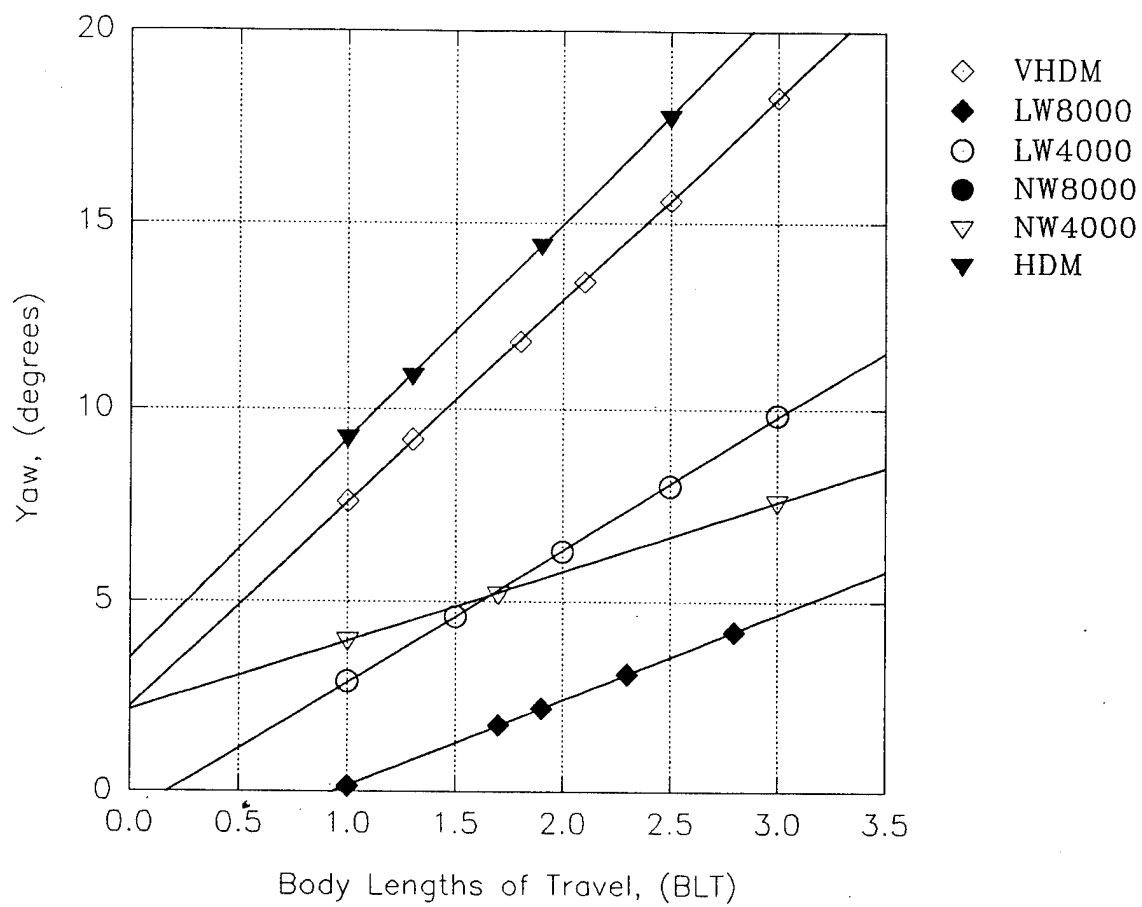


Figure 55. Yaw versus Body Lengths of Travel for Grid Type 16.

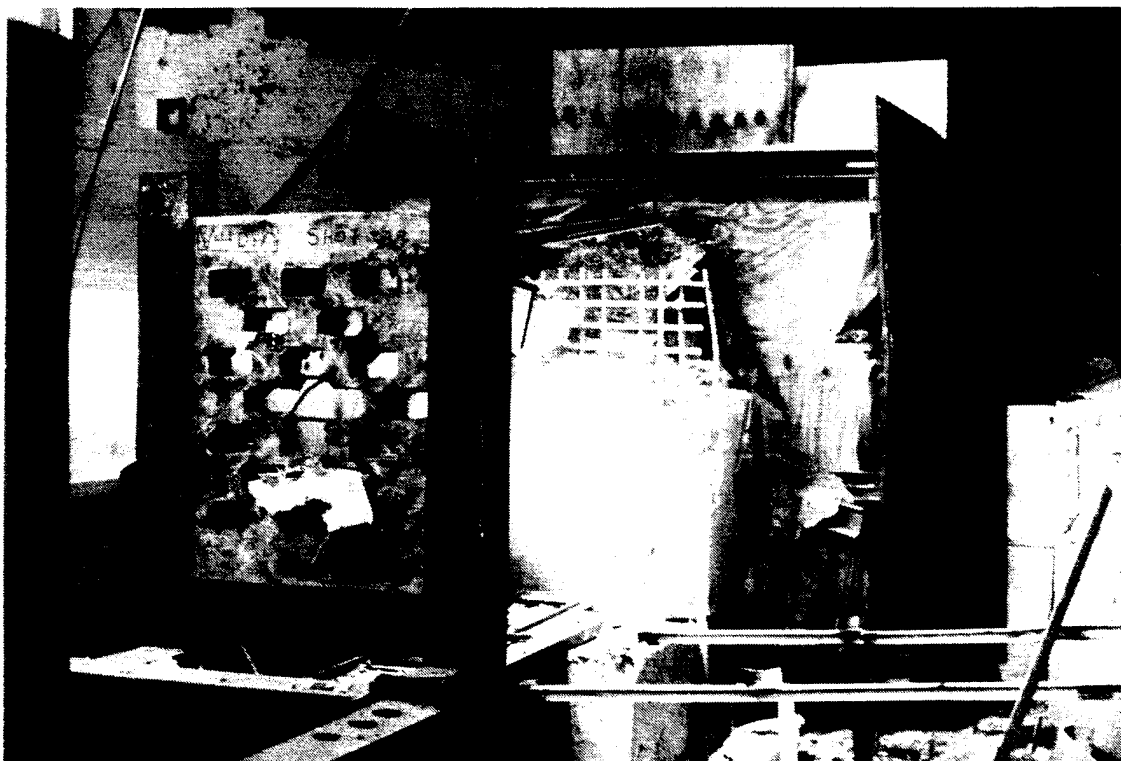


Figure 56. Posttest Photographs of Shot 39.

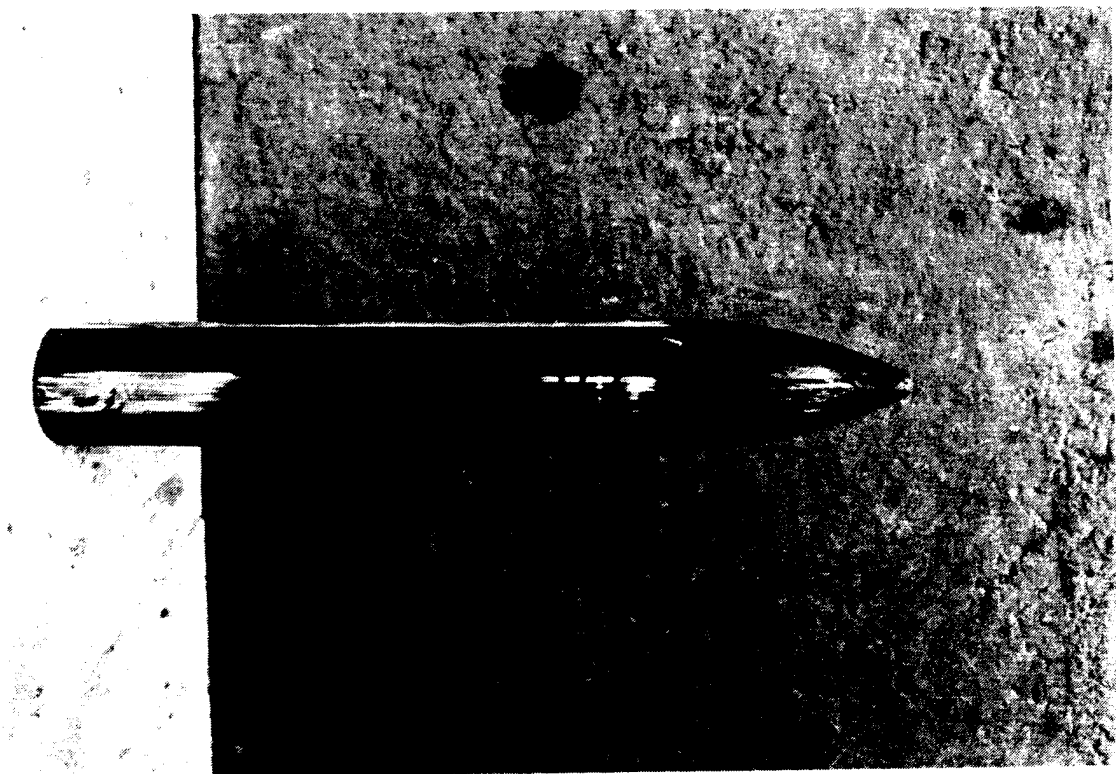


Figure 57. Posttest Photographs of Shot 41.

resulted in a yaw angle of 2.8 degrees at the burster slab. The projectile suffered little damage, and was found intact in the sand berm behind the burster slab. Figure 58 shows collateral damage to the deflection grid in the lower right quadrant from the remains of the nylon pusher plug, which continued down range after failing to be stopped by the sabot stripper.

Shot 50 used the NW 8000 mix design, with a unit weight of 153 pcf and a static compressive strength of 9,853 psi. The strike point was centered in the web, and resulted in a total yaw at the burster slab of 12.5 degrees. The upper right quadrant of the burster slab was destroyed, with the projectile lying 4 feet into the sand berm with the case slightly bent and missing the end cap, as shown in Figure 59. It is debatable whether a real projectile would have detonated upon impact of the burster slab, under these conditions.

Shot 52 used the NW4000 mix design, with a unit weight of 151 pcf and a static compressive strength of 5,320 psi. The initially planned strike point was located on a web centered on the deflection grid, but was relocated to determine if edge effects would come into play and alter the performance of the deflection grid. Figure 60 shows the secondary strike point and the posttest conditions, which yielded 12.5 degrees of yaw at the burster slab. As the projectile struck the burster slab, it deflected upwards and sustained collateral damaged from the concrete containment structure at the rear of the laboratory. As in Shot 50, the impact of the casing on the burster slab could have caused a fuse disruption in a live weapon.

Shot 55 used the HDM mix design, with a unit weight of 305 pcf and a static compressive strength of 8,615 psi. The strike point was centered on the web, and resulted in a total yaw at the burster slab of 14.1 degrees. Figure 61 shows the deformation of the penetrator case and the missing end cap. The penetrator was found lodged in the burster slab, unable to perforate.

The data on yaw achieved per body length of travel plotted in Figure 62 shows a close grouping for VHDM, HDM, NW8000, and NW4000 concretes. The slopes of these lines range from 5.4 DBLT to 7.5 DBLT. The projectiles were either stopped by the burster slab or received extensive damage to the penetrator case. Of all the tests conducted, the 20-hole geometry showed the most consist performance. Figures 63 and 64 indicate a consistent relationship between total yaw and unit weight, and an almost linear relationship between toughness (JCI Method) and total yaw. When displaying the data in a 3D plot, Figure 65, of unit weight versus compressive strength, and total yaw, the significance of the independent variable, unit weight, is obvious. Figure 66 indicates a general trend of increased total yaw as compressive strength increases but lacks the linearity of Figure 64.

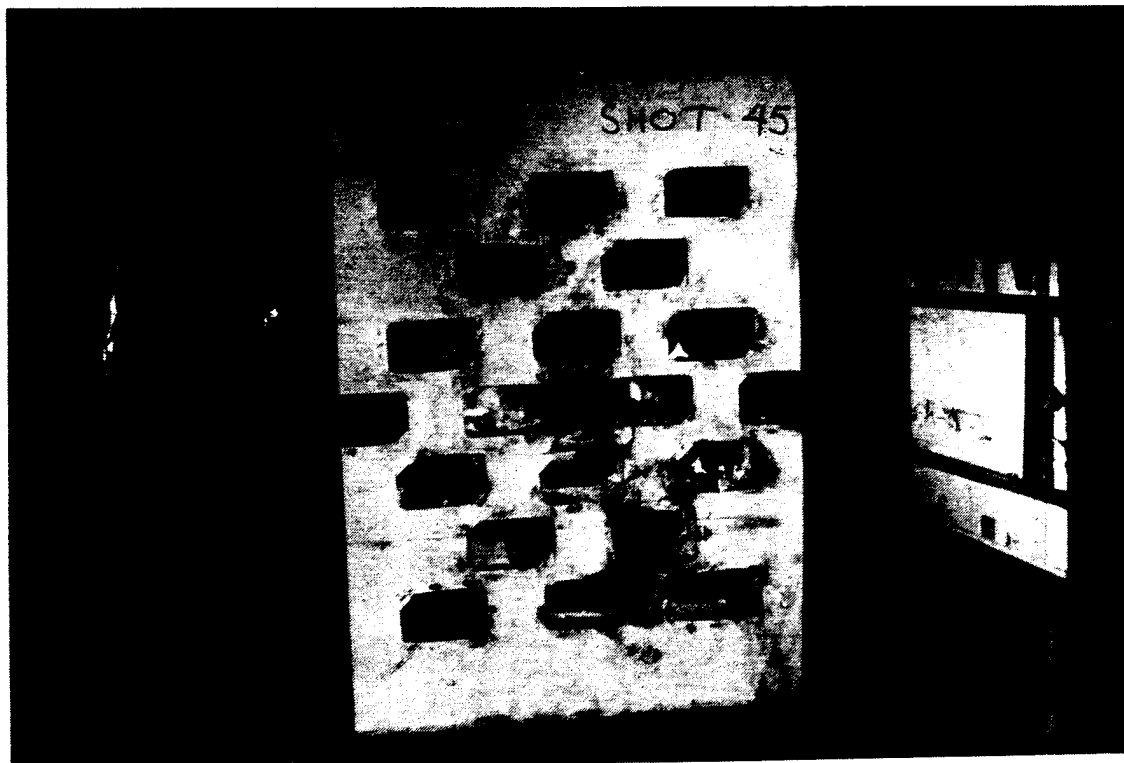
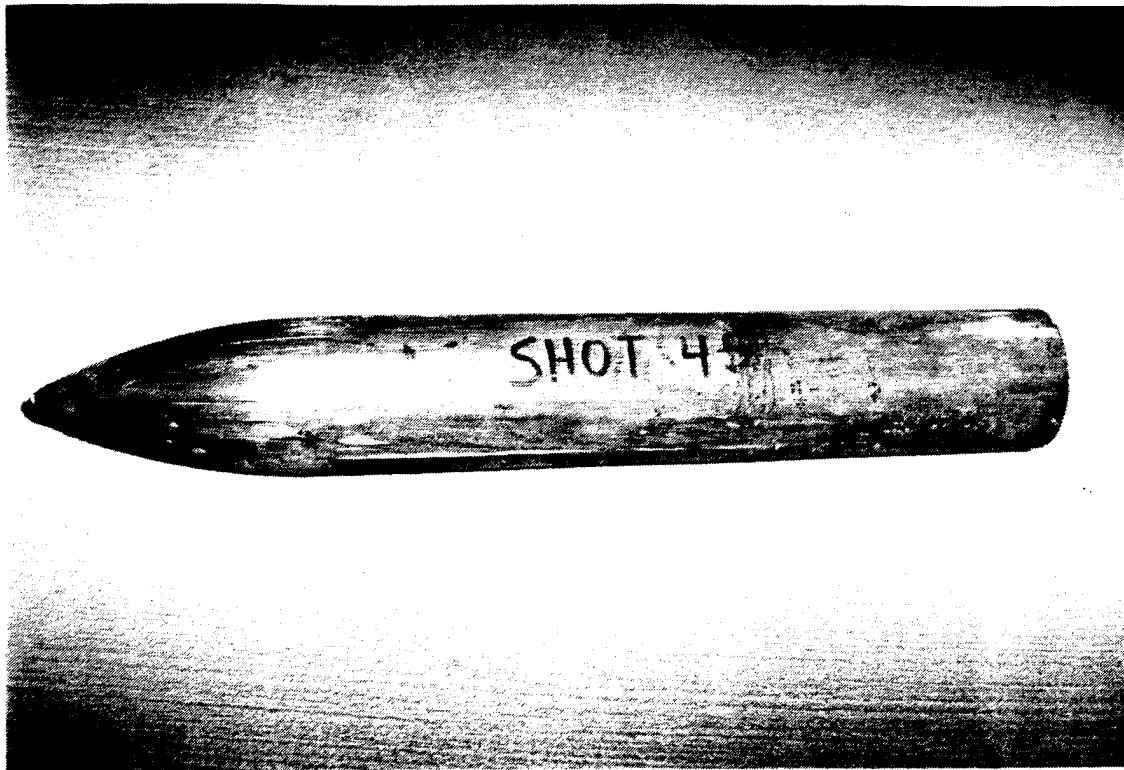


Figure 58. Posttest Photographs of Shot 45.

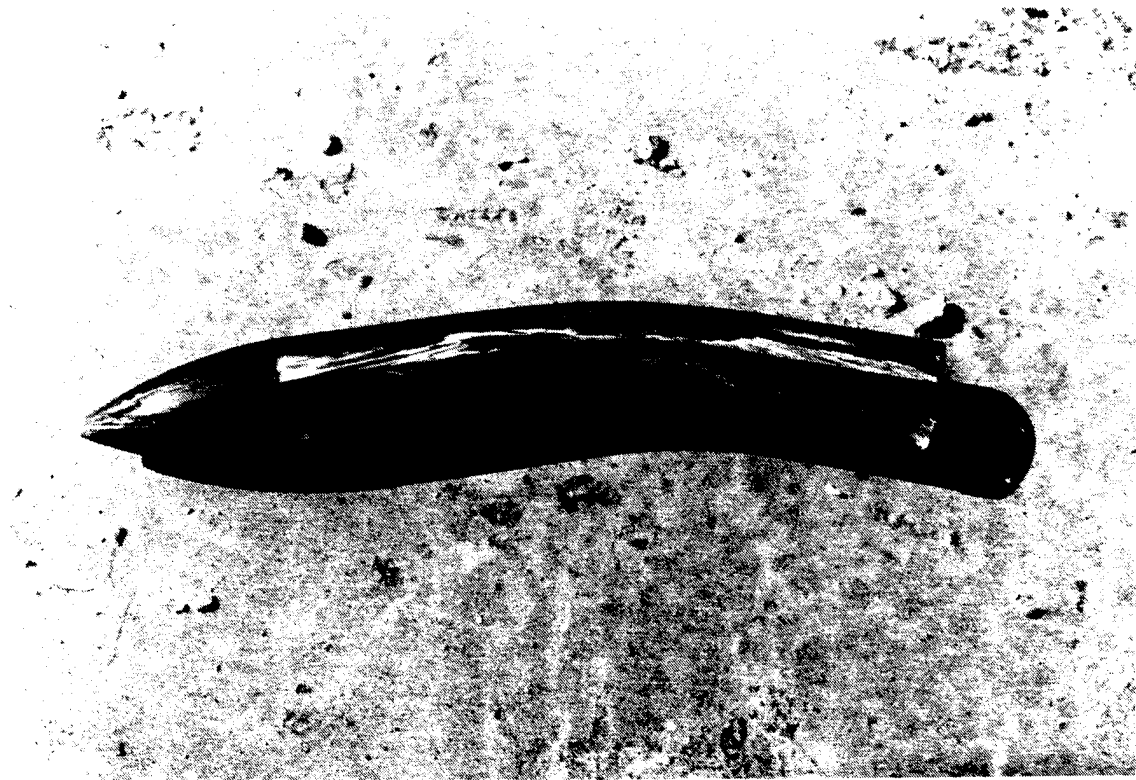


Figure 59. Posttest Photographs of Shot 50.

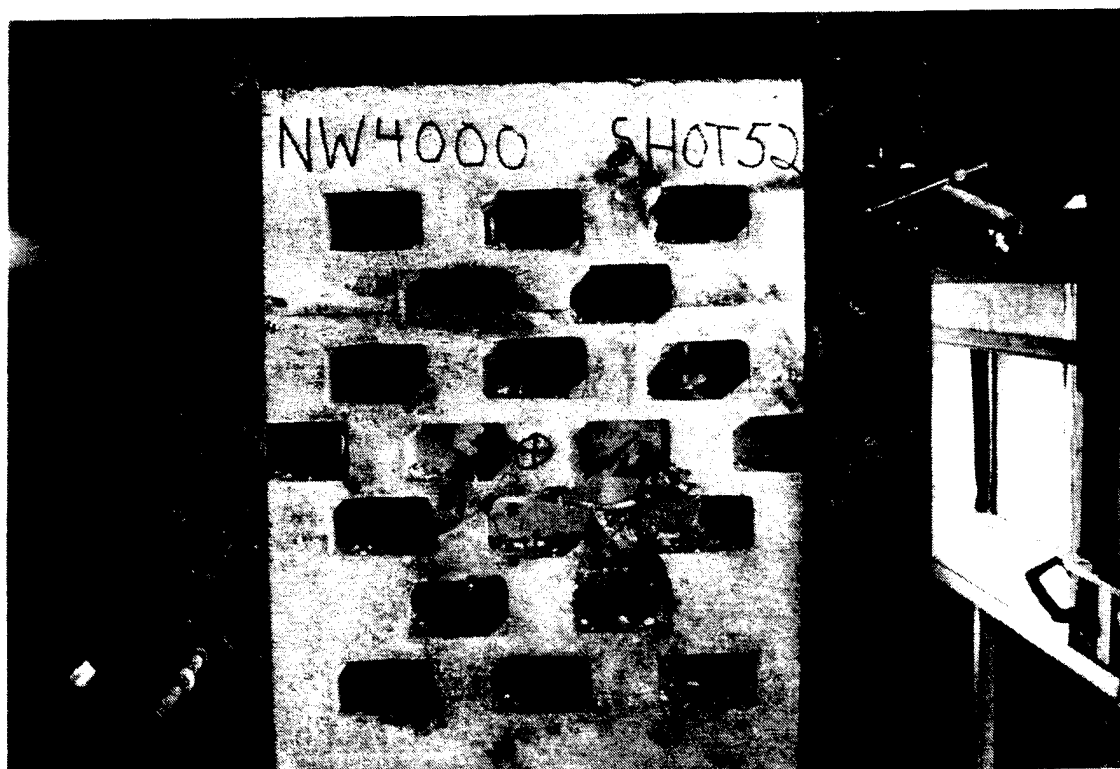
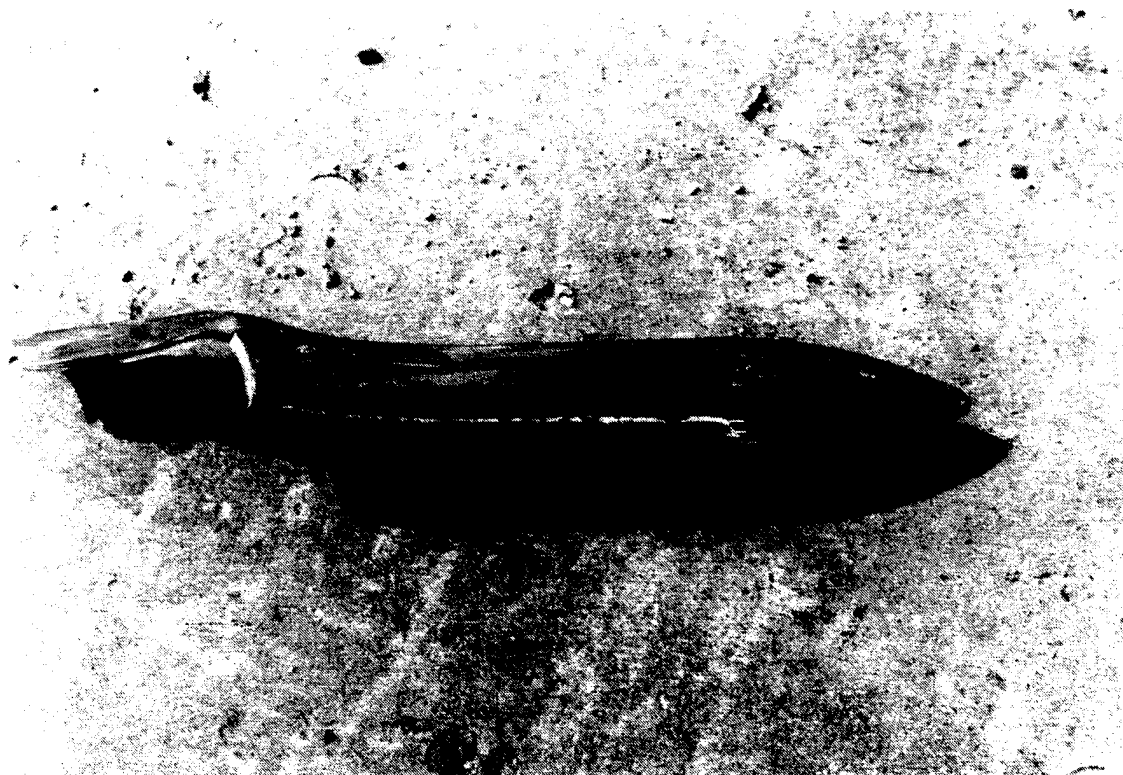


Figure 60. Posttest Photographs of Shot 52.



Figure 61. Posttest Photographs of Shot 55.

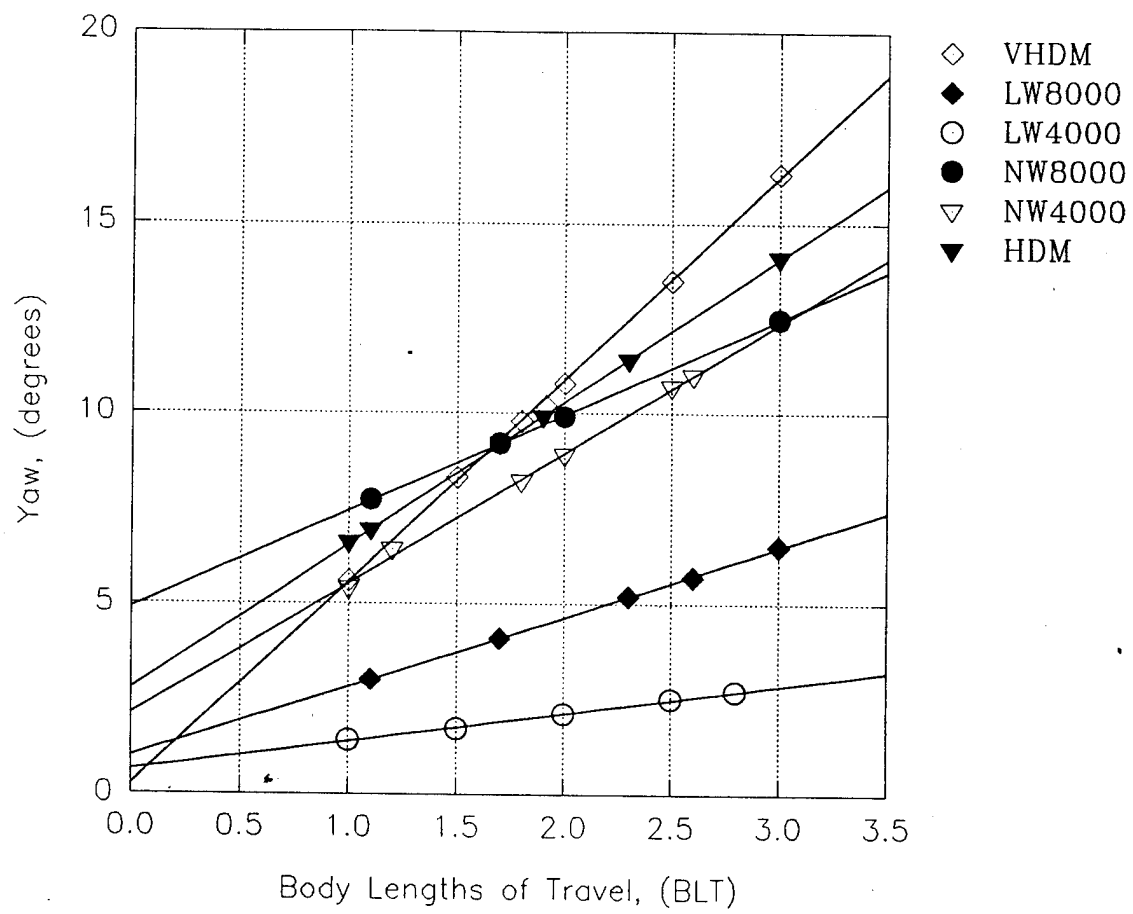


Figure 62. Yaw versus Body Lengths of Travel for Grid Type 20.

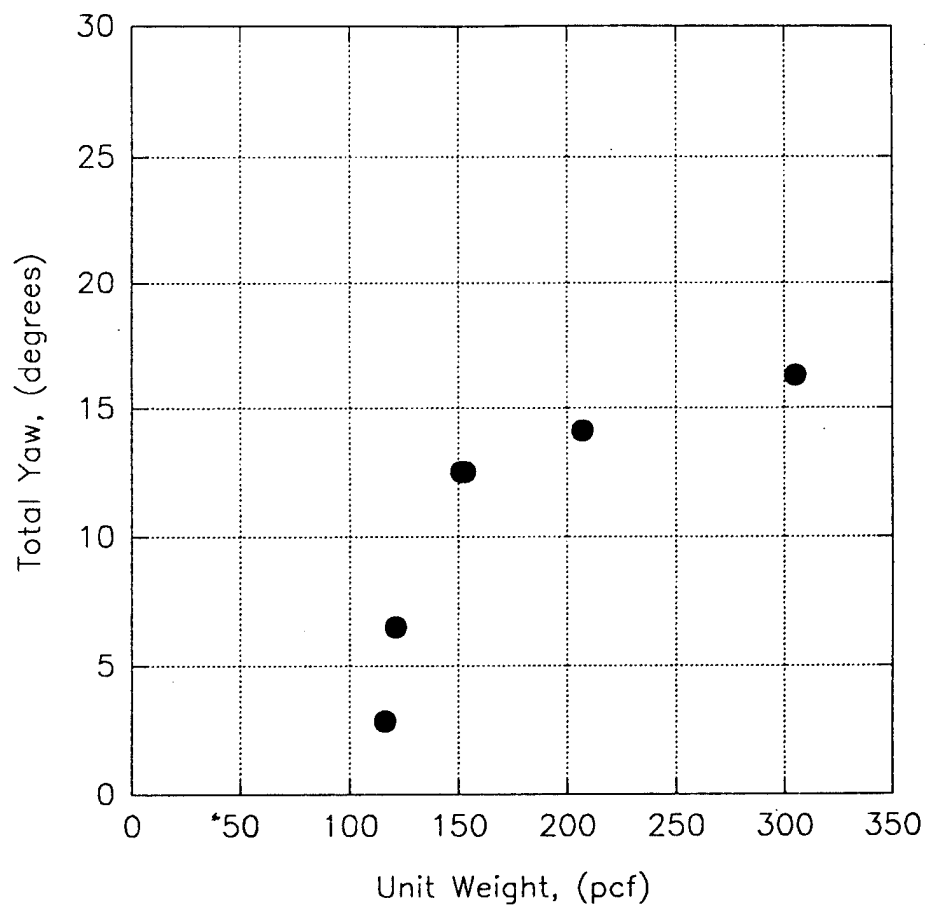


Figure 63. Unit Weight versus Total Yaw for Grid Type 20.

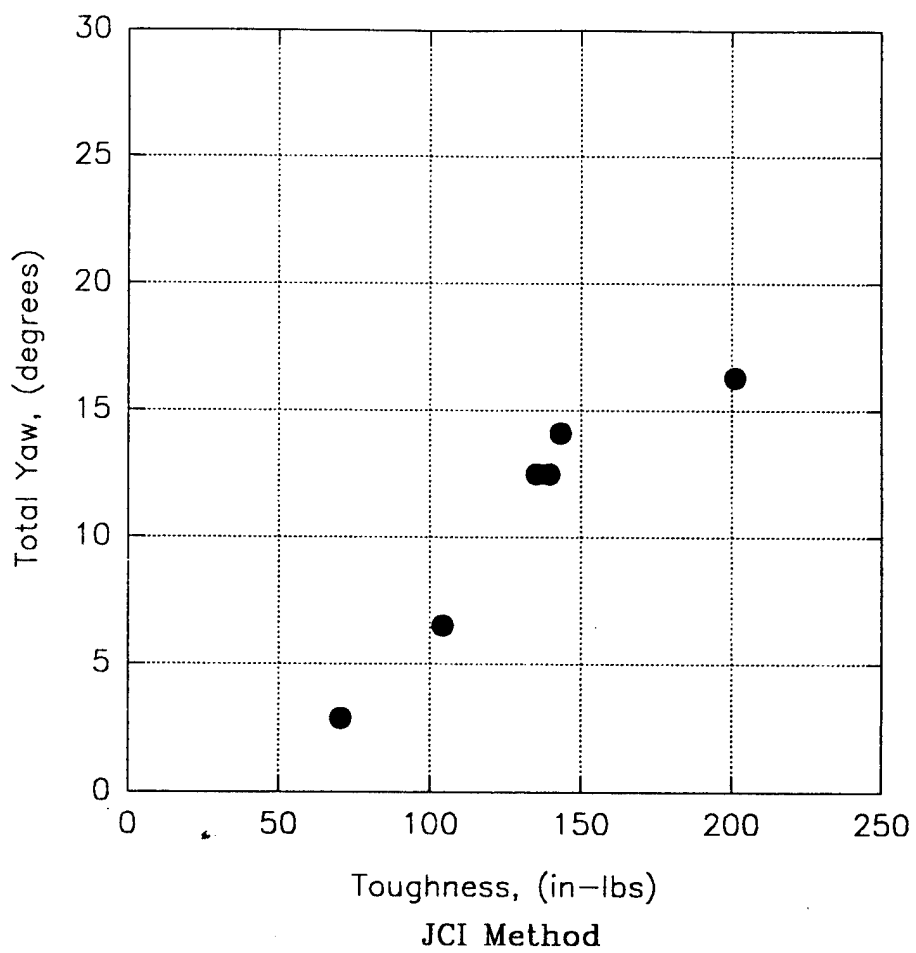


Figure 64. Toughness versus Total Yaw for Grid Type 20.

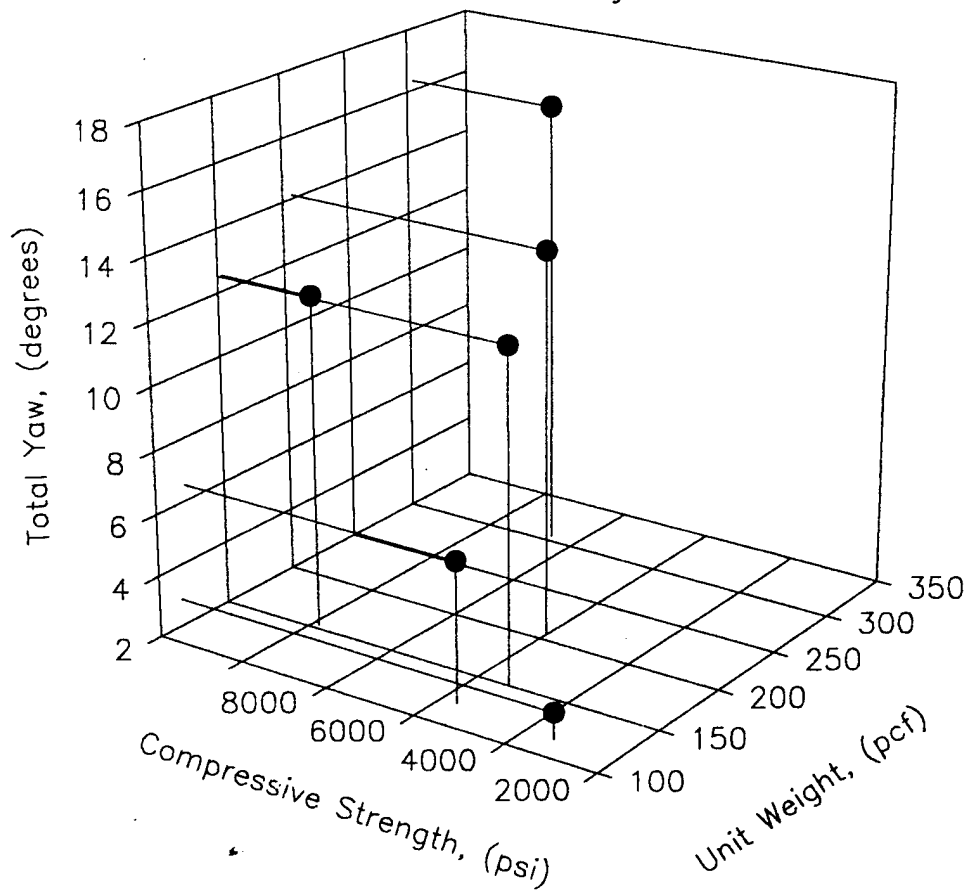


Figure 65. Material Property Comparison for Grid Type 20.

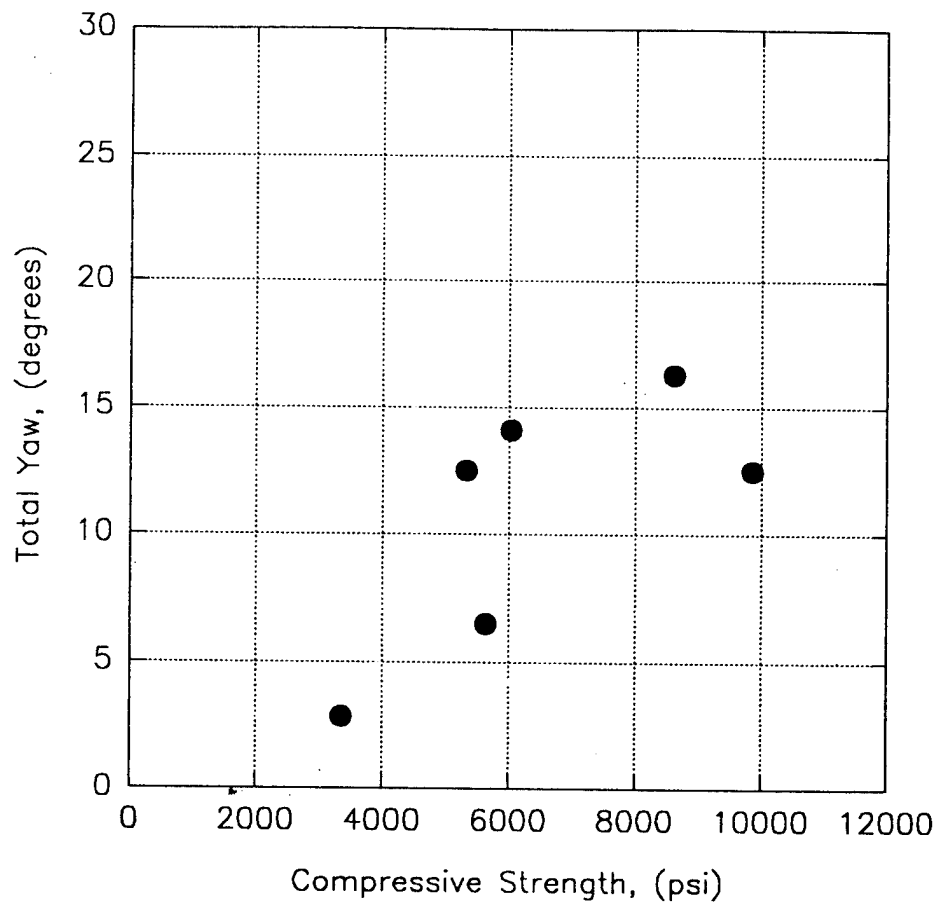


Figure 66. Compressive Strength versus Total Yaw for Grid Type 20.

3. Grid Type 25

The six tests using Grid Type 25 were Shots 38, 43, 44, 46, 48, and 51. Shot 38 used the VHDM mix design, with a unit weight of 305 pcf and a static compressive strength of 8,615 psi. The strike point was centered on the web, and resulted in 27.6 degrees of yaw upon impact with the burster slab. The projectile was severely cracked and the back end was flattened, as shown in Figure 67. The burster slab was not penetrated, and minimal damage was inflicted on the deflection grid.

Shot 43 used the LW8000 mix design, with a unit weight of 121 pcf and a static compressive strength of 5,634 psi. Since the light weight mix designs showed low rates of rotation at the center of the web, the strike point was changed to a location that might achieve a greater rotation rate. Strike Location Three, shown in Figure 37, was chosen. The projectile struck the top edge of the burster slab as it translated upwards to a total yaw of 18 degrees. Had the projectile struck the burster slab in the center section, as in earlier shots, the projectile would have been defeated. Figure 68 shows the posttest condition of the penetrator and the deflection grid.

Shot 44 used the HDM mix design, with a unit weight of 207 pcf and a static compressive strength of 6,028 psi. The strike point was located at the center of the web, and resulted in a total yaw at the burster slab of 26.5 degrees. Damage to the burster slab was limited to a two inch deep by two foot square spall area. The projectile was broken in two, as shown in Figure 69, with severe deformation of the tail section. Damage to the deflection grid was limited to a 1.5 projectile-diameter circle.

Shot 46 used the LW4000 mix design, with a unit weight of 116 pcf and a static compressive strength of 3,346 psi. The strike point was relocated to Strike Location Four, shown in Figure 37, which caused a translation of the projectile to the upper quadrant of the burster slab and achieved a yaw angle of 13.9 degrees. The projectile struck the upper quadrant of the burster slab and caused severe bending of the projectile, loss of the end cap, and a major split in the tail section, as shown in Figure 70.

Shot 48 used the NW8000 mix design, with a unit weight of 153 pcf with a static compressive strength of 9,853 psi. Strike Location Five, shown in Figure 37, was selected, and achieved 7.7 degrees of rotation at the burster slab. The projectile perforated the burster slab, penetrated eight feet of sand, and was still intact with no structural damage, as shown in Figure 71.

Shot 51 used the NW4000 mix design, with a unit weight of 151 pcf with a static compressive strength of 5,340 psi. The strike location was centered on the web, and resulted in a total yaw at the burster slab of 8.5 degrees. The projectile penetrated the burster slab and exhibited no significant damage, as shown in Figure 72.

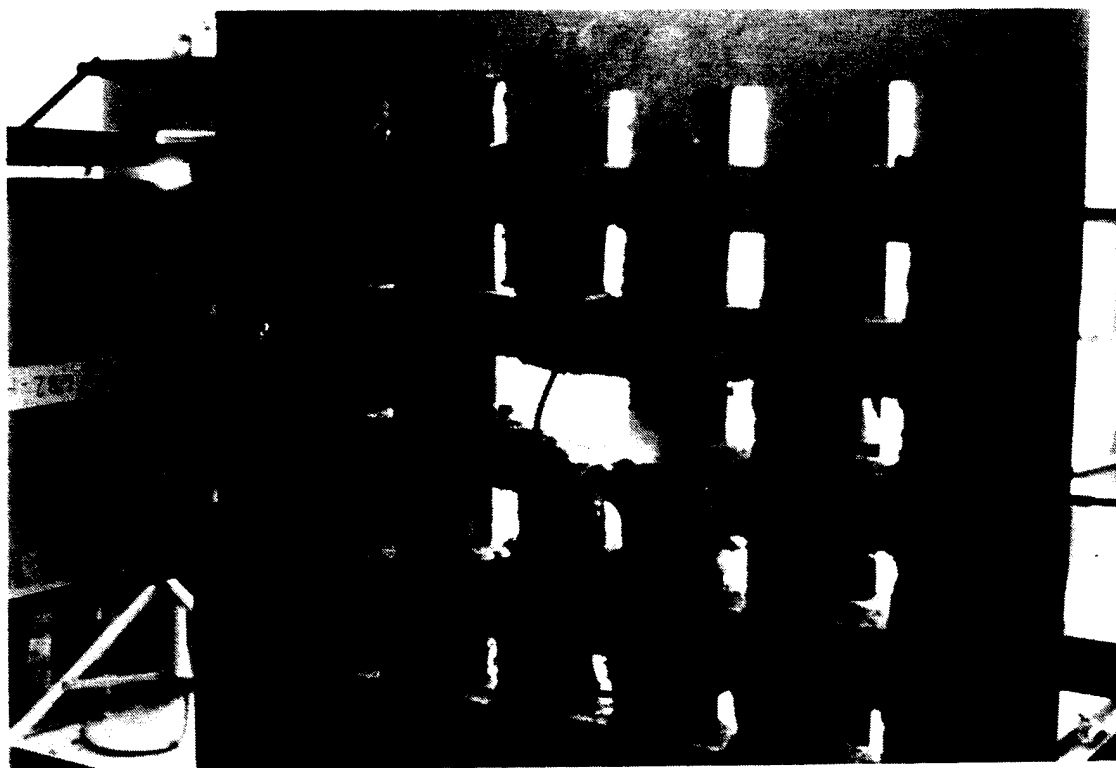
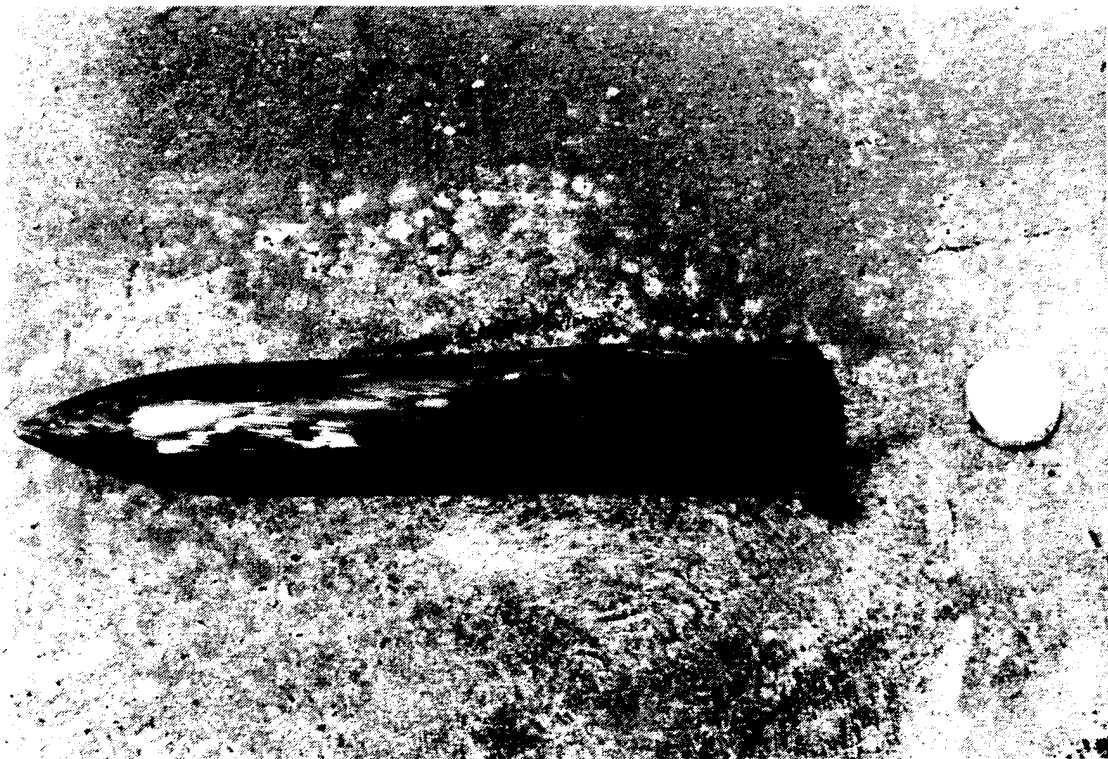


Figure 67. Posttest Photographs of Shot 38.

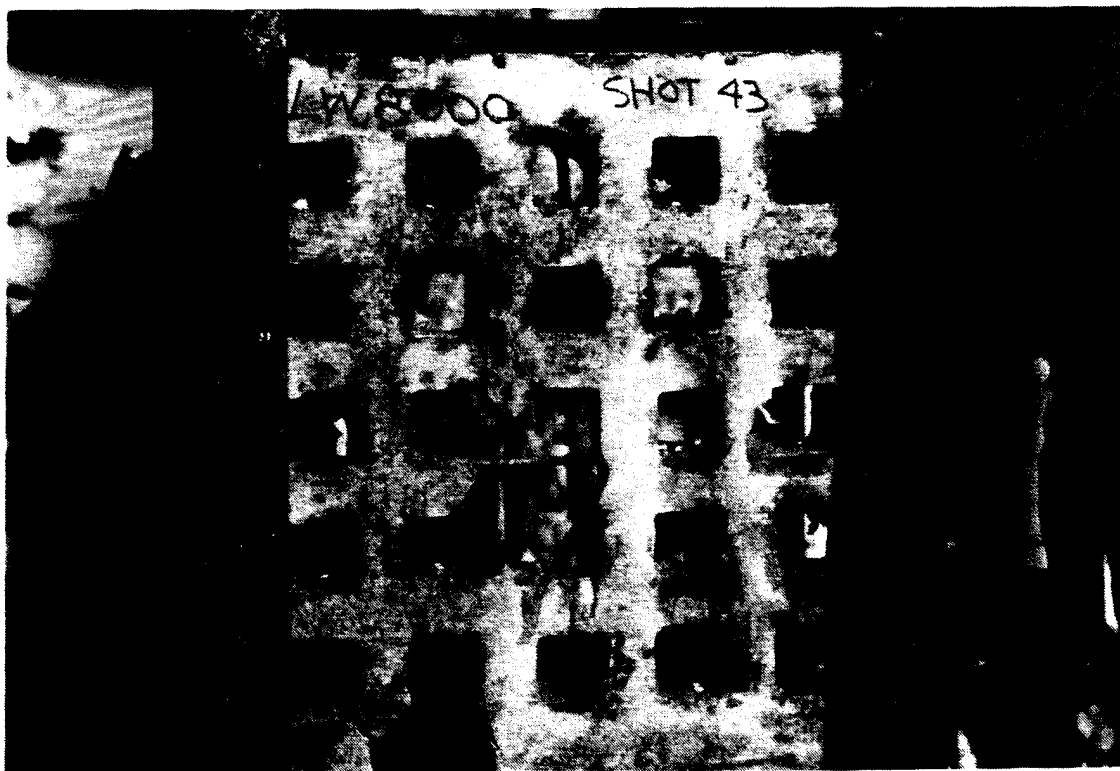


Figure 68. Posttest Photographs of Shot 43.



Figure 69. Posttest Photographs of Shot 44.

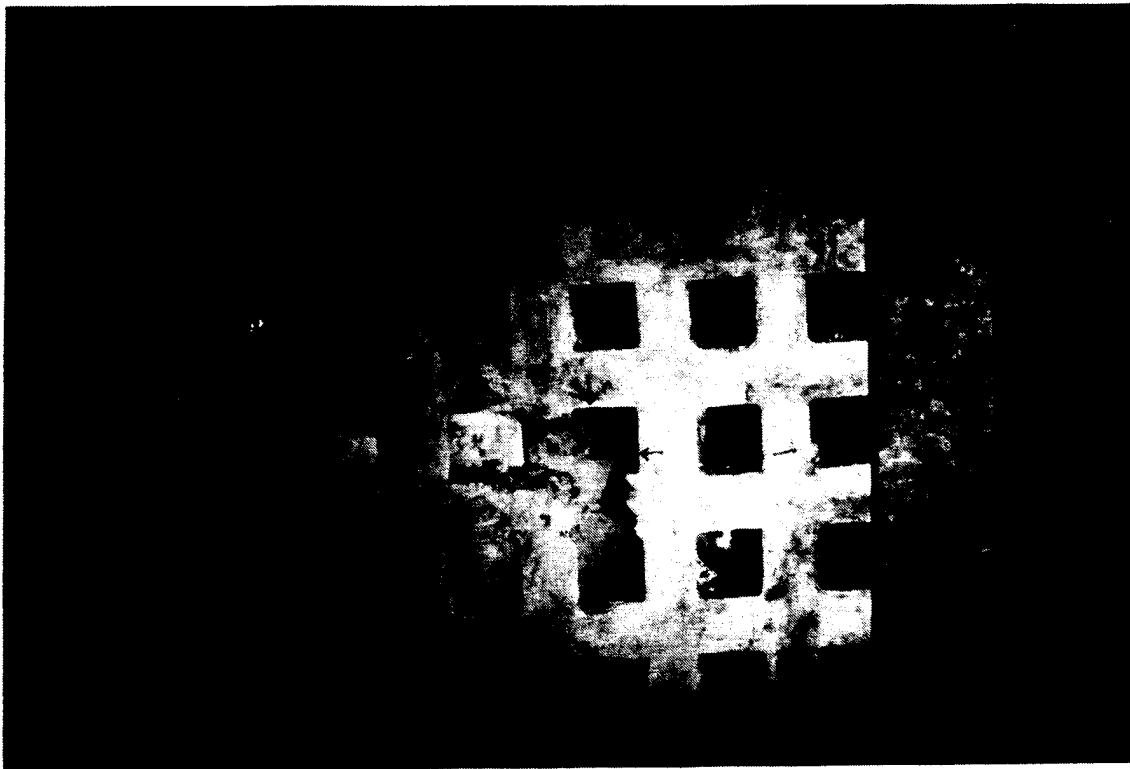


Figure 70. Posttest Photographs of Shot 46.



Figure 71. Posttest Photographs of Shot 48.

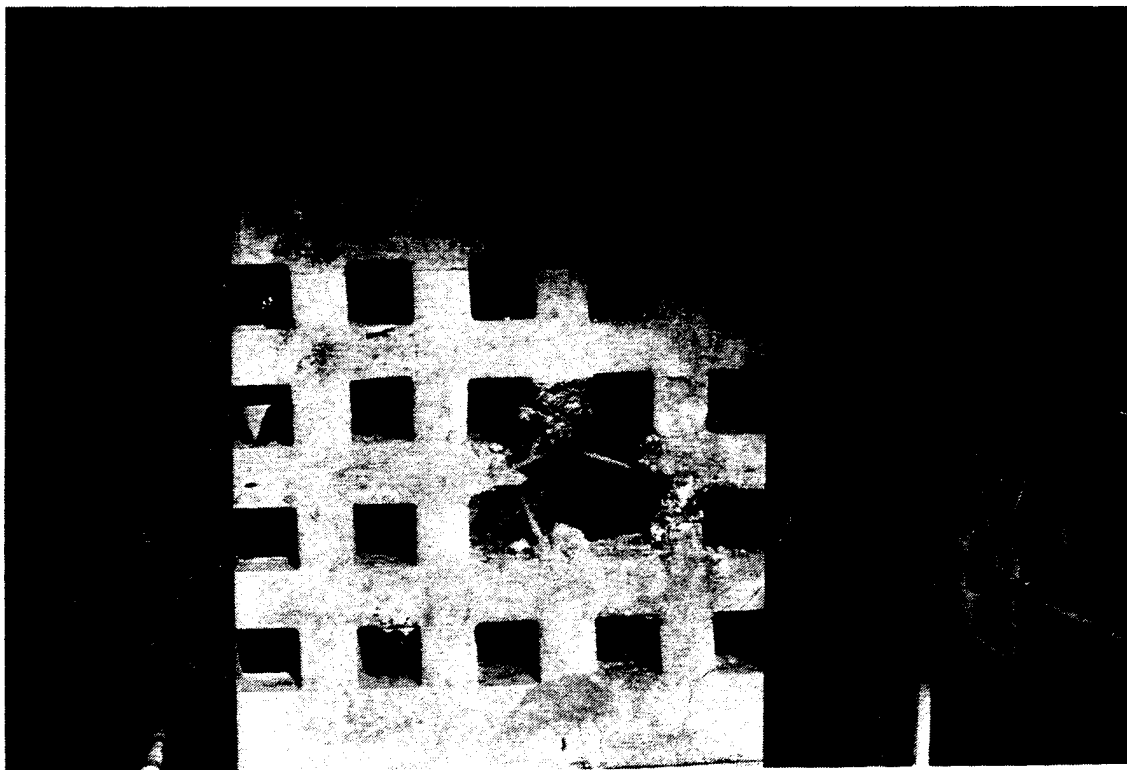
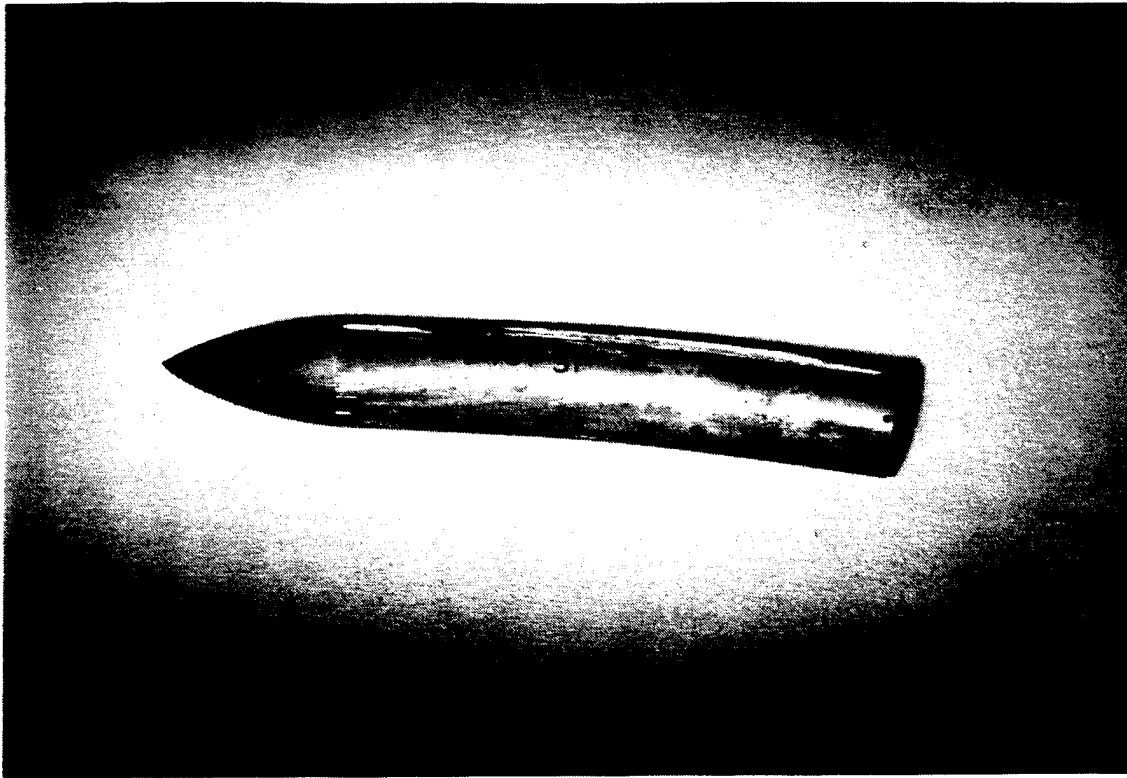


Figure 72. Posttest Photographs of Shot 51.

Figure 73 shows the a wide variation in rotation rates induced by the grid geometric pattern. This can be attributed to the deliberate relocation of the impact points. But even with the impact location changed to enhance the rotation rates of the lighter weight concretes, the VHDM and HDM grids performed in a superior manner with total yaws at the burster slab of 27.6 degrees and 26.5 degrees, respectively. Lighter weight designs can be just as effective, provided there is sufficient distance between the deflection grid and the burster slab, or strike locations stray from the center of the web. But this is not always practical or cost effective, due to the amount of real estate required and the confidence level required for sensitive or high risk assets. Figures 74 and 75 show the relation between unit weight, compressive strength and total yaw. Although the strike location has been altered, a relationship can be observed between unit weight and total yaw.

C. COST ANALYSIS

All penetrators stopped by the burster slab had an angle of attack of at least 12.5 degrees. The light weight concretes showed increased fracturing as the compressive strength was increased, and did not perform as well as did the heavier concretes. This could be related to the contact time of the penetrator and the deflection grid and the associated angular impulse. Lightweight, high-strength concretes have a shorter time to failure, and do not provide the contact time required to overcome inertia forces in the shorter distances.

To determine if a deflection grid system is a viable alternative to present construction practices, an example is presented, comparing a stand-alone burster slab system over a buried hardened structure, to the use of a deflection grid system and a thinner burster slab.

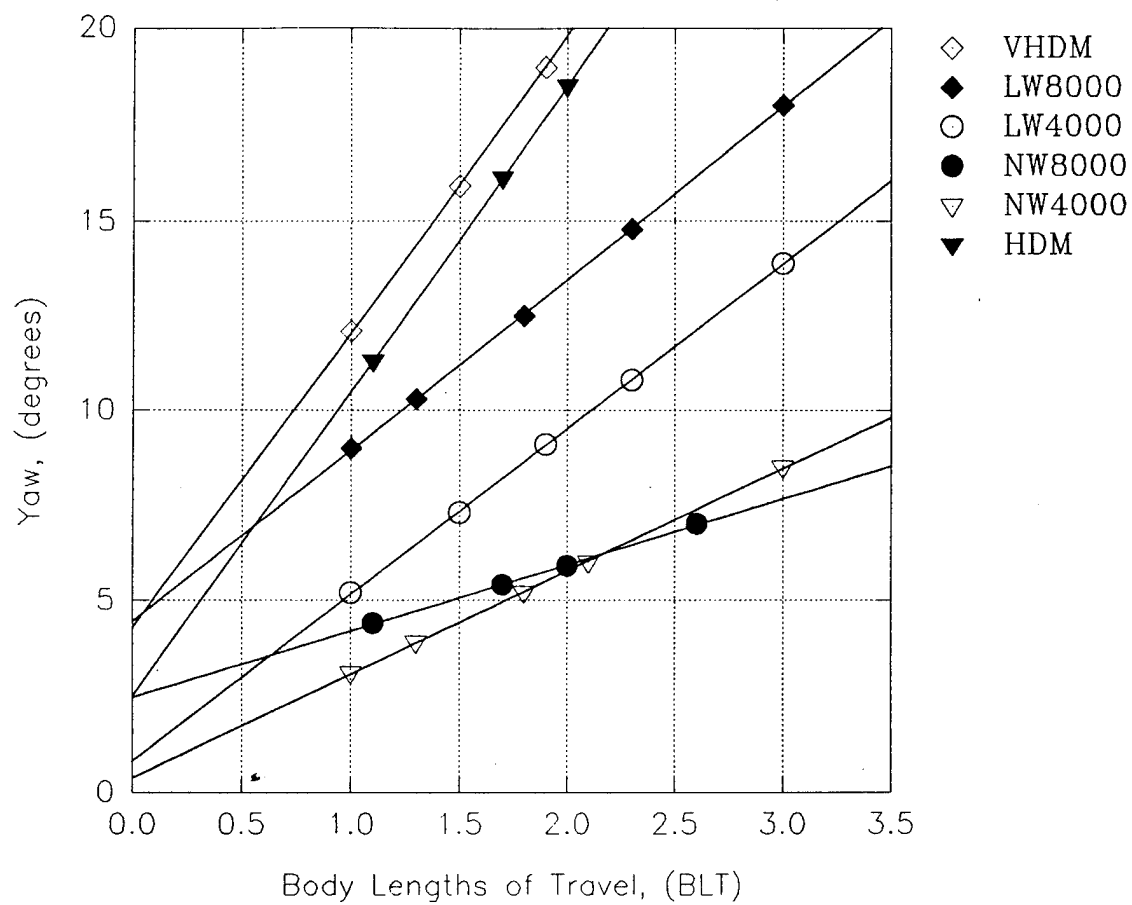


Figure 73. Yaw versus Body Lengths of Travel for Grid Type 25.

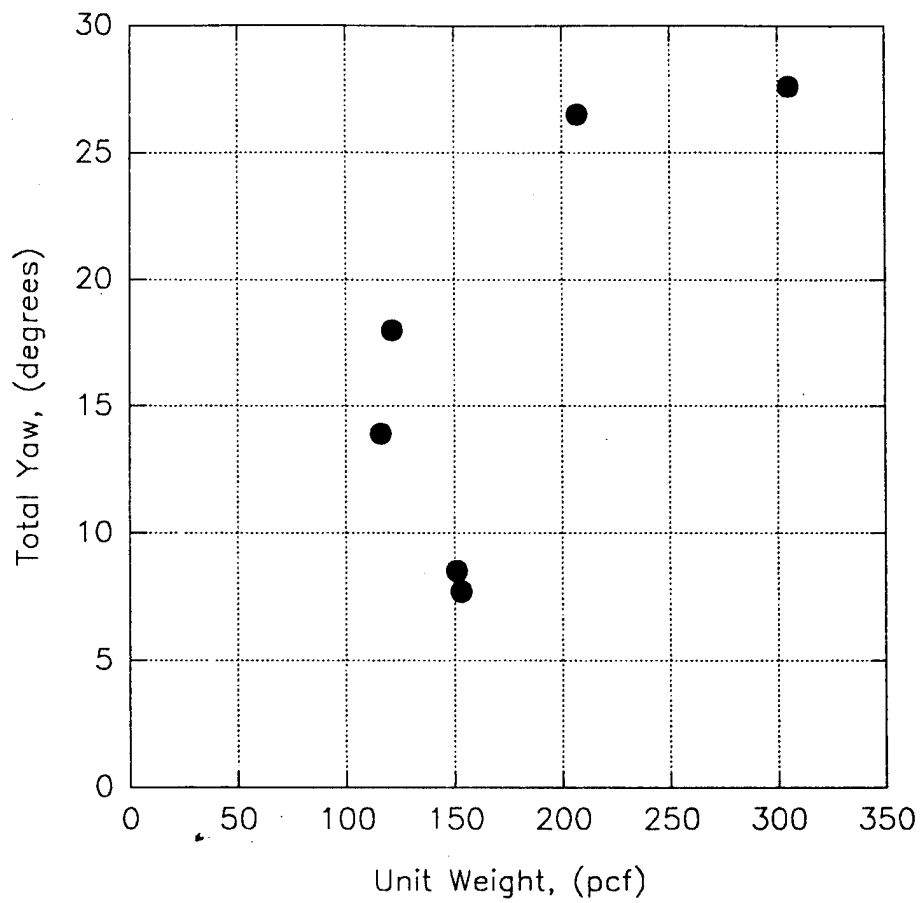


Figure 74. Unit Weight versus Total Yaw for Grid Type 25.

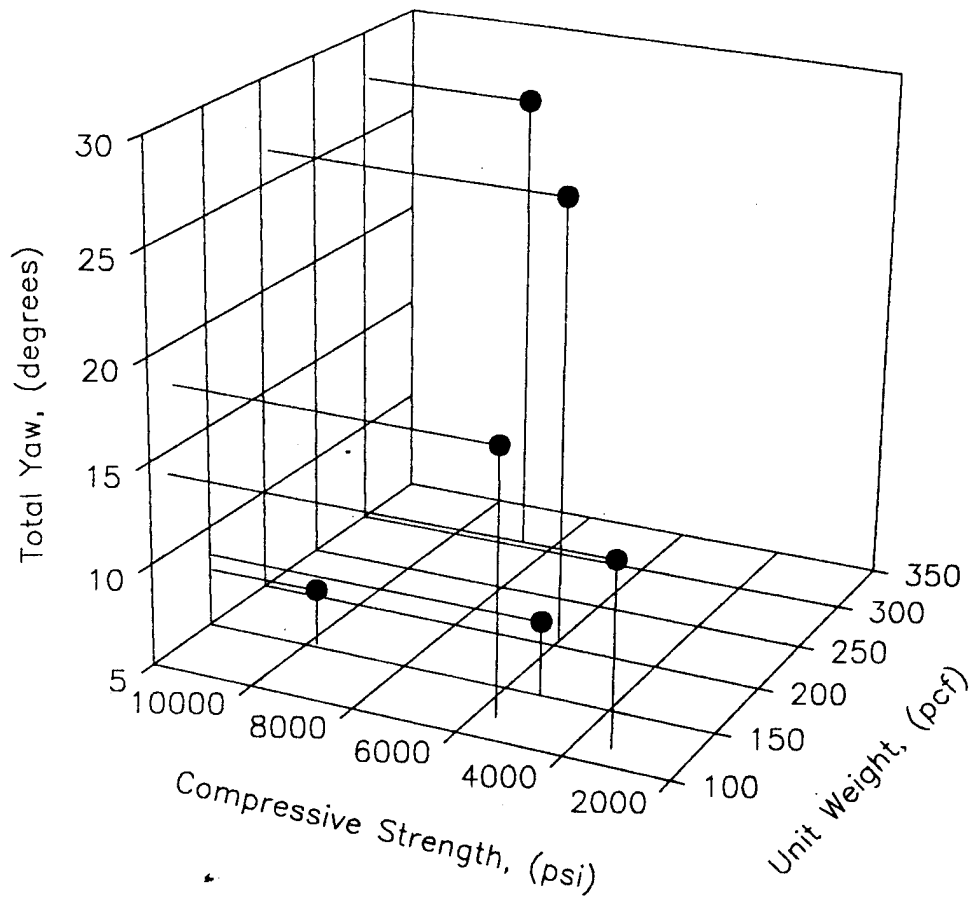


Figure 75. Material Property Comparison for Grid Type 25.

1. Burster Slab Upgrade

The approach taken in this example is to design the slab with a thickness to prevent penetration of the weapon. Concrete f'_c will be established at 4,000 psi, since quality control for massive concrete pours is difficult to maintain. The weapon will have the same parameters as tested in the laboratory for both scenarios.

- x = Absolute penetration depth (in)
- t = Thickness required to prevent perforation (in)
- V = Velocity of the projectile (1000ft/sec)
- f'_c = Compressive strength of concrete (psi)
- W = Weight of projectile (lb)
- d = Diameter of projectile (in)
- N = Factor for projectile nose shape
- n = Caliber radius head

Using the NDRC equation for penetration, (Reference 8)

$$N = 0.72 + 0.25\sqrt{n - 0.25} = 0.72 + 0.25\sqrt{8.75 - 0.25} = 1.4$$

$$x = \frac{180NW(V/d)^{1.8}}{\sqrt{f'_c}} + d = \frac{180(1.4)(28)(1.1/3.35)^{1.8}}{\sqrt{4000}} + 3.35 = 18.37in$$

$$t = 1.24(x) + 1.32(d) = 1.24(18.37) + 1.32(3.35) = 27.2in$$

Therefore, the thickness of a burster slab required to prevent perforation is equal to 27.2 inches of concrete having a unit weight of 150 pcf. Total weight of a 10-foot by 10-foot section of the slab would be 34,000 pounds.

2. Deflection Grid with Burster Slab Upgrade

Since heavier concrete mixes performed 100% of the time in preventing perforation, an HDM Grid Type 20 is selected, resulting in a unit weight of 207 pcf. Using the design parameters in the FY 92 test program, the deflection grid requires a thickness of 4 inches, followed by a 72-inch air gap, terminating at an 18-inch burster slab. The overall depth of the combined system is 94 inches. The weight of the deflection grid

is 5,520 pounds for 26.6 cf of concrete at 207 pcf. The weight of an 18 inch burster slab is 22,500 pounds, for a combined weight of 28,020 pounds. This results in a 17 percent weight reduction and a 22 percent volume reduction based on a sectional slice of the overall system.

A cost breakdown was performed on the six mix designs according to the data given in Section IV based on materials required for a 1-yard volume. The following represents the amounts based on bulk quantity purchases and there ranking in performance.

<u>Mix Design</u>	<u>Cost per Cubic Yard</u>	<u>Performance</u>
LW4000	\$ 108.16	6
LW8000	\$ 178.13	5
NW4000	\$ 111.95	4
NW8000	\$ 121.44	3
HDM	\$ 206.10	2
VHDM	\$ 1,623.10	1

All the costs include a set price of \$50 per 10 pounds of nylon fibers, which is excessively high. This was a price established by the supplier for both small and large quantities. Alternate materials could be substituted at a much lower price, but were not tested because of lack of time. In the construction of a full-scale deflection system, there would be a reduction in weight and volume of materials over existing protective construction practices. This would translate into a decrease in total labor costs and a reduction in material construction costs for the facility being protected, due to the reduced overburden pressure of the deflection grid system.

SECTION VI

CONCLUSIONS

In reviewing the laboratory data on the compression and flexural tests, a significant relationship was observed between unit weight and material toughness. An almost linear relationship exists when toughness is calculated using the JCI Method as shown in Figure 76. Total yaw was related to unit weight, compressive strength, and toughness, where again toughness exhibited excellent linearity based on the FY 92 data. For this particular penetrator, angles of attack greater than 12 degrees upon impact with the burster slab defeated the weapon. The work performed by WES corroborates this statement.

In designing a deflection system, the threat must be known, as well as the depth of the protected facility. This information will be used to compute the physical dimensions of the deflection grid, length of the air gap, and thickness of the burster slab. The following computational procedures are valid only within the range of conditions described in the body of this report, and require modification to account for scale effects. Change in weapon characteristics will have a definite impact on the procedure. Efforts are being investigated to augment these calculations for a variety of weapon types, and will be presented in a subsequent report.

From the data collected on grid geometry performance it was determined that the thickness of the deflection grid be at least 1.2 projectile diameters. The grid perforations should be laid out in a pattern to promote irregular cracking. The grid surface area facing the threat at any point within two projectile-diameter circle must not exceed 3.5 times the presented area of the projectile (solid area ratio no greater than 7/8). The air gap distance is designed so the weapon will achieve a minimum of 12 degrees of yaw at the burster slab, after impacting at the most conservative grid strike location. If the material acquisition is based on cost, select the most economical design mix, and determine the toughness index using the JCI Method. Once samples have been prepared, take the average toughness index and apply it in the following formula:

Z = Air gap distance between deflection grid and burster slab (in)
 x = Toughness index of material based on JCI Method (in lb)

$$Z = 67.985 - 1.15605x + .00676256x^2 - .000013131x^3$$

This is an empirical equation based on toughness index performance and induced yaw, assuming center-of-the-web strike to provide a conservative estimate. A strike on the

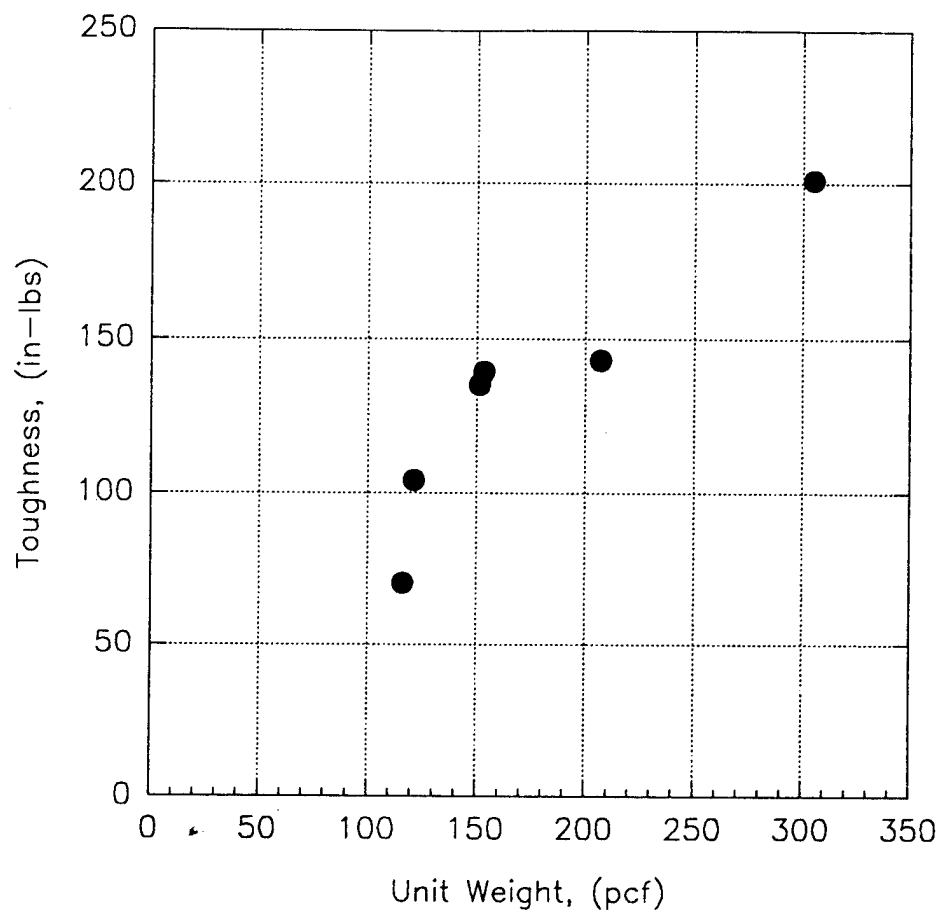


Figure 76. Unit Weight versus Toughness for JCI Test Method.

grid outside this area will provide a greater amount of rotation. The burster slab is designed using PENCO2D for a 12-degree angle of attack impact condition. Total span distance of the deflection system can be determined and compared to the space available for construction, and can be reevaluated if space constraints exist. If problems do exist, select a mix design with a higher toughness index, then recalculate. Structural details of connections and support structure were beyond in the scope of this effort.

The advantages of such a protective system become more apparent every day. With rising costs in the construction industry, and the penetration capability of advanced weapons increasing, current construction practices do not yield effective protection for critical airbase resources. This effort has developed an innovative design, and has achieved the objective stated in Section I. Based on the observations and deductions of the FY 91 and FY 92 programs, this concept has displayed: (1) consistency in performance, as shown by the 20-hole geometry design; (2) limited damage to the deflection grid with increased penetrator contact time, as a result of the nylon fibers; and (3) overall 17 percent weight and 22 percent volume reductions as compared to standard protective construction practices. The nylon fibers performed better than did the steel fibers in this particular application. At very high strain rates, the steel fibers failed from pullout, while the nylon fibers stretched to absorb the mechanical energy. These findings dictate a continued effort to exploit this extremely promising technology.

SECTION VII

RECOMMENDATIONS

Investigations should be conducted to evaluate additional mix design performance with variations of velocity and projectile size, to increase the existing data base. Full scale tests should be conducted against inert and live 2000-pound class weapons, once scaling issues have been investigated. The deflection grids should be constructed as modular panels in a factory environment, to ensure strict quality control.

REFERENCES

1. Rohani, B., "Shielding Methodology for Conventional Kinetic Energy Weapons," Technical Report SL-87-8, U.S. Army Engineer Waterways Experiment Station, Vicksburg, MS, 1987, Secret.
2. Austim, C.F., Halsey, C.C., Clodt, R.L., and Berry, S.L., "Protective Antipenetration Systems Development," Technical Report ESL-TR-83-39, Engineering and Services Laboratory, Air Force Engineering and Services Center, Tyndall Air Force Base, FL, 1982.
3. Gelman, M.D., Nelson, R.B., and Ito, Y.M., "Non-Normal Impact of AP Projectile into Array of Large-Caliber Boulders," Technical Report SL-91-2, U.S. Army Engineer Waterways Experiment Station, Vicksburg, MS, September 1991.
4. Cargile, J.D., and Cummins, T.K., "Effectiveness of Yaw-Inducing Bar Screens for Defeating Low Length-to-Diameter Armor-Piercing Projectiles," Technical Report SL-92-10, U.S. Army Engineer Waterways Experiment Station, Vicksburg, MS, March 1992.
5. Creighton, D.C., "Non-Normal Projectile Penetration in Soil and Rock: User's Guide for Computer Code PENCO2D," Technical Report SL-82-7, U.S. Army Engineer Waterways Experiment Station, Vicksburg, MS, September 1982.
6. Nemegeer, D., "An Identity Chart for Steel Fibres," Fiber Reinforced Cements and Concretes Recent Developments, Elsevier Applied Science, 1989, pp.401-410.
7. Zhao, J., Xu, P., and Fan, C., "An Investigation of the Toughness and Compressive Toughness Index of Steel Fiber Reinforced Concrete," International Symposium on Recent Developments in Concrete Fiber Composites, Transportation Research Record No. 1226, 1989, pp.88-93.